THE UNIVERSITY OF CHICAGO

QUANTITATIVE MAGNETIC RESONANCE IMAGING OF MULTIPLE SCLEROSIS

A DISSERTATION SUBMITTED TO

THE FACULTY OF THE DIVISION OF THE BIOLOGICAL SCIENCES

AND THE PRITZKER SCHOOL OF MEDICINE

IN CANDIDACY FOR THE DEGREE OF

DOCTOR OF PHILOSOPHY

COMMITTEE ON MEDICAL PHYSICS

BY

ADAM JAMES HASSE

CHICAGO, ILLINOIS

MARCH 2022

To Eileen, Katelyn, Megan, Mom, and Dad

TABLE OF CONTENTS

LIST OF FIGURES

LIST OF TABLES

LIST OF EQUATIONS

ACKNOWLEDGEMENTS

I would first and foremost like to thank my advisor, Dr. Tim Carroll. He constantly pushed me to think outside of the box, to reach for goals that I did not think were possible, and most importantly, always fought for what he thought was best for me. I am incredibly grateful for his support, his enthusiasm, his witty remarks, his movie recommendations, and his guidance over the past five years.

I also would like to acknowledge my thesis committee, Drs. Steffen Sammet, Sean Foxley, Sam Armato, and Adil Javed for always being available to answer my questions and steer me in the right direction. A special thank you goes to both Dr. Adil Javed for being such an enthusiastic supporter of this project, and Dr. Sean Foxley for helping to acquire all the data from the healthy volunteer study during the middle of the pandemic.

I was incredibly honored to have worked with some incredible people during this journey in the Carroll research group. I specifically want to highlight a few people. A special thank you to Dr. Yong Jeong for not only starting this work but helping me through any issues I had. I am also thankful for both Mira and Julian. I have had the pleasure to watch both of them grow from nervous first years into two of the most promising and inquisitive people I have ever met. I cannot wait to see what the two of them achieve in their graduate research and beyond.

My fellow GPMP students were essential in getting me to where I am now. Interviewing here early on, I was told how much we would lean on each other during our time here, and I am so thankful that I had the peers that I had to do just that. Specifically, Jennie, Sam, and Scott, you were always available to answer my questions, listen to my complaints, and grab a cup of coffee and a bite to eat.

I would also like to thank the entire GPMP faculty and staff. Their doors were always open for whatever I needed, and I could not have done this without their support. The GPMP is an incredible tight-knit group that pushes all its students to their fullest potential, and I am thankful to have been a part of it.

This dissertation would not have been possible without the support of the National Institute of Biomedical Imaging and Bioengineering of the National Institutes of Health (NIH) under grant number T32 EB002103 and the National Institute of Neurological Diseases and Stroke of the NIH under grant number F31NS118930-01A1.

I would like to thank my family. I would especially like to thank my parents for their unrelenting love and support. My mom is my constant source of inspiration, and always knows the right things to say to get me out of my own head. My dad always encourages me to be the best I can be while staying true to myself. I am so thankful to have two incredible older sisters, Katelyn and Megan, to look up to. Katelyn is the one who showed me what medical physics is, and I am grateful for her endless supply of advice and knowledge on that subject and on life in general. Megan continuously shows me what strength really is and is always there for me when I needed anything, especially if it involves a game night.

Finally, I would like to thank my wonderful wife Eileen, for being a constant source of love, support, patience, and active listening skills when I drone on about some random topic. None of this would have possible without her.

ABSTRACT

Data harmonization is an important issue in computerized analysis of medical images, and especially with magnetic resonance imaging (MRI). MRI consists of a complex system of radiofrequency pulses at various times that allow for incredible control over the imaging contrast. However, with that comes a lack of uniformity in imaging datasets. While radiologists do not necessarily need a uniform imaging dataset, this presents a problem when trying to train machine learning algorithms to perform tasks using these heterogeneous datasets. Without any uniformity, certain imaging features may be skewed or not present, even if the training dataset consists of the same MR weightings.

Relaxometry or quantitative MRI is a potential solution to this issue. An MR signal is created, at its most basic, by adding energy into the tissue in the form of radiofrequency pulses and observing how the tissue of interest returns to its original state. The relaxation of the tissue back to equilibrium can occur in two ways, either by spin-lattice (T1) relaxation or spin-spin (T2) relaxation. The contrast seen in T1-weighted and T2-weighted MRIs between tissues is primarily due to this difference in T1 and/or T2 relaxation between tissues of different types. The other parameters used to generate the MR image (such as the repetition time, echo time, flip angle, etc) are used to highlight certain aspects of the image or affect the image quality or duration. Therefore, if it were possible to remove the user-defined scan parameters and generate an image of only T1 or T2, the issue of a heterogeneous dataset could be solved, and variations in these relaxation times would be indicative of some sort of underlying physiology.

Current relaxometry techniques are slow, computationally expensive, and not often performed. Most clinicians find no additional value in performing these scans, so very few datasets include relaxometry images. Because of this, there are few MR imaging datasets that can be used

for machine learning applications. It would be beneficial, then, to be able to retrospectively remove the effect of scan parameters on previously-acquired MR images and artificially produce quantitative T1 and T2 maps for big data studies. By doing this, it would not disrupt any clinical workflow and instead be a step in a machine learning pipeline.

The research presented in this dissertation presents the following results. First, an algorithm to retrospectively quantitate T1 from T1-weighted MR images was developed using a combination of sequence-specific MR signal equations and literature values for healthy tissue as references. This algorithm, referred to as T1-REtrospective Quantification Using Internal REferences (T1-REQUIRE), was tested for two specific MR sequences: T1-weighted spin-echo and T1-weighted magnetization prepared gradient echo (MPRAGE). It was validated by a combination of digital simulations, a dual T1/T2 phantom, and a healthy volunteer study. The results demonstrate that T1-REQUIRE is comparable to the reference standard to a clinically-relevant degree and within a range of T1 values that are inclusive of most brain tissue and neuropathology. In addition, it was shown that T1-REQUIRE also effectively harmonizes data across both sequences and across scanners. This is shown by comparing the results from T1-REQUIRE for both the spin-echo and MPRAGE images, before completing a study consisting of two subjects having repeated scans across multiple scanner models and manufacturers. Finally, T1-REQUIRE was applied for a pilot study to determine if it was effective at data harmonization and if it provided any additional predictive power. A study was completed looking at the contrast enhancement status of Multiple Sclerosis (MS) lesions using a combination of two separately acquired datasets. Although the study was too small to find significant differences in the predictive power of T1-REQUIRE, improved data harmonization was shown, especially when training on one dataset and testing on the other.

The medical significance of this research is that it has the potential to be an important addition to big data and machine learning studies. These studies are of increasing importance as the medical system recognizes the importance of harnessing the patient data to improve patient outcomes. The REQUIRE algorithm would allow for a simple an efficient way to harmonize MRI data and help answer important clinical questions.

Keywords: MRI, data harmonization, relaxometry, T1, machine learning, big data, Multiple Sclerosis, gadolinium-based contrast agents

CHAPTER 1

INTRODUCTION

Magnetic resonance imaging (MRI or MR imaging) is an essential tool for diagnosis and management of a multitude of diseases. Annually in the US, upwards of 30-40 million MRIs are performed, with a significant portion of these being anatomical and/or functional scans of the brain.[1] This has led to a large amount of medical imaging data that is often unused for research purposes. A primary reason why it remains unused is due to the heterogeneity of the images collected; unlike with other imaging modalities, most MRIs only show relative contrast between different tissue types, and the contrast can change depending on which scan parameters are used. Because of this, it is difficult to complete retrospective studies with previously acquired data. In this dissertation, a method for harmonizing retrospective MRI data using a physics-based approach is presented and applied to a disease where it could potentially be useful.

The introduction of this thesis begins with a general overview of MRI and more specifics including weightings, relaxometry, and pulse sequences. It then transitions into the disease that is of interest for this work, Multiple Sclerosis (MS), before a brief introduction on machine learning. Finally, it is concluded with a discussion of the scope and aims of this dissertation research, as well as an outline of the structure of this thesis.

1.1 Introduction to MRI

1.1.1 Overview of Spin Physics

MRI is a noninvasive diagnostic procedure involving the use of non-ionizing radiation to produce a detailed anatomical or functional image. By manipulating magnetic gradients and radiofrequency (RF) pulses, hydrogen nuclei (the most abundant atom in the human body due to

its presence in water molecules) are excited and allowed to relax in specific manners that allow for either high soft tissue contrast or useful functional information. This makes MRI a very advantageous tool in the fight against both diseases (cancer, stroke, Multiple Sclerosis (MS)) and traumatic soft-tissue injuries (muscle, ligament, and tendon tears).

To generate MR images, the patient or subject is placed inside of a MR scanner that produces a strong magnetic field referred to as B_0. This B_0 field (with strengths typically 1.5 Tesla [T] or 3T – about 5 orders of magnitude larger than the Earth's magnetic field) causes the randomly-oriented nuclear spins of the hydrogen nuclei to align either parallel or anti-parallel with the direction of the B_0 field. A small majority, approximately 1 spin per million, align parallel to the B_0 field, producing a net magnetization vector M that points in the same direction as the B_0 field.[2]

In addition, a short RF pulse, which is simply a magnetic field oscillating at the resonance frequency of hydrogen nuclei, is applied in a direction orthogonal to the B_0 field. This RF pulse causes the net magnetization vector to tip into the transverse plane as energy is added to the system, causing more hydrogen nuclei spins to align anti-parallel to the B_0 field. When the RF pulse is turned off, the net magnetization vector relaxes back towards its initial equilibrium by releasing the energy it had gained from the RF pulse. By repeating this process, adding gradient coils to position the nuclei gaining and releasing energy from RF pulses, and measuring the amplitude of the RF energy released by those nuclei, we can produce a MR image.

However, the signal that is produced in this process is not the MR image itself. Instead, it is the Fourier transform of the image. As the frequency and phase encoding gradients are turned on and off, the phase and frequency that nuclei precess at begins to vary depending on where they are spatially in relation to the gradient coils. Thus, when we input RF energy into the system and

perturb it, the read out will be the time-varying signal of all combined nuclei that were excited in a domain referred to as k-space. K-space does, however, have a direct relationship with the image domain itself: because the gradient strengths, durations, and sequence timings are all known, it is possible to calculate the signal in the image domain as the Fourier transform of the signal in k-space.

1.1.2 T1 and T2 Relaxation

The key to MRI is the way that the excited hydrogen nuclei relax back to equilibrium. The composition of the tissue being excited and surrounding those nuclei being excited have a drastic effect on how quickly or slowly these excited nuclei return to their resting state. By altering the timing parameters and strength of the RF pulse and magnetic gradients, we can maximize the different relaxation times between tissues and generate very high tissue contrast, a hallmark of MR imaging.

There are two ways that the excited hydrogen nuclei relax back to equilibrium. First, the hydrogen nuclei can give up their energy to the lattice of tissue surrounding it. This is referred to as longitudinal relaxation, spin-lattice relaxation, or T1 relaxation, and is characterized by a constant known as the T1 relaxation time. The second refers to how the spins of the hydrogen nuclei de-phase with one another. When the nuclei are tipped into the transverse plane by the RF pulse, their spins are initially aligned. But, through interaction with other nuclei, the spins will de-phase with one another. This kind of relaxation is referred to as transverse relaxation, spin-spin relaxation, or T2 relaxation, and is characterized by a constant known as the T2 relaxation time.

Because the T1 and T2 relaxation times of tissue vary within the body, we can use sequence parameters such as the pulse repetition time (TR) and echo time (TE) to generate the contrast, or

weighting, of the MR image. For a T1-weighted image, a short TR and short TE result in a T1-weighted image, where the difference in contrast between tissues is primarily due to their different T1 relaxation times. For a T2-weighted image, a long TR and long TE produces a T2-weighted image, where the difference in contrast between tissues in the final image is due to their different T2 relaxation times.

1.1.3 MR Sequences and Signal Equations

One of the most basic MR sequence is a spin-echo. In this sequence, a 90-degree RF pulse selectively excites a thin region determined by the slice-selection gradient. This tips the net magnetization vector into the transverse plane with all the nuclei spins being in-phase. During this time, a phase-encoding gradient that is turned on and off spatially encodes phases in a direction orthogonal to the B_0 field. After a period of TE/2, a 180-degree RF pulse causes the spins which are dephasing start to rephase. At the total time of TE, a spin-echo occurs and is read out. This repeats after a time of TR for all necessary phase-encoding steps before moving on to the next slice.

The signal (S) that is produced by a spin-echo sequence at any voxel in the MR image is dependent on the proton density (ρ), machine parameters and gain (k), TR, TE, T1, and T2 of the tissue located within that voxel (*Equation 1.1*).[3]

$$S = k\rho\left(1 - e^{-TR/T1}\right)e^{-TE/T2} \qquad \textit{Equation 1.1}$$

This gives us a relationship that directly relates any signal intensity produced with either a T1- or T2-weighted MR image to its corresponding T1 or T2 relaxation time.

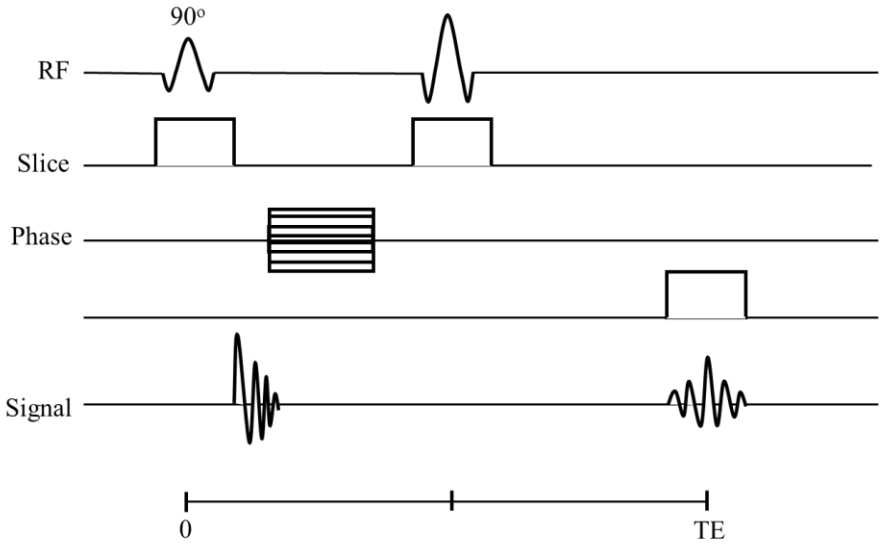

Figure 1.1: Pulse sequence diagram for a spin-echo MRI.

Of course, there are much more complicated MR sequences that do not have such a simplistic pulse sequence diagram and signal equation. A few of importance for the purposes of this thesis are the magnetization-prepared rapid gradient echo (MPRAGE), a 3-dimensional, usually T1-weighted sequences that uses a 180-degree inversion pulse followed by a rapid echo train readout with small flip angles (see *Figure 1.2*), and a fluid-attenuated inversion recovery (FLAIR), a T2-weighted sequence that uses a 180-degree inversion pulse strategically with the known relaxation time of fluid to remove any signal from fluid from the image.

1.1.4 MR Relaxometry

MR relaxometry is a broad term referring to the measurement of the relaxation variables of the tissue in MRI. There are three types of relaxation variables: T1, T2, and T2*. T1 and T2 have been discussed previously, and T2* relaxation is a combination of T2 relaxation (spin-spin) and the magnetic field inhomogeneities. For the purposes of this thesis, though, T2* relaxometry is not discussed in detail. It is important to note the differences between quantitative T1 and T2

(qT1/qT2), the actual measurement of the relaxation variables, and T1- and T2-weighted, the use of the differences in T1 and T2 to generate contrast in an MR image.

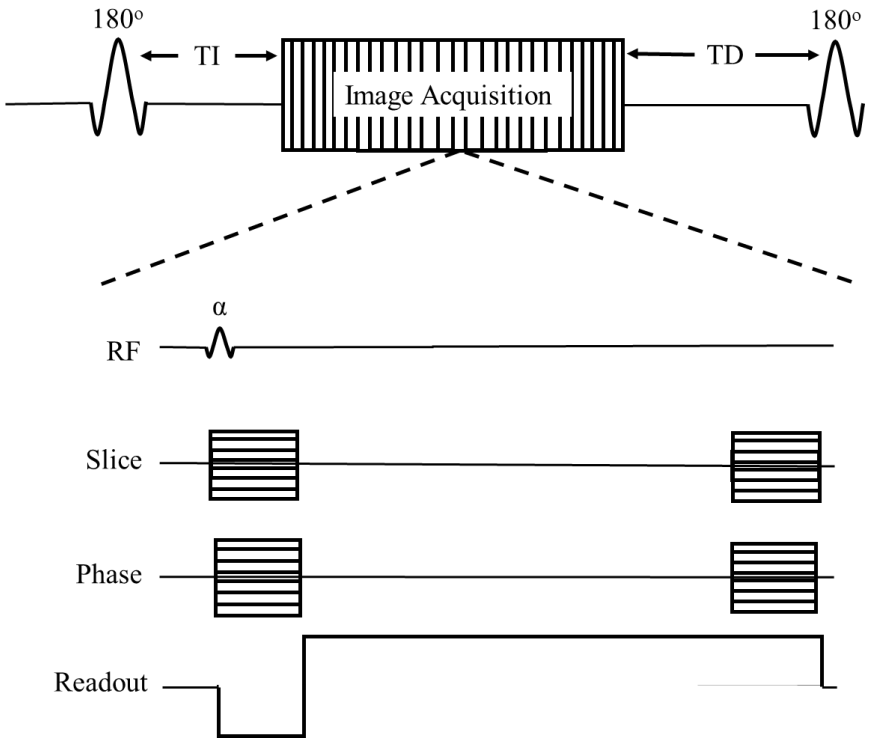

Figure 1.2: The pulse sequence diagram for MPRAGE MRI shows a much more complex acquisition.[4]

MR relaxometry is a very useful technique. By generating qT1 and qT2 images, there is no longer a dependence on machine parameters like gain, filters, TE, or TR; instead qT1 and qT2 maps are only dependent on the tissue properties located in each voxel. This can be advantageous when looking for both subtle differences in tissue pathophysiology, like finding regions of hypoxia in tumors or regions of demyelination in MS, and in large datasets, like trying to normalize MRIs across scanner vendors or different sequences.[5-12]

To create the qT1 and qT2 images, all variables in a specific sequence (and corresponding signal equation) are kept constant except for one. For each voxel, a fit can be applied using the signal intensity and dependent variable to solve for either T1 or T2. For the simplest case, a series of T1-weighted spin-echo images with varying TR allows for *Equation 1.2* to be solved for T1, and a series of T2-weighted spin-echo images with varying TE allows for *Equation 1.3* to be solved for T2. Another technique for calculating T1 involves the use of a series of T1-weighted inversion recovery (IR) images. This sequence involves a 180-degree RF inversion pulse, followed by a spin-echo sequence after some inversion time (TI). Instead of using *Equation 1.1* and varying TR under the assumption that there will be minimal T2 weighting, *Equation 1.2* can be used with the independent variable TI to generate a qT1 map.[3]

$$S = k\rho\left(1 - 2e^{-TI/T1}\right) \qquad \textit{Equation 1.2}$$

The methods mentioned above, however, take too much time to be run during a routine MRI exam of a patient. There are more complicated techniques that can be used to generate similar qT1 and qT2 maps much more quickly. One of these used to generate a qT1 maps is a Look-Locker technique. Developed for cardiac applications, the Look-Locker uses a 180-degree inversion pulse with a train of smaller RF pulses after a delay of TI followed by a readout to generate an image. TI is again varied, and *Equations 1.3-1.4* can be fit to calculate T1 from a voxel-wise fit.[13]

$$S = \mathrm{A} - \mathrm{B}e^{-TI/T1^*} \qquad \textit{Equation 1.3}$$

$$T1 = T1^*\left(\frac{B}{A} - 1\right) \qquad \textit{Equation 1.4}$$

For a quicker qT2 method, there are clinically available sequences that essentially run a series of T2-weighted images with multiple echoes. These multiple echoes occur at different TEs and can be fit as mentioned previously using *Equation 1.2* under the assumption that there will be minimal

T1 weighting.

In addition to these techniques, researchers have developed tools such as MR Fingerprinting (MRF) and synthetic MR for measurement of relaxation variables in clinically appropriate scan times.[14,15] These sequences use a combination of innovative pulse sequences and mathematical reconstructions to produce quantitative MR images, and synthetic MR can even generate weighted images with almost any desired contrast. However, these tools have not yet been integrated into clinical workflow.

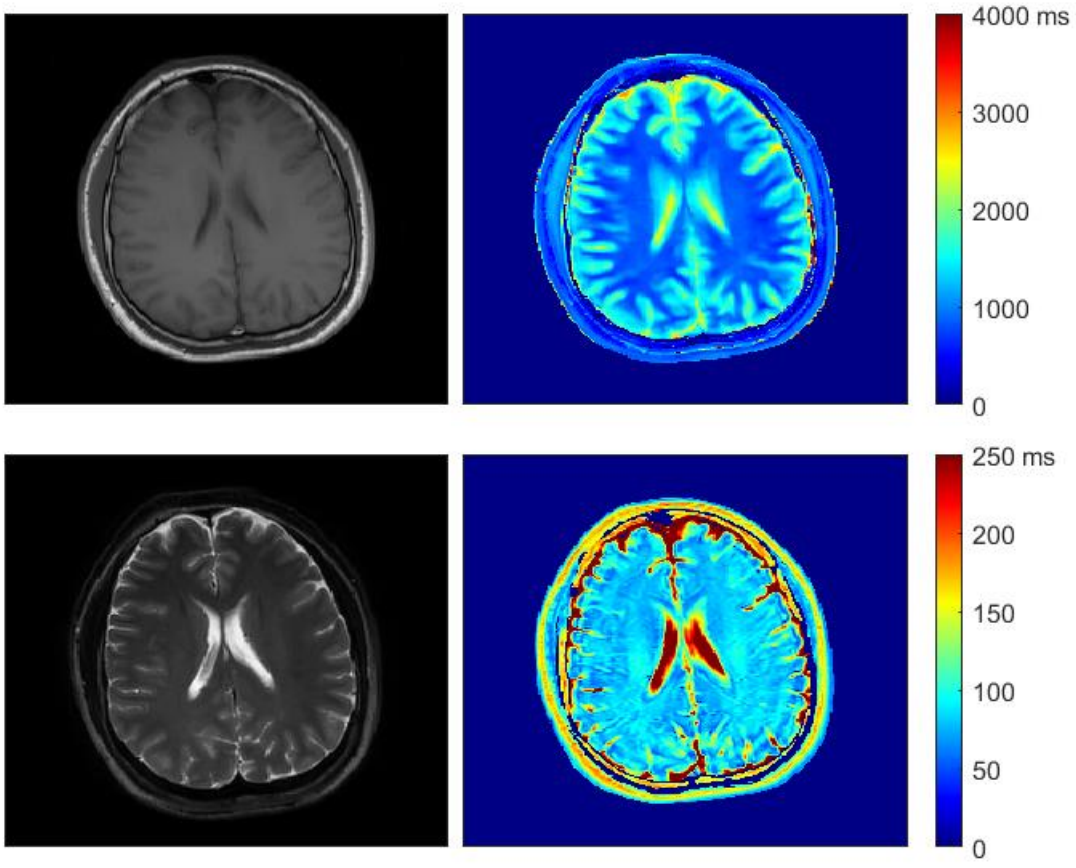

Figure 1.3: Example T1w image (top left), qT1 map (top right), T2w image (bottom left), and qT2 map (bottom right). All images are of the same subject and are approximately the same axial slice.

MR relaxometry is used in a variety of clinical applications, mostly on the research side as scientists try and uncover the relationships between quantitative MR maps and corresponding pathology. Such applications include cancer detection and progression, iron overload in tissue, MS, and aneurysms, to name a few. In addition, relaxometry is a perfect data normalizing method for big data and machine learning applications. Yet, there are few large datasets of relaxometry data that have been taken.

1.2 Introduction to MS

1.2.1 Pathology of MS

MS is a chronic neuroinflammatory disease of the central nervous system (CNS) characterized by the focal demyelination of axons into "lesions" or "plaques" in white matter, along with a more diffuse demyelination throughout the CNS. More specifically, MS is an autoimmune disease resulting from the loss of oligodendrocytes that form the myelin sheath around axons. This myelin sheath helps carry action potentials quickly through the CNS by reducing the capacitance of the axonal membrane, resulting in saltatory conduction and the "jumping" of the action potential down the length of the axon. In MS, an inflammatory process caused by T cells enter the brain via disruptions in the blood-brain barrier (BBB) and recognize myelin as foreign, thereby promoting an inflammatory response. Without myelin, the neuron is unable to function properly. Remyelination can occur early in the disease but is often unable to be completed fully. Repeated attacks by the immune system lead to the build-up of a scar-like plaque (hence the name sclerosis). This can occur throughout the CNS, often involving both the brain and spinal cord.[16-22]

Because of the interruption in the CNS signaling pathway, patients with MS can have a variety of clinical disabilities, including autonomic, visual, motor, and sensory symptoms. There

is no known cause for MS, but a multifactorial etiology is generally accepted involving both a genetic component and environmental factors such as the Epstein-Barr virus and vitamin D. The global prevalence of MS is 33 per 100,000 people, although there is a great variance between different regions, especially different longitudes. MS primarily affects people between the ages of 20-40 years, with a 3:1 female-to-male predominance.[16-18, 22-23]

1.2.2 Clinical Presentation and Progression of MS

The range of clinical symptoms that MS patients can experience is vast and includes pain, cognitive dysfunction, gait ataxia, and vision or sensory loss.[24,25] However, the hallmark of a MS diagnosis is the dual criteria of dissemination of time and space. For clinical symptoms, this would be marked by symptoms lasting longer than 24 hours and occurring in two separate anatomical locations at two distinct times, e.g. vision loss in one eye followed by a constant tingling in the right hand a month later. Without those two criteria fulfilled, MS cannot be diagnosed.

There are four MS disease courses that have been classified based on symptom onset and evolution: clinically isolated syndrome (CIS), relapsing-remitting MS (RRMS), secondary-progressive MS (SPMS), and primary-progressive MS (PPMS). To quantify the evolution of these clinical symptoms as MS progresses, neurologists developed the Expanded Disability Status Scale (EDSS) ranging from 1 (normal neurological exam) to 10 (death due to MS), although the accuracy of the EDSS is disputed due to its over-reliance on motor function and subjective nature.

CIS refers to the first clinical manifestation of the disease that is, as stated in the name, isolated by definition. CIS may relapse in the same anatomic location over time as well. Although the criteria for diagnosis of MS is not fully met by CIS, it is considered a subclass of MS, as CIS will lead to a MS diagnosis 80% of the time when lesions are present on the initial baseline MRI and 10-20% when lesions are not present.

RRMS is the initial diagnosis of about 85% of patients with MS. The RRMS phenotype is characterized by relapses of acute neurological symptoms followed by a period of recovery before repeating. This recovery period may lead to a complete return to the baseline before the relapse or could result in a partial remission and permanent accumulation of some disability with irreversible CNS damage.

SPMS, often evolving from RRMS, consists of the progressive worsening of neurologic symptoms (mainly gait impairment) over time with or without distinct relapses. About 80% of RRMS patients will evolve into some form of SPMS withing 20 years.

Finally, PPMS, consisting of about 15% of initial MS diagnoses, is characterized by the progressive worsening of neurologic symptoms from the onset of initial symptoms. Much like SPMS, there can be periods of relapses and remission, but there is the constant progression of symptoms over time.[16-18,24-28]

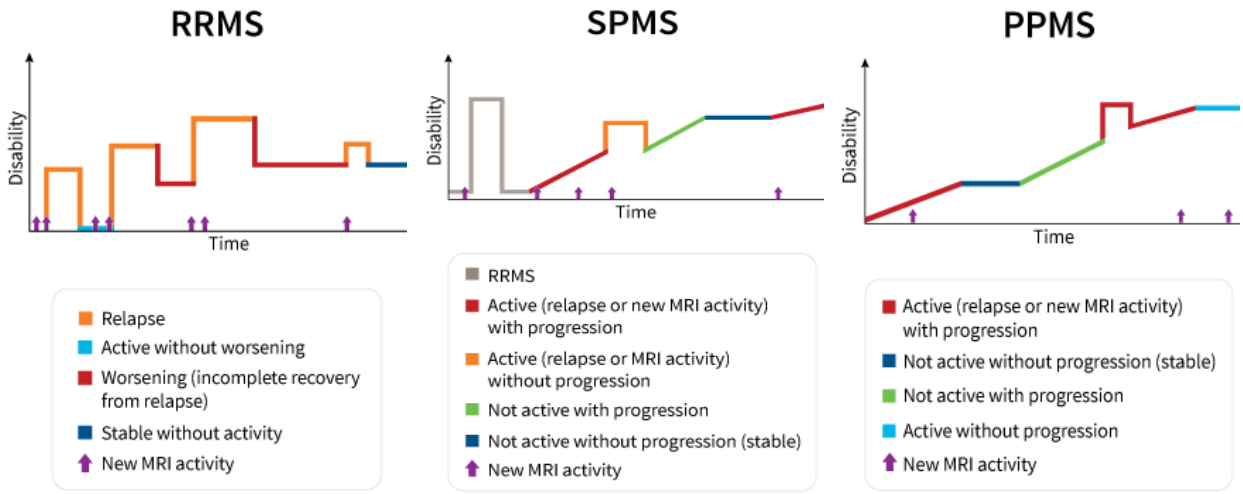

Figure 1.4: Varying clinical progression of different types of MS over time.[29]

Because the clinical course of MS is so widely varied from patient to patient, it can be difficult to predict when relapses will occur, whether they will result in an accumulation of disability, and whether a specific treatment is effective or if normal remission is occurring.

1.2.3 Role of MRI in MS

The first documented usage of MRI to evaluate MS lesions occurred in 1981 by Young *et al* and has since been a staple for the assessment of disease diagnosis, monitoring, and progression.[30] The McDonald Criteria, developed in 2001 by neurologist Ian McDonald and colleagues, incorporates clinical evaluation with MRI techniques to establish MS.[31-32] The Criteria, last updated in 2017, provides an outline for MS diagnosis based on clinical presentation, radiological findings, and laboratory tests that allows for the fulfillment of both the dissemination of space and time requirements. For example, if a patient has clinical presentation of two or more attacks and clinical evidence of one lesion, the dissemination of space criteria can be satisfied by either an additional clinical attack implicating a different CNS site or one or more MS-typical T2 lesions in two or more areas of the CNS.

Besides the diagnosis of the disease, MRI is typically used regularly to monitor and evaluate MS patient both on and off treatment. The most recent guidelines, published via a consensus of experts in the imaging of MS, call for routine MRI scanning at least once a year, with duration between consecutive scans varying depending on what treatment, if any, the patient is using.[33] Commonly used sequences on these monitoring scans tend to focus on the brain instead of the spinal cord and include a 3D FLAIR, MPRAGE, T2-weighted sequences, and T1-weighted sequences pre- and post-injection of gadolinium contrast agent, which shortens the T1 relaxation time in areas where there is active inflammation.

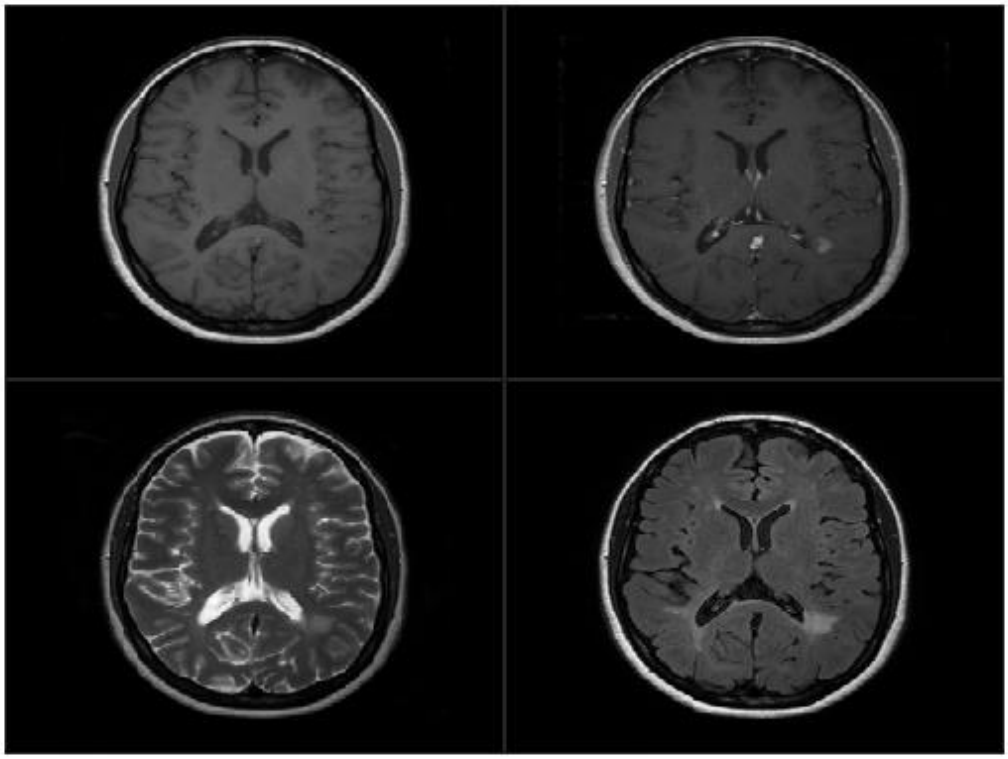

Figure 1.5: Example MRIs of subject with MS showing the varying contrasts between T1w pre-contrast (top left), T1w post-contrast (top right), T2w (bottom left), and FLAIR (bottom right).

1.2.4 Role of Quantitative MRI in MS

Much work has been done to assess disease progression of MS including clinical, laboratory, and radiological measures. Currently, the most widely used clinical assessment of clinical disease progression is the EDSS, which measures 7 functional scores related to neurological performance on ex-amination and is a global score. However, EDSS has been shown to have high interobserver variability.[34] MRI, by far the best biomarker of disease activity, provides a wide range of image contrasts (T1, gadolinium-enhanced T1, T2, susceptibility weighted, MTR, quantitative susceptibility mapping (QSM)) each reflecting a different pathophysiologic signature: loss of myelin/axons/gliosis, acute inflammation breakdown of the blood-brain barrier, total volume of tissue injury, myelin density, and the combination of iron deposition in activated

macrophages and chronic inflammation. Thus, MRI could provide an objective measure of disease progression in MS.

Many studies have correlated various MRI markers of disease activity to clinical measures of disease progression. Such studies have included correlating the number of T1 contrast-enhancing lesions, hypo- or hyper-intense lesions, and the magnetization transfer ratio (MTR) to EDSS scores.[35-44] More recently, assessment of brain atrophy has become an important marker of MS disease progression. Brain atrophy occurs in normal aging population but is enhanced two- to three-fold in MS, even at early stages of MS. Brain atrophy is not only correlated with EDSS but also several measures of cognitive disability.[45-46] The correlations of MRI measures of disease activity to clinical scores of disease progression have been at best moderate, furthering the notion that MS is a 'clinico-radiological paradox' where disease seen radiologically is not necessarily captured on clinical exams of disability.[47]

Previous studies have shown that MRI relaxometry (T1, T2, T2*) correlates well with histopathology, which is expected as tissue relaxation times change when tissue microstructure changes (such as demyelination or inflammation).[48-53] However, few have shown that relaxometry changes can be correlated with disability. Manfredonia et al found that normal-appearing brain T1 relaxation times can predict disability in early primary-progressive MS.[54] This study provides evidence for the hypothesis that cerebral MR relaxometry can be correlated and predictive of disability of MS patients, and can potentially be used to quantify treatment response. It reasons that MR relaxometry may be used in combination with other geometric- and intensity-based features previously described in the literature for improved analysis of MS patients. In turn, relaxometry can also be thought of as a standardizing metric, providing further argument of the use of quantitative MR maps as input to classification algorithms instead of weighted images.

1.3 Machine Learning

In recent years, machine learning has been a topic of increasing interest as the collection of large datasets and the development of more powerful computers and algorithms to analyze those datasets have become prevalent. Using these large datasets and improved computational efficacy, statistical models can be derived and applied to aid physicians with their normal tasks (such as computer-aided detection of lesions) or augment the physician's knowledge where they have limited success (such as computer-aided diagnosis of malignancy). Combining trained machine learning algorithms with the expertise of physicians can lead to fewer mistakes or misinterpretations of information.

There are two broad categories of machine learning algorithms, supervised and unsupervised. Supervised learning requires a dataset that is annotated with the ground truth, like malignancy versus non-malignancy. One can then train a machine learning algorithm with the annotated dataset and then apply on non-annotated datasets for prediction. Supervised machine learning models are often used in the case of medical imaging, as a radiologist (or multiple radiologists) has previously read the image and made a diagnosis. In contrast, unsupervised learning does not require annotated data for training, and instead uses inherent differences between subsets of data to develop its predictive model.[55-57]

To further complicate the matter, there are another two broad categories that machine learning algorithms can be separated into, classification and regression. Classification algorithms are those whose desired output is a class label. For example, the determination of malignancy versus benign tumors would be a classification task. This can be expanded to more than just two classes, such as assigning labels to handwritten numbers and letters. Most regression algorithms, on the other hand, predict a numerical label from a continuous spectrum. An example of where a

regression algorithm is useful could be by predicting housing prices based on the neighborhood and features of the house. The outlier of regression algorithms is logistic regression for classification of only two classes, where each class is assigned either a 0 or 1 during training and a logarithmic curve is fit using the desired features. This produces a curve that is continuous, but thresholds can be applied to discriminate between the two classes.[55-57]

There are also a range of complexities of machine learning algorithms to choose from depending on your application. Linear regression can be considered a machine learning technique, as it uses acquired data to form a linear model that can then be used to predict an outcome. This is a simplistic model, however, and may have little-to-no practical use in the case of medical imaging. Moving up in complexity, linear discriminant analysis (LDA) can be used to separate subsets of data for classification purposes. If, for example, we wanted to find the optimal separation of lesions that were either malignant or non-malignant using features extracted from those lesions, LDA may be an appropriate choice. However, LDA can be susceptible to outliers and can only generate a linear classifier, making its utility limited for medical imaging. Moving to the more complex algorithms, convolutional and deep neural networks use interconnected layers to complete some tasks. For the purposes of this thesis, only simple classification algorithms, such as logistic regression, will be used.

1.4 Research Objectives and Scope of Thesis

Currently, relaxometry is not clinically relevant for most scenarios, including for MS. This is because there is no defined benefit for radiologists and other clinicians. Because of this, there are limited datasets that are available to have quantitative MR maps included. For applications such

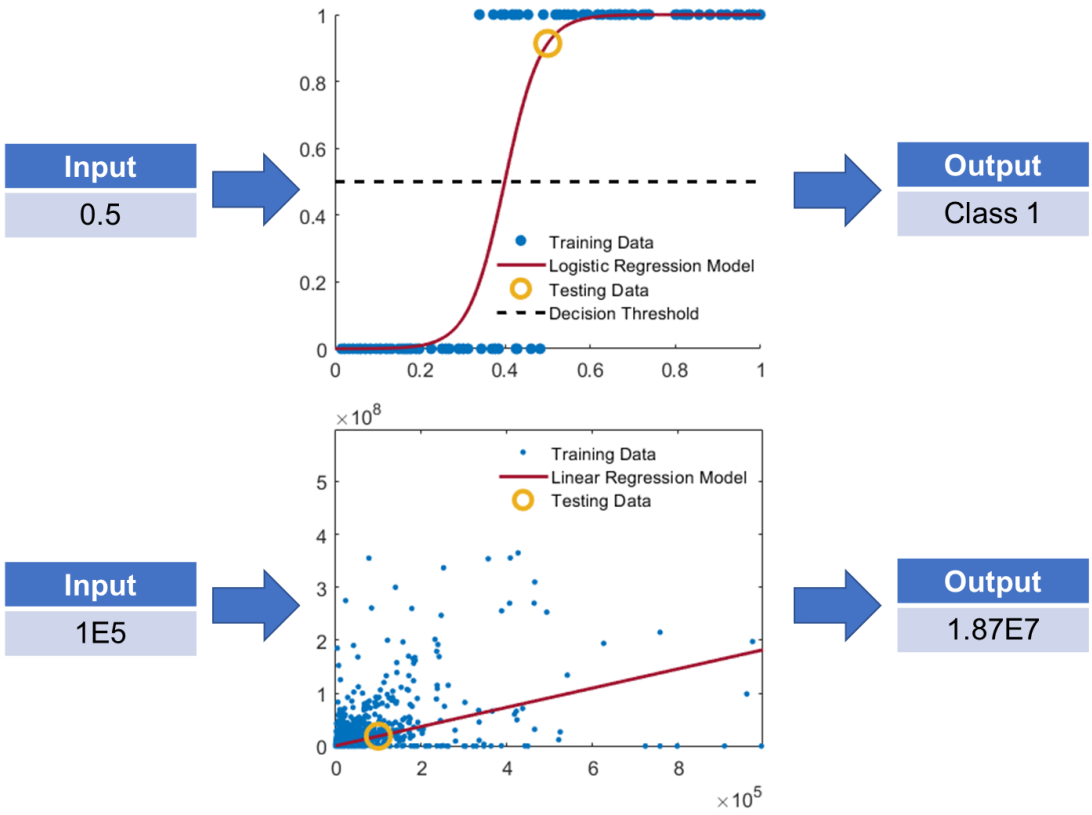

Figure 1.6: Example of logistic regression as a classification algorithm (top) and linear regression as a continuous prediction algorithm.

as machine learning, this can potentially be problematic, as weighted MR images can vary drastically depending on the sequence run and the scan parameters. Therefore, it would be beneficial to have a methodology that uses weighted MR scans to artificially generate estimates of quantitative MR maps for analysis. By doing this, we can use previously acquired weighted datasets for quantitative MR research without adding any additional scans to clinicians' workflow.

Chapter 2 of this dissertation will provide an overview of the proposed algorithm to retrospectively quantify weighted MR images into estimated MR maps. A further discussion into the important physics and mathematics of the algorithm, referred to as the REtrospecitve Quantification Using Internal REferences (REQUIRE) algorithm, will be discussed to provide a

better understanding and overview of both the theory behind the algorithm and the actual implementation of the REQUIRE algorithm.

Chapter 3 will discuss the application of the REQUIRE algorithm to the most basic scenario: a weighted, spin-echo MR image. Computer simulations on digital phantoms will allow for a better understanding of potential pitfalls of the methodology. In addition, phantom studies using a dual T1/T2 phantom will be discussed, along with a healthy volunteer study to determine the applicability of this method *in vivo*.

Chapter 4 will be the continuation of the method described in Chapter 3. However, the application will be on more complicated weighted MR sequences to ensure that the REQUIRE algorithm is translatable across whatever MR sequence is run. The results are presented and compared with the reference standard, as well as with the results in Chapter 3.

Chapter 5 is the application of this REQUIRE with real world data involving patients with MS. The datasets acquired were taken at different times and with different parameters and sequences, providing an opportunity to test the developed methodology and apply it to a problem with a potential machine learning application. For this thesis, the chosen problem was predicting what MS lesions would enhance (or are actively inflaming) by using only features derived from T1-weighted pre-contrast MR images and their corresponding estimated T1 maps. Chapter 5 will also discuss the issues with gadolinium contrast deposition in the brain, and why this is a source of concern for patients with MS.

Finally, Chapter 6 will summarize the results of this dissertation and provide guidelines for future endeavors into related research topics.

CHAPTER 2

OVERVIEW OF REQUIRE ALGORITHM

This section will be dedicated to a general overview of the REQUIRE algorithm, specifically focusing on the two sequences highlighted in Chapters 3 and 4 of this dissertation. An overview of the theory behind the REQUIRE algorithm will be discussed before more specifics on the signal equations and derivations are given. The implementation of the algorithm will also be discussed, as the REQUIRE algorithm must be adjusted from an analytical solution for simple MR sequences to an iterative solution for more complicated MR sequences.

2.1 Theory

As described in Chapter 1, there are a multitude of ways to generate an MR signal that can be transformed into an image (T1- versus T2-weighted, 2D versus 3D images, etc). However, all have the following in common: inherent microstructural and physiological differences in tissue (i.e. white matter versus gray matter) are used to generate contrast in an MR image. This means, for example, that to generate a T1-weighted image, the contrast is due to primarily the differences in T1 relaxation times between tissues. Additionally, because the entire MR image was acquired using the same sequence and parameters, the difference in signal intensities must be only from the differences in the inherent tissue properties themselves. Therefore, it should be feasible, if we have an appropriate model of the signal in an MR image and references in the image, to calculate these tissue properties for each voxel of the image. This is the basis of the REQUIRE algorithm. In the next few sections, more details will be provided into how this process unfolds for two scenarios: a T1-weighted spin-echo image of the brain and an MPRAGE MR image of the brain.

2.1.1 T1-weighted Spin-Echo

As given in Chapter 1 via *Equation 1.1*, the theoretical signal equation of a T1-weighted spin-echo MR image is as follows:

$$S = k\rho\left(1 - e^{-TR/T1}\right)e^{-TE/T2} \qquad \textit{Equation 2.1}$$

where S is the signal intensity, k is comprised of various scanner settings such as ADC gain, ρ is the proton density, TR is the repetition time, T1 is the T1 relaxation time, TE is the echo time, and T2 is the T2 relaxation time.[3] Inverting this equation and solving for T1, which is the primary goal of this portion of the thesis, we find the following:

$$T1 = \frac{-TR}{\log\left(1 - \frac{Se^{TE/T2}}{k\rho}\right)} \qquad \textit{Equation 2.2}$$

This equation shows how the T1 value of each voxel of the image varies with the signal intensity of the image. However, although the TR and TE are fixed imaging parameters, there are still four unknowns in the equation: T1 (what we're trying to solve for in this instance), T2, k, and ρ. Two of those can be estimated by reference values in the literature. If we know, for example, a voxel is comprised of primarily gray matter, we can assign a T2 and ρ value for that specific voxel. After this occurs, now only two unknowns remain, T1 and k. Much like with the T2 and ρ assumptions, we can again make another assumption, this time about T1. If we accept that the T1 relaxation time of a specific tissue type as found in the literature is correct on average, we can then solve for k. So, for the instance of the brain, if we compute the average signal intensity across three different healthy tissue types (gray matter, white matter, and cerebrospinal fluid) and set their corresponding T1 values to those found in the literature, it is possible to estimate k and then have an equation that relates any S to a corresponding T1 relaxation time in the image.

2.1.2 MPRAGE

Unlike the T1-weighted spin-echo image, MPRAGE is a much more complicated MR sequence. Because of that, there is no compact analytical signal equation and corresponding inversion to said signal equation. Instead, a step-by-step iterative solution can be used to estimate the signal intensity at each T1 value, compare that to the actual average signal intensities of healthy tissues in the image, and then iterate until it converges on the best possibly solution. To do this, however, some sort of signal equation is required to estimate signal intensity. Luckily, the one described by Brant-Zawadzki *et al* is a good approximation. Those equations are given as follows:

$$S_N = M_N e^{-TE/T2^*} \qquad \textit{Equation 2.3a}$$

$$M_N = M_0\left(1 - e^{-TR/T1}\right)\sum_{i=0}^{\frac{N}{2}-2}\left(cos\alpha \cdot e^{-TR/T1}\right)^i + M_0\left(1 - e^{-TR/T1}\right) + M_{eq} \cdot e^{TI/T1}\left(cos\alpha \cdot e^{-TR/T1}\right)^{\frac{N}{2}-1} \qquad \textit{Equation 2.3b}$$

$$M_{eq} = \frac{1}{1 - X \cdot e^{-T_{rec}/T1}} \cdot M_0\left(1 - e^{-T_{rec}/T1}\right) \qquad \textit{Equation 2.3c}$$

$$X = \left(1 - e^{-TR/T1}\right)\sum_{i=0}^{\frac{N}{2}-2}\left(cos\alpha \cdot e^{-TR/T1}\right)^i + \left(1 - 2e^{-TI/T1}\right)\left(cos\alpha \cdot e^{-TR/T1}\right)^{\frac{N}{2}-1} \qquad \textit{Equation 2.3d}$$

In *Equations 2.3a-d*, S_N is the signal at the N^{th} phase encoding step, M_N is the magnetization at the N^{th} phase encoding step, α is the flip angle, M_{eq} is the equilibrium magnetization, TI is the inversion time, T_{rec} is the recovery period after readout until the next inversion, and X is the fraction

remaining as a result of small-angle excitation. For our purposes, the signal decay due to $T2^*$ effects was ignored, as they would be small due to the small TE of the sequence.[58]

Using *Equations 2.3a-d*, it is possible to estimate the signal intensity for the T1s of the healthy reference tissues (again, gray matter, white matter, and cerebrospinal fluid). An initial guess of M_0 can be given, the error between the actual signal intensity and the theoretical signal intensity calculated, and then a new value assigned for M_0. This can occur until a certain threshold is achieved, whatever that may be, and then the signal intensity for each T1 can be calculated. In this way, an estimated T1 map can be generated from the MPRAGE image.

2.2 Algorithm Implementation

Ideally, for both implementations of the T1-REQUIRE algorithm described above, an analytical solution could be used. However, due to the complexity of MPRAGE, this is not possible. This section will walk step-by-step through the implementation of the algorithm in MATLAB for both the T1-weighted spin-echo and MPRAGE. Due to the similarities of some portions, steps that are individual to one or the other will be noted in the subsection heading; otherwise, that subsection will be describing a step that is shared by the two implementations.

2.2.1 Conversion to NIFTI Format

To begin, all images were converted to NIfTI file format from either DICOM or PAR/REC file formats. This was done so that the images could be easily imported into both MATLAB and used by Statistical Parameter Mapping version 12 (SPM12 - Wellcome Centre for Human Neuroimaging, University College London, UK), a toolbox developed specifically for MATLAB and originally applied to functional neuroimaging data. To do this, the tool developed by Xiangrui

Li called dicm2nii was used. This set of MATLAB functions, useful on both DICOMs and PAR/RECs, was used to convert all the images in whichever dataset we were interested into the NIfTI file format.

2.2.2 Segmentation via SPM12

After the images are converted to NIfTI format, they can be manipulated in MATLAB using the functions included in the SPM12 toolbox. One of these functions is the brain segmentation function. The point of it is to take an MRI of the brain and segment out different tissue types. SPM12 does this in four steps. First, a bias correction algorithm is run on the MR image that removes the spatially varying artifact often present in MR images. Second, the corrected MR image is spatially warped onto a reference tissue probability map. This tissue probability map consists of spatial probabilities that a specific type of tissue occurs in a specific area. Third, SPM12 uses these spatial probabilities along with intensity-based information within the image to generate a tissue probability map for that MR image, but still warped to the reference space. By incorporating both spatial and intensity information, the segmentation returns accurate results, even if there is evidence of disease (such as intensity loss in T1-weighted images due to demyelination). Finally, the calculated tissue probability map is returned to the original image space for use within the REQUIRE algorithm.

For the purposes of the REQUIRE algorithm, three of the six default healthy tissue segmentations are used: white matter, gray matter, and cerebrospinal fluid. The other three (bone, soft tissue, and air/background) are not useful for the purposes of the algorithm. SPM12 returns these tissue probability maps as NIfTI files to be imported and manipulated by both SPM12 and MATLAB.

2.2.3 Skull Stripping

Once the segmentation was completed, the brain was then segmented away from the soft tissue and skull using the tissue probability maps produced in the previous section. To do this, the white matter, gray matter, and cerebrospinal fluid segmentations were added together, each with a threshold applied such that only voxels with a probability that it belonged to one of those tissue types had to exceed 0.8. Once the three tissue types were added, the resulting mask was dilated, filled, and then eroded, with the element used for both the dilation and erosion being equivalent. This generated a brain mask that was then applied to the MR image to produce an MR image of only the brain.

2.2.4 Proton Density/T2 Correction for Spin-Echo

For the case of the T1-weighted spin-echo images, we found that including both a proton density and T2 correction to estimate T1 produced the most accurate qT1 maps.. To do this, the healthy tissue segmentations (gray matter, white matter, and cerebrospinal fluid) were all assigned a T2 value and proton density value based off previously acquired values found in the literature (*Table 2.1*).[59-62] The term $\frac{e^{TE/T2}}{\rho}$ from *Equation 2.4* was then calculated for each voxel. However, this produced harsh gradients at points where the tissue segmentation changes, so a gaussian smoothing filter was applied to generate a smooth estimation of the dual proton density/T2 correction. The original T1-weighted spin-echo image was then multiplied by this correction, generating an image that is, theoretically, only dependent on T1.

$$\frac{Se^{TE/T2}}{\rho} = S_{T1} = k\left(1 - e^{-TR/T1}\right) \qquad \textit{Equation 2.4}$$

Table 2.1: Healthy Brain Tissue T2 and ρ Values at 3T		
Tissue Type	**T2 Relaxation Time ± σ (ms)**	**ρ ± σ (Relative to H_2O)**
Gray Matter	110 ± 8.7	.807 ± 0.0160
White Matter	79.6 ± 2.6	.679 ± 0.0168
Cerebrospinal Fluid*	1447 ± 52	1
*Note: The T2 of cerebrospinal fluid was so long compared to TE values for T1-weighted spin-echo images, as well as compared to the other tissue types, that no T2 effects were accounted for in the cerebrospinal fluid		

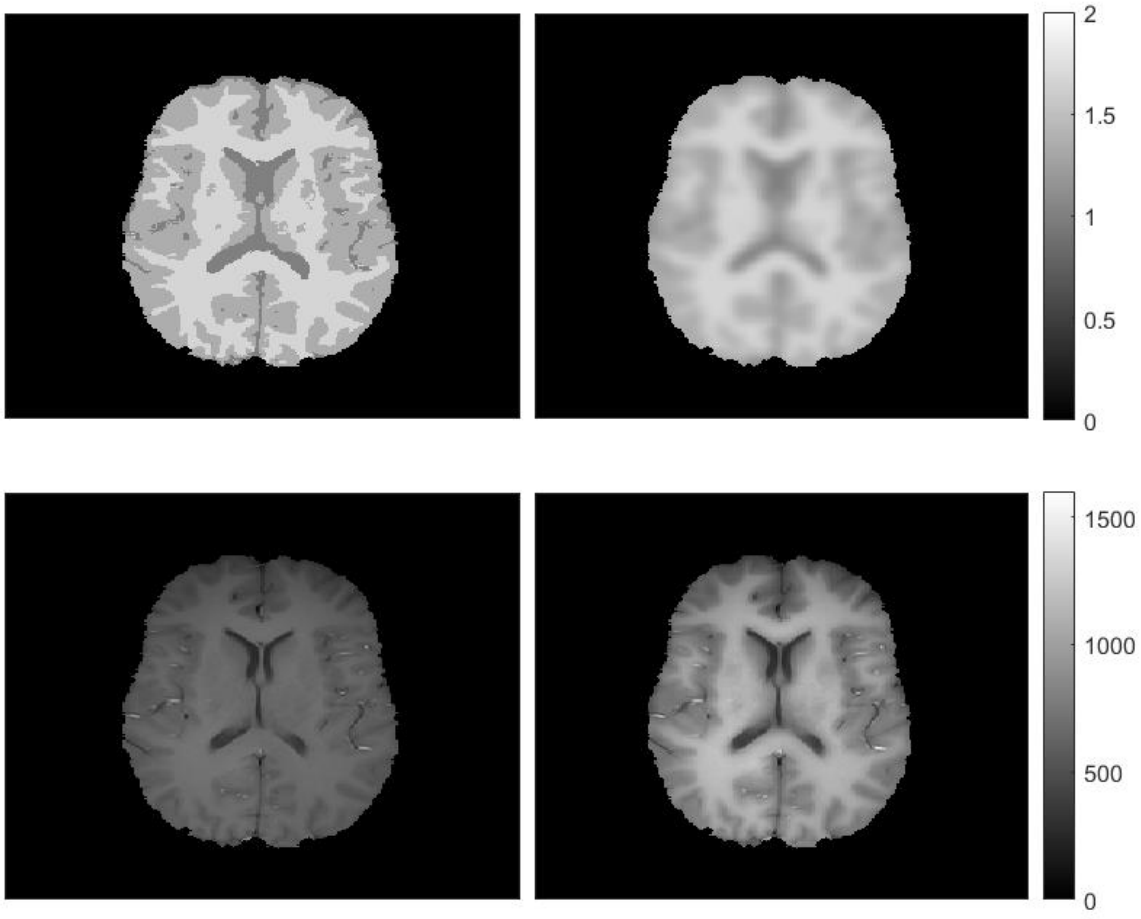

Figure 2.1: Proton density correction before (top left) and after (top right) Gaussian filter applied. T1-weighted spin-echo MR image before (bottom left) and after (bottom right) T2/PD correction applied.

2.2.5 Solving the Spin-Echo Signal Equation

Once the dual proton density/T2 correction was applied to the T1-weighted spin-echo image, the resulting image should be one that, if the scanner settings *k* is consistent, is only affected by varying T1 values. So, to solve for *k* so that we can relate any signal intensity in the corrected image to a corresponding T1 value, internal references were used.

To do this, the average intensity values for our three healthy tissues (gray matter, white matter, and cerebrospinal fluid) were calculated from the tissue probability maps and the weighted images. Because this needs to be more precise, a threshold of 0.9 was applied to determine which voxels were included in this calculation. Once these average signal intensities were calculated, a non-linear curve fit was applied in MATLAB using *Equation 2.4,* the average signal intensities, and reference values for T1 of healthy gray matter, white matter, and cerebrospinal fluid found in the literature (*Table 2.2*).[59-61] This non-linear curve fitting was completed using a least-squares optimization method to solve for *k.* After this is solved for, *Equation 2.4* was manipulated such that the entire corrected image could be manipulated to solve for T1 at each voxel. Because this process does not use a voxel-by-voxel fit, it is incredibly efficient, reducing computation times by over 100x compared to a reference standard T1 mapping algorithm.

Table 2.2: Healthy Brain Tissue T1 Values at 3T

Tissue Type	T1 Relaxation Time ± σ (ms)
Gray Matter	1331 ± 57
White Matter	832 ± 44
Cerebrospinal Fluid*	2500

*Note: The T1 of cerebrospinal fluid was set to 2500 to increase contrast between gray and white matter. Literature values ranged from 2000 to over 4000 ms.

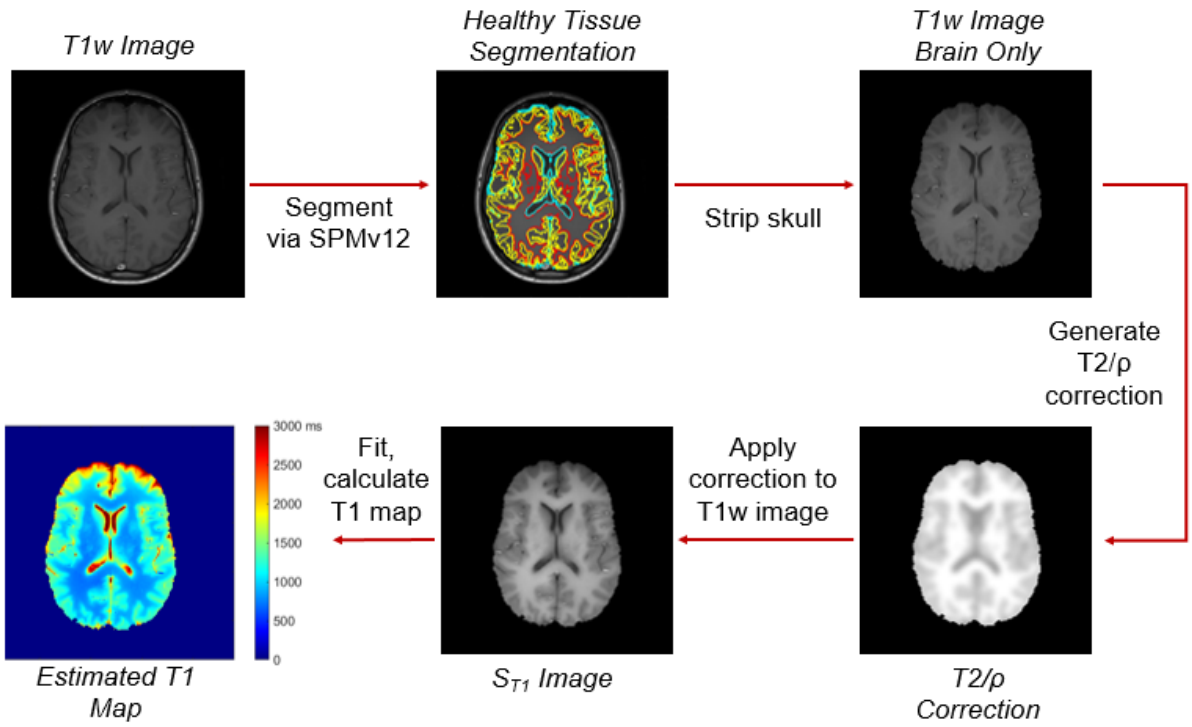

Figure 2.2: Flowchart of T1-REQUIRE algorithm for a spin-echo MRI.

2.2.6 Simulating the MPRAGE Signal Equation

Compared with the spin-echo MR sequence, MPRAGE is a much more complicated MR sequence, and likewise, has a much more complicated signal equation. Instead of solving the signal equation directly, though, it is possible to iteratively estimate the unknown parameter M_0 by guessing an initial value and minimizing the error between the estimated and actual values.

To do this, much like with the spin-echo case, the average intensity values of gray matter, white matter, and cerebrospinal fluid were calculated, and they were assigned a T1 value from the literature. From there, a set of M_0 values are calculate by equally spacing 100 steps between 0 and ten times the maximum signal intensity in the image. Iterating through those 100 steps, the MPRAGE signal equations, *Equations 2.3a-d*, are used to calculate the estimated signal intensity of the three tissue types. These values are compared with the actual signal intensities, and the root

mean square error (RMSE) is calculated. Using the RMSE, the minimum error is found. Then, using the M_0 values one index above and below that, the process is repeated. This continues until the step size between consecutive steps in the range of M_0 is less than 0.1% of the maximum MPRAGE image intensity. This gives us our M_0 value which then can be used to solve the MPRAGE equations. This allows for the generation of a lookup table for T1 values ranging from 10-3000 ms, which can be used to assign a T1 value for every signal intensity in the image.

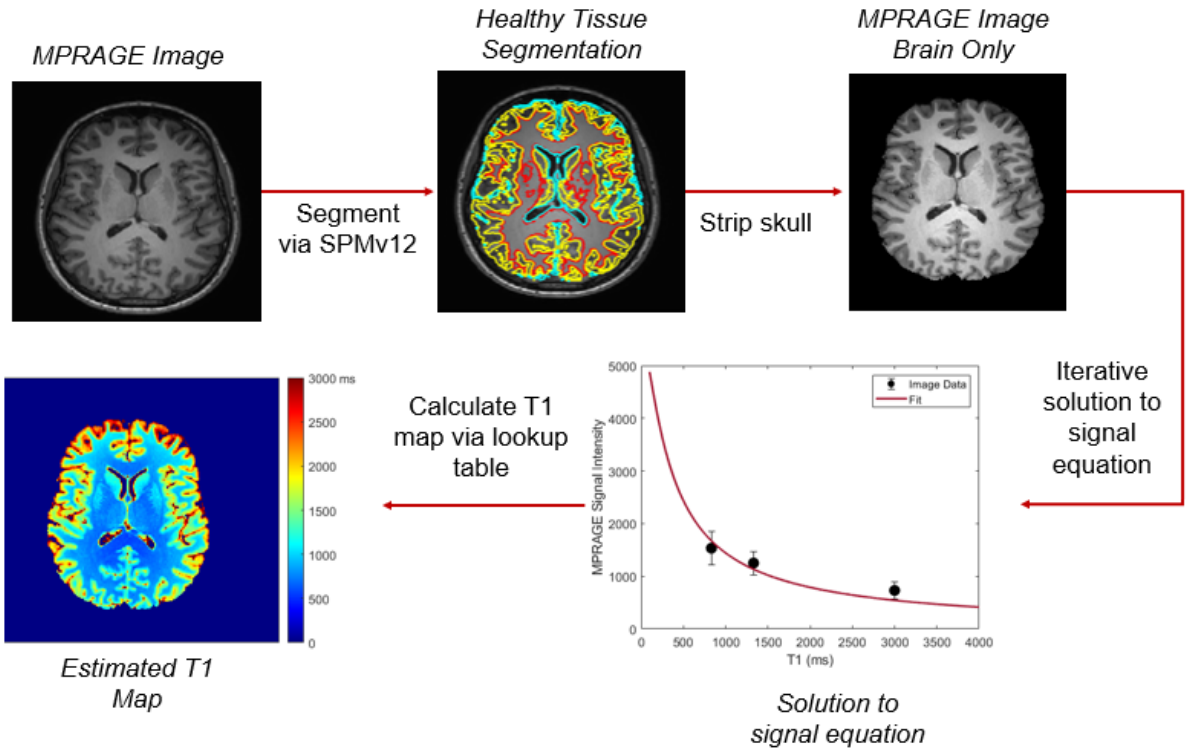

Figure 2.3: Flowchart of T1-REQUIRE algorithm for an MPRAGE MRI.

2.3 Discussion

The above chapter described two different implementations of the T1-REQUIRE algorithm. However, because the algorithm is entirely self-sufficient, relying only on the input of a T1-weighted MR image and the scan parameters surrounding that image, this algorithm should be able to be extended to any T1-weighted MR sequence with a defined signal equation or

approximation of the signal equation, as well as potentially being extended to include T2 and other weightings of MR images. That being said, the scope of this dissertation will include only T1-weighted MR images taken by either a spin-echo or an MPRAGE sequence. In the following chapters (Chapters 3 and 4), the results of applying the T1-REQUIRE algorithm on digital phantoms, physical phantoms, and healthy volunteers will be discussed. In Chapter 5, the utility of the T1-REQUIRE algorithm will be explored in the setting of MS.

CHAPTER 3

VALIDATION OF T1-REQUIRE ON T1-WEIGHTED SPIN-ECHO MR IMAGES

This chapter will introduce the validation process of T1-REQUIRE on T1w spin-echo MR images. For clarity, it will be organized as follows: the introduction, digital simulation methods followed by the results of the simulation, construction and scanning of a dual T1/T2 phantom and the results of that experiment, and finally the healthy volunteer study methods followed by the results. All of this will be followed by an overall discussion of this chapter as a whole.

3.1 Introduction

Quantification in MR is a normalization procedure performed to remove the mechanical and environmental properties embedded into the MR signal by the imaging process and retain only the tissue property that the signal contrast is dependent on, e.g. the T1 (spin-lattice) or T2 (spin-spin) relaxation times. By successfully quantifying these, along with other tissue properties not pertaining to this study, researchers and clinicians can both compare MR information from scans take with different imaging systems or imaging parameters, as well as relate these properties to the underlying tissue structure and function to potentially find imaging biomarkers of underlying physiological processes. However, current quantification techniques are slow and have poor resolution, thus limiting clinicians to only taking quantifiable data in cases where it has previously been shown to add important information for diagnosis or management of treatment.

The REQUIRE algorithm described in Chapter 2 of this dissertation is a novel attempt to solve those issues. By using the signal equations of commonly used MR sequences and healthy tissue as reference, it may be possible to remove those mechanical and environmental properties and efficiently estimate the tissue properties. This can result in a quantitative MR map that retains

the same resolution as the original MR scan with no additional scan time, essential for leaving the clinical workflow uninterrupted.

To ensure that the REQUIRE algorithm is performing at an acceptable level, it is necessary to validate the algorithm. To do this, we will begin with the simplest MR imaging sequence, a spin-echo. Specifically, this chapter focuses on a T1-weighted spin-echo, as T1-weighted MR imaging is key for the work completed in Chapter 5. Validation was completed in three different ways. First, digital simulations were used to explore the potential viability of the algorithm as a whole, along with determining the effect that assumptions may have on the overall performance of T1-REQUIRE. Second, a combined T1/T2 phantom was built and scanned to determine the accuracy of T1-REQUIRE as it compares to reference standard T1 mapping sequences, along with a comparison between T1 mapping sequences themselves. Finally, a healthy volunteer study determined the ability for T1-REQUIRE to be used *in vivo* in a controlled setting, and a range of T1 values that it would be valid in was quantified.

3.2 Digital Simulation

3.2.1 Digital Phantom Construction

Since the primary purpose of this research revolves around neuroimaging, a digital T1 phantom was constructed in MATLAB with relaxation times commonly found in the brain, including fat, gray matter (GM), white matter (WM), and cerebrospinal fluid (CSF). To construct the phantom, four regions were placed inside a 100x100x20 matrix. Each region was then assigned one of the four tissue types. Each pixel inside a tissue region was randomly assigned a T1 relaxation time from a Gaussian distribution incorporating the mean and standard deviation of T1 values of that tissue type found in the literature.[59-61] Further, a similar process was completed with

T2 relaxation times to make a digital T2 phantom, which was used to determine the effects of T2 and varying TEs within the simulation.

Table 3.1: MR Relaxation Values for Digital Phantom

Tissue Type	T1 Relaxation Time ± σ (ms)	T2 Relaxation Time ± σ (ms)
Fat	371 ± 8	133 ± 6
Gray Matter	1332 ± 57	110 ± 8.7
White Matter	832 ± 44	79.6 ± 2.6
Cerebrospinal Fluid	3302 ± 170	1447 ± 52

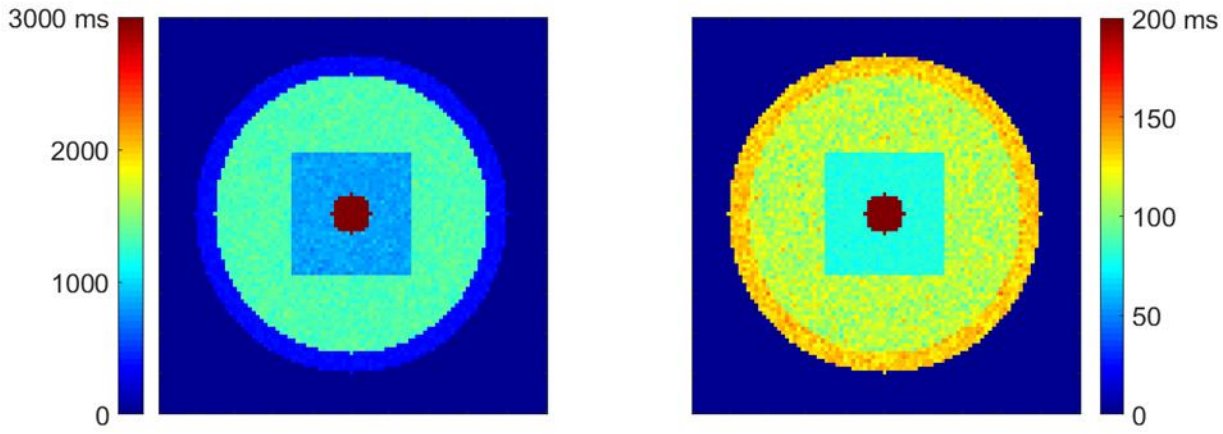

Figure 3.1: Center slice from the digital T1 (left) and T2 (right) phantoms with added gaussian noise. From the outside to the center, the tissue types represented are fat, GM, WM, and CSF, respectively.

3.2.2 Simulation Design

The simulation was designed to take the T1 and T2 digital phantoms and process them through a mock spin-echo sequence, then use the tissue types and known average T1 values to back calculate the original T1 phantom. To do this, the phantoms were placed into the spin-echo signal equation with user-defined parameters. Then, Gaussian noise was added to the simulated MR image, as Rician noise in an image with a signal-to-noise ratio (SNR) higher than three can be approximated with a Gaussian distribution. From there, the average signal intensity for each

tissue type was measured and fit to a modified version of the spin-echo equation for T1-weighted images. This fitting procedure was completed in MATLAB using the native non-linear fitting function. Finally, statistical methods were applied to compare the resulting calculated T1 map and the original digital T1 phantom. It is important to note that the fitting algorithm used, while similar to the end T1-REQUIRE algorithm, varied slightly. No T2 or proton density variations were accounted for in the early iterations of the algorithm while the digital simulations were being run.

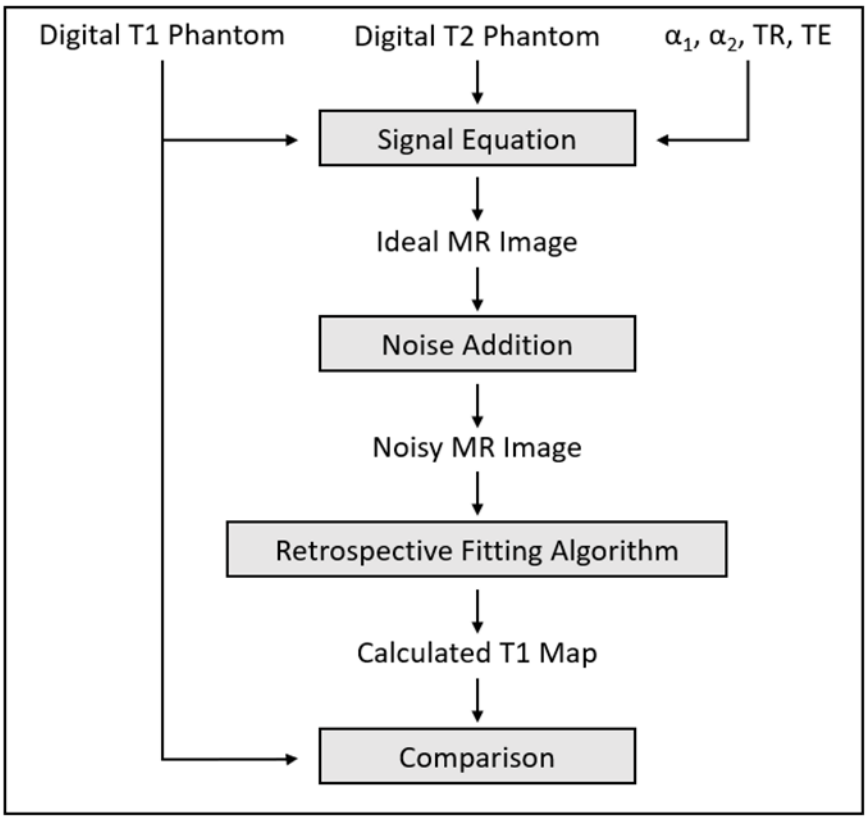

Figure 3.2: Flowchart depicting the simulation design.

3.2.3 Variation of Imaging Equation Parameters

Using this simulation, it is straightforward to vary many of the physical parameters present in the more precise signal equation and determine the accuracy of fitting the simpler T1-weighted

spin-echo equation retrospectively. For this analysis, the flip angles α_1 and α_2 (taken to be 90° and 180° pulses, respectively, to produce a true spin-echo) were varied within 20° of their assigned values. TR was varied between 25-5000 ms, and TE between 1-200 ms. Further, analysis was completed in the ideal case, where there is no T2 effect and no additional noise from the imaging system (TR = 525 ms) and exact flip angles, along with addition of T2 effects (TR = 525 ms, TE = 10 ms) but no additional noise from the imaging system and exact flip angles. Finally, the noise was varied so that the error could be calculated with different SNRs to determine how the amount of noise added by the imaging system affects the fitting procedure. The calculated SNR was determined by taking the average signal inside of a region within the GM and dividing it by the standard deviation of a region within the signal in the background.

3.2.4 Data Analysis

Correlation plots were generated on a pixel-wise basis for non-zero pixels, and linear regression was performed to find the correlation slope and coefficients of determination (R^2) for each scenario. Further, Bland-Altman plots were created to find bias within the results, further confirmed by inspecting the histogram of the percent error images generated automatically. Finally, the average of the absolute value of the error was used to compare various scenarios such as varying the TR to generate plots for visual analysis.

3.2.5 Results

To begin, the digital T1 phantom was run through the simulation with a TR of 525 ms, no T2 effects, ideal flip angles, and no noise from the MR imaging systems. This resulted in an almost perfect fit, with a correlation slope of 1.00, a correlation coefficient of 1.00, almost no bias present (mean bias from Bland-Altman plot of -0.333 ms), and an average percent difference of 0.04%.

This was to be expected, as the fitting equation was the same as the signal equation used to generate the simulated MR. The purpose of the ideal situation was to ensure that the simulation was functioning properly with no outside influence.

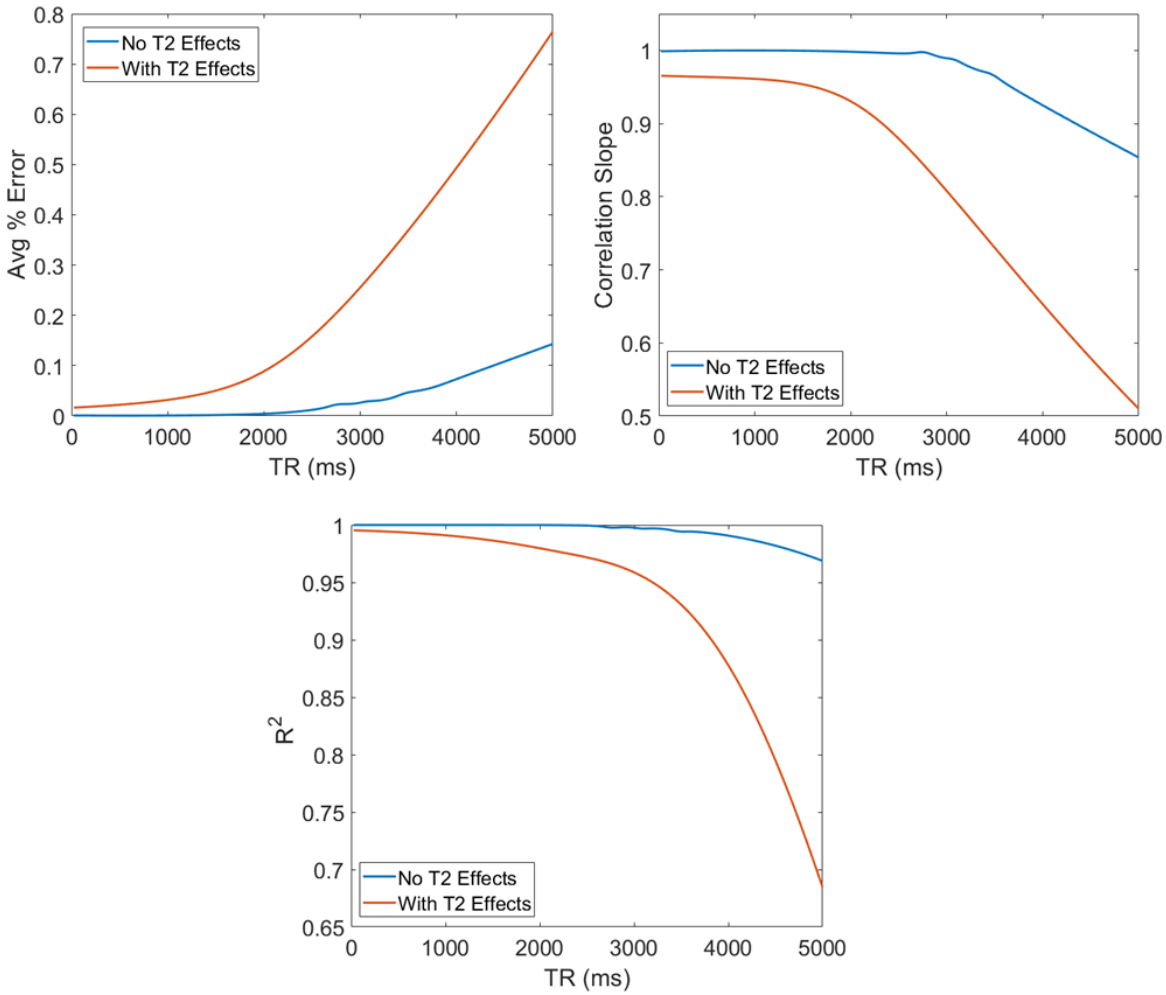

Figure 3.3: Average percent error (a), correlation slope (b), and R^2 values with varying TR, along with (orange) and without (blue) T2 effects (TE = 10ms).

After the initial run to test the efficacy of the simulation's fitting procedure, the input TR was varied between 25-5000 ms with and without T2 effects. The purpose of this was to determine the impact of fitting with the incorrect TR and that of including T2 effects when the fitting algorithm ignored them. The TE of the varied TR with T2 effects was set at 10 ms. *Figure 3.3*

shows the average percent error, correlation slopes, and R^2 with and without T2 effects as a function of TR. No additional MR noise was added to the system to only analyze the effect of TR. At a TR of 525 ms and a TE of 10 ms, the average percent error when T2 effects are included increased from 0.04% to 2.24%. The correlation slope decreases from 0.9998 to 0.9636, and the R^2 decreases from 1.000 to 0.9937. This indicates that T2 effects may be a significant source of error in T1-REQUIRE if they are ignored.

With a set TR of 525 ms, the TE was then varied from 0-200 ms to determine its effects on the fit, which does not include any T2 effects. As expected, the higher TEs produced more T2 effects, which resulted in the fit underestimating the actual T1 relaxation time, as shown with a higher average percent error and lower correlation slope and R^2 values (*Figure 3.4*). This shows, again, that ignoring T2 effects may not be appropriate, and the impact of doing so increases as TE increases.

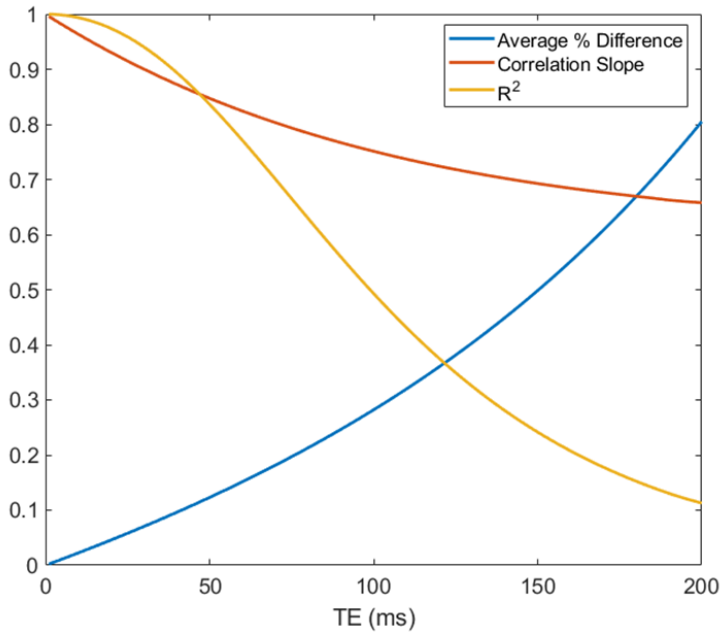

Figure 3.4: Statistics resulting from varying the TE with a constant TR.

Keeping a constant TR of 525 ms with no T2 effects or additional MR noise, both flip angles (α_1 and α_2) were varied within 20 degrees of their specific values. However, this produced no increase in error, as the fitting algorithm was able to account for this in M_0 such that this effect was nullified.

Noise was introduced into the system by multiplying the simulated MR image with a zero-mean gaussian distribution with a set variance. By altering the variance of this distribution, the SNR could also be altered. The range of variances was set from 0.005% to 1% of the maximum signal intensity of the simulated MR image, resulting in statistics shown in *Figure 3.5.* As expected, higher SNRs resulted in better retrospective fits when looking at the average percent error, the correlation slope, and the R^2 values.

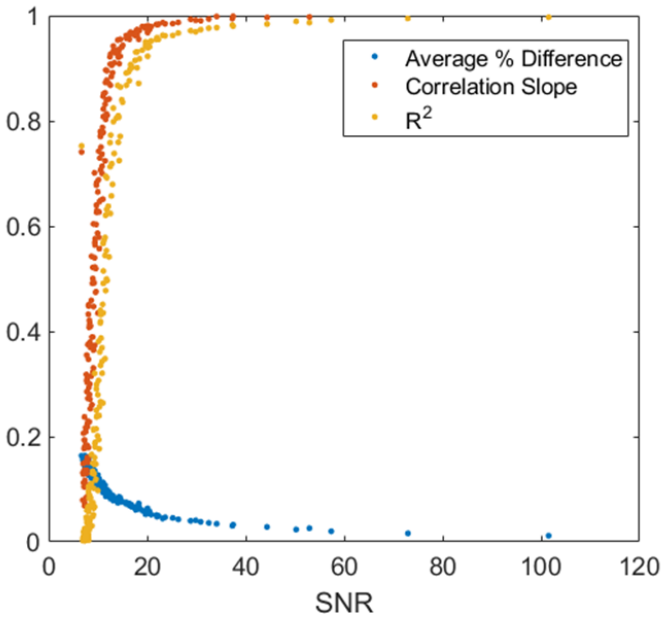

Figure 3.5: Statistics resulting from varying the added imaging noise with a constant TR (525 ms) and no T2 effects.

For a realistic example, the simulation was run with a TR of 525 ms, a TE of 10 ms, ideal flip angles (as this does not affect the overall accuracy), and a SNR of 30 (well below what most

systems currently operate at). The simulation output is shown in *Figure 3.6*. The average percent error across the phantom was 4.61%, with a correlation slope of 0.969 and a R^2 of 0.966. There is a slight bias of the retrospective fit to overestimate the actual T1, with a mean bias of 24 ms.

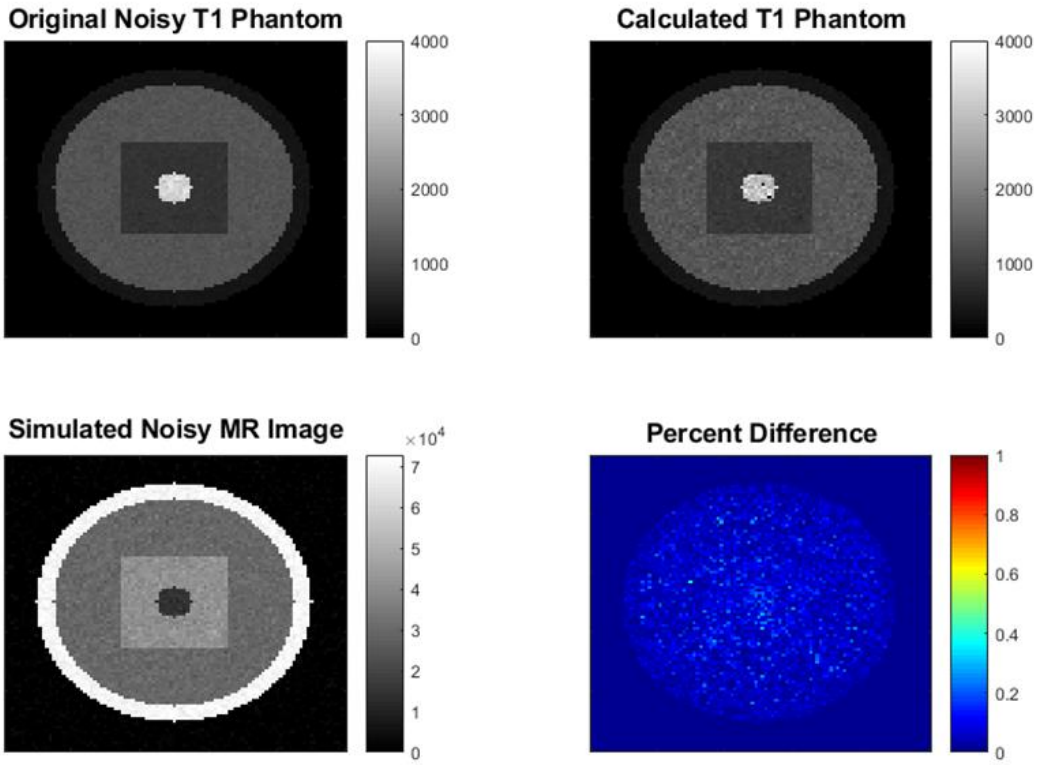

Figure 3.6: Output from simulated T1-weighted spin-echo imaging simulation and corresponding REQUIRE T1 mapping.

3.3 T1/T2 Phantom

3.3.1 Construction of the T1/T2 Phantom

The phantom to be used for this MRI study was constructed from 29 syringes filled with varying concentrations of both gadolinium and agarose gel. Agarose was chosen due to its similar T2 relaxation time when compared to human tissue (~40-150 ms) and the ability to vary this relaxation time by varying the concentration of agarose in the syringe. To begin construction of

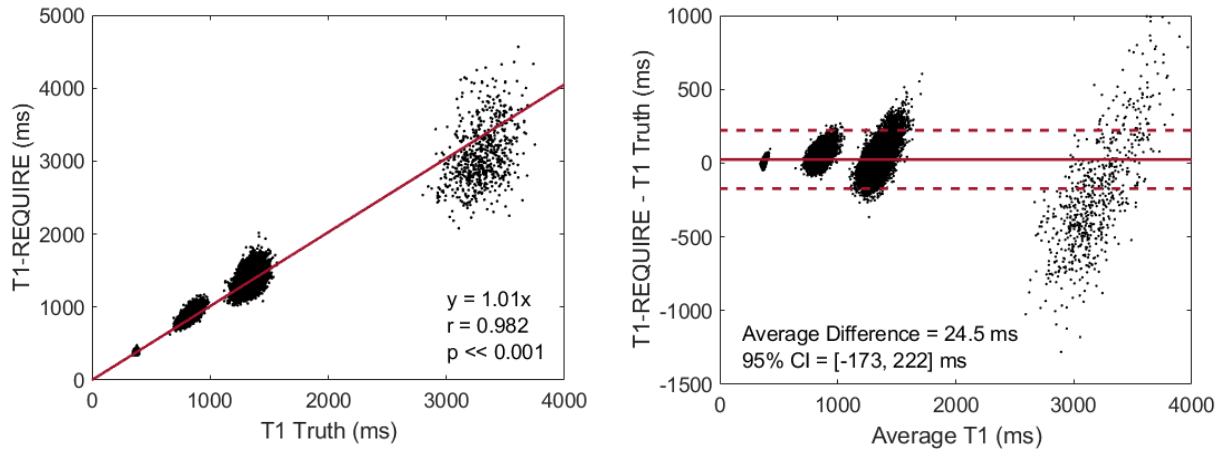

(a) (b)

Figure 3.7: Correlation (a) and Bland-Altman (B) plots for a realistic simulation using the digital phantoms.

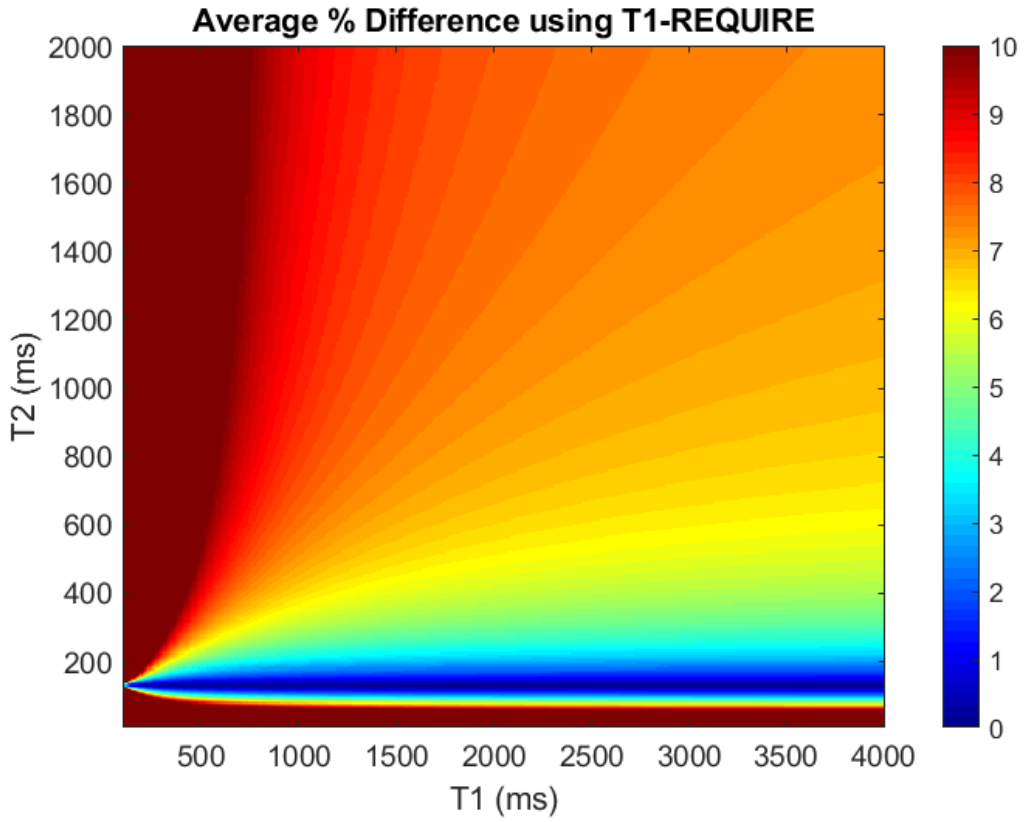

Figure 3.8: Heat plot showing the average percent difference using T1-REQUIRE with variations in T1 and T2. TR and TE were set at 525 ms and 10 ms, respectively

.

the phantom, a serial dilution of the gadolinium-based contrast media was performed to reduce concentration to the desired levels. The media of choice was Omniscan from GE Healthcare, often used in a clinical setting for MR contrast. The gadolinium was diluted with distilled water such that 5 mL of each concentration in a 100 mL total volume would yield the desired concentration. 10 mL of each concentration was made in case replication of the process was necessary.

After the serial dilutions were made, 5 mL of each concentration were placed in a beaker along with 95 mL of distilled water. Agarose powder was added to achieve the first desired concentration of agarose by heating and stirring the solution. After fully dissolved, a syringe was used to measure 20 mL of the solution, with extra care being taken to remove any air pockets. The process was then repeated with the remaining 80 mL of solution, adding agarose to achieve the second concentration, heating and stirring until dissolved, measuring 20 mL. This was done four times to each solution, bringing the total number of syringes to 28. Table 2 describes each syringes' concentration of both agarose and gadolinium, with the position in the table corresponding to the position in the final phantom. The 29th vial was filled with canola oil to represent fat. After the syringes were cooled, a holding container was constructed by cutting circular holes in a sponge. The syringes were inserted into the holes and secured by filling the remainder of the container with rice.

3.3.2 MR Imaging of the T1/T2 Phantom

These test tubes were imaged in a Philips Ingenia 3T scanner located at the Magnetic Resonance Imaging Research Center (MRIRC) at the University of Chicago. Sequences run include a T1-mapping Look-Locker with multiple inversion times (TE = 4.6 ms, TR = 8 ms,

Inversion Times (TI) = 150, 400, 750, 1500, 3500 ms, $\alpha = 12^{o}$), a T1-weighted spin-echo (TE = 10 ms, TR = 525 ms), and a progression of T1-weighted inversion-recovery (IR) images with varying TI for ground truth (TE = 7 ms, TR = 7000 ms, TI = 50-5000 ms).

3.3.3 Data Analysis

Gold standard T1 maps were created in MATLAB by fitting *Equation 1.2* using the multiple-TI IR images. The T1-mapping Look-Locker sequence was used to compare with the gold standard, as it is the reference standard in the University of Chicago Medical Center's MS imaging protocol. To create a T1 map from the images, the REQUIRE algorithm for spin-echo MR images described in Chapter 2 of this dissertation was completed.

Data analysis was completed in MATLAB and consisted of correlation plots with fits via linear regression and Bland-Altman plots to determine bias. These plots were generated using regions-of-interests (ROIs) placed over a single slice of the test tubes via a gray-level thresholding method followed by erosion in MATLAB, and visual inspection ensured only voxels in the test tube were included. In addition, Pearson's Correlation Coefficients was calculated to show the relationship between the two mapping methods.

3.3.4 Results

The constructed phantom resulted in calculated T1 values ranging from ~100 ms to ~ 1650 ms when using the gold-standard inversion recovery (IR) with multiple inversion time (*Figure 3.9*). From these values, test tubes 1 (top row, first column), 8 (second row, fourth column), and 29 (containing vegetable oil, located between rows 1 and 2) were selected as reference for the T1-REQUIRE method due to their approximation of the T1 relaxation times of CSF, GM, and fat, along with their wide range of T1 values to fit the signal equation as accurately as possible.

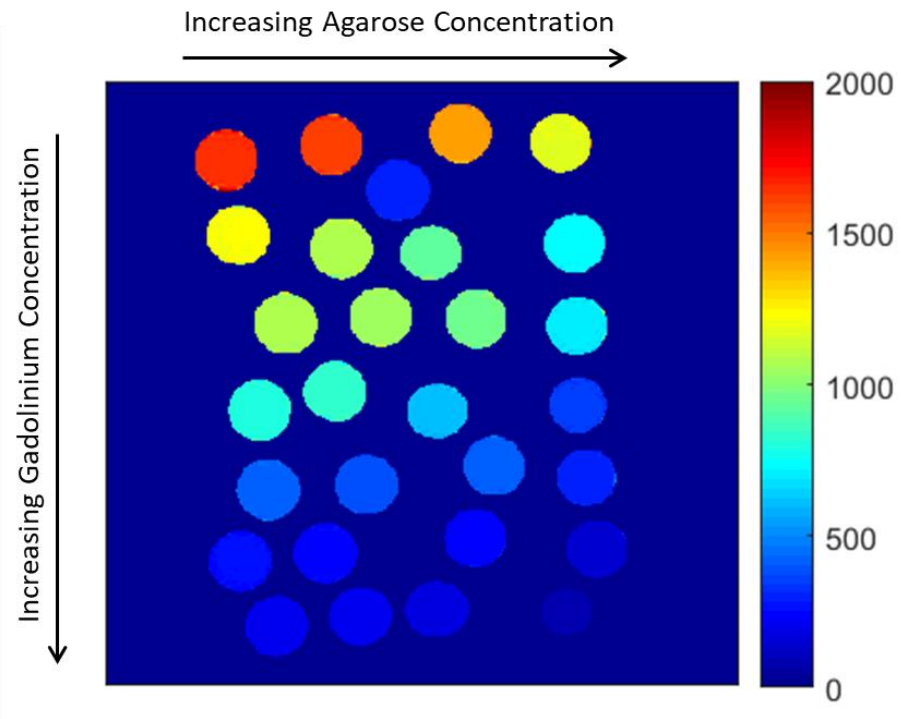

Figure 3.9: T1 Map of Agarose/Gadolinium phantom. 29th vial (fat) is placed in between rows 1 and 2.

The slopes, p-values, Pearson's correlation coefficients (R) derived from the linear regression of the correlation plots, and mean biases from the Bland-Altman plots are summarized in *Table 3.2.* Correlation and Bland-Altman plots are shown in *Figures 3.10-3.12.* A high correlation coefficient between the T1-REQUIRE and gold-standard IR method along with a correlation slope close to one confirms that T1-REQUIRE is a good estimate with the gold-standard T1 quantification method. This table also shows us that the Look-Locker tends to underestimate the true T1 value by about 11%. To correct for this, all Look-Locker T1 maps will be corrected by dividing the fit image by 0.89. Once this is completed, T1-REQUIRE also agrees well with the corrected Look-Locker T1 quantification method.

Table 3.2: Summary of Results of T1/T2 Phantom Study				
T1 Quantification Method	**Correlation Slope**	**p**	**R**	**Mean Bias [95% CI] (ms)**
Look-Locker vs IR	0.890	<< 0.001	0.975	-100 [-306, 106]
T1-REQUIRE vs IR	0.987	<< 0.001	0.905	-28.9 [-485, 427]
T1-REQUIRE vs Look-Locker (uncorrected)	1.09	<< 0.001	0.900	71.5 [-410, 553]
T1-REQUIRE vs Look-Locker (corrected)	0.971	<< 0.001	0.900	0.458 [-485, 486]

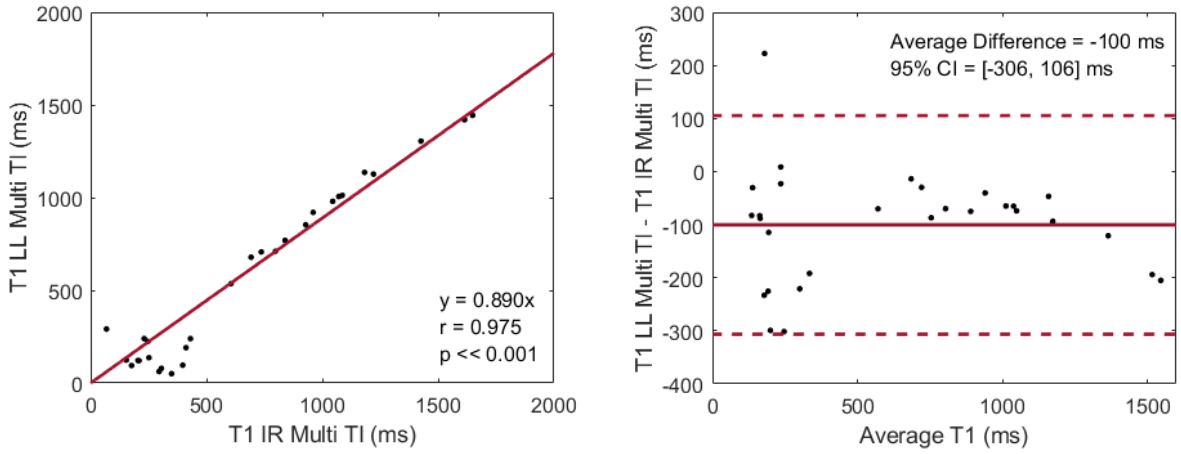

(a) (b)

Figure 3.10: Correlation (a) and Bland-Altman (b) plots for the phantom study between the Look-Locker and Inversion Recovery T1 mapping techniques.

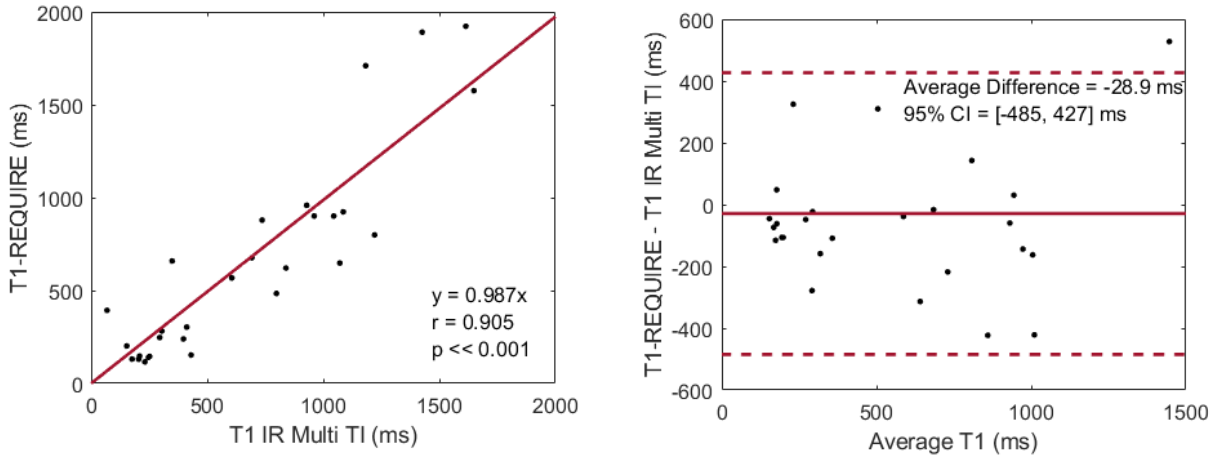

(a) (b)

Figure 3.11: Correlation (a) and Bland-Altman (b) plots for the phantom study between T1-REQUIRE and Inversion Recovery T1 mapping techniques.

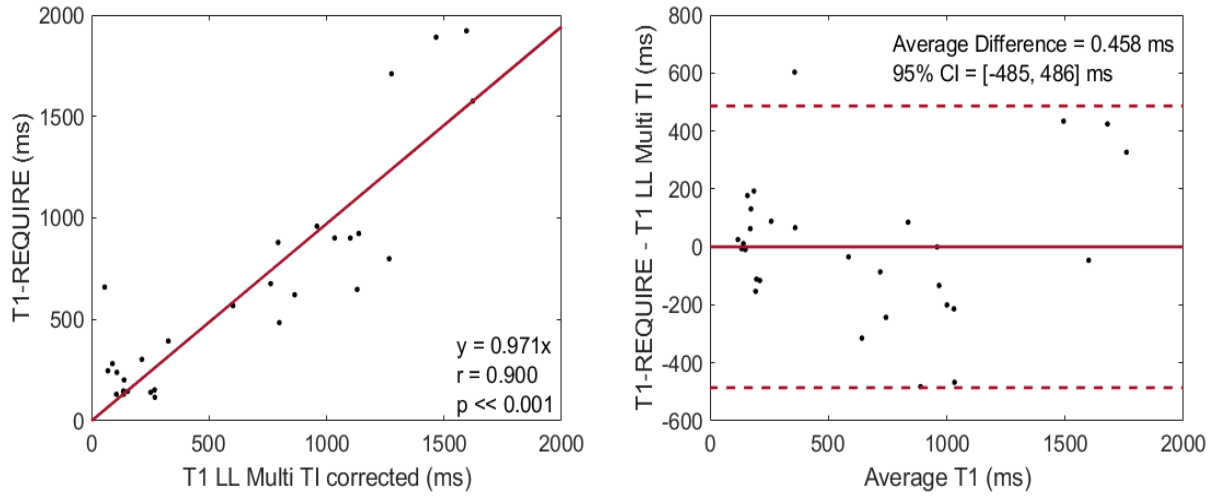

(a) (b)

Figure 3.12: Correlation (a) and Bland-Altman (b) plots for the phantom study between T1-REQUIRE and corrected Look-Locker T1 mapping techniques.

.

3.4 Healthy Volunteer Study

3.4.1 MR Imaging of Subjects

Ten healthy controls (34.1 ± 10.3 years, 7 males, 3 females) were scanned in the same Philips Ingenia 3T MRI scanner at the University of Chicago MRIRC. This was a HIPAA compliant investigation that was approved by the Institutional Review Board of our institution. The protocol for these studies included a T1-mapping Look-Locker with multiple inversion times (TE = 4.6 ms, TR = 8 ms, TI = 150, 400, 750, 1500, 3500 ms, $\alpha = 12^{o}$, 240x196x65 mm^3 [240x240x13 pixels] FOV) and a T1-weighted spin-echo (TE = 10 ms, TR = 525 ms, 240x196x65 mm^3 [240x240x13 pixels] FOV). These two sequences were run back-to-back-to-back to reduce the risk of movement in between the three scans.

3.4.2 Data Analysis

Images were exported into MATLAB and converted into T1 maps either by the T1-REQUIRE algorithm as described in Chapter 2 or via the Look-Locker method described by *Equations 1.3-1.4.* The T1 map generated via the Look-Locker was then corrected due to the underestimation found in the phantom study. The T1w spin-echo was registered to the Look Locker images via SPM12 prior to analysis. After conversion to T1 maps, both were convolved with a 4x4x1 Gaussian smoothing kernel to reduce noise prior to analysis. Like both the digital simulation and phantom studies, correlation plots were generated, and both Pearson's and Lin's Concordance Correlation Coefficients were calculated.[63]

3.4.3 Results

The resulting comparison T1 relaxation times from the ten healthy controls using the Look-Locker reference standard and T1-REQUIRE with the spin-echo MRIs are shown in *Figure 3.13*. For each

data set, the T1-REQUIRE method for the was completed in less than a minute on a spin-echo image, including the conversion of files from DICOM to NIFTI formatting, and the conversion of multiple TI Look-Locker images to T1 maps was completed in an average 106 minutes on the same machine at the same resolution, a more than 100x increase in computational efficiency.

When comparing the T1 relaxation times from the T1-REQUIRE on spin-echo images with those from the reference standard Look-Locker, we found a correlation slope of 0.939, intercept of 84.2 ms, Pearson's correlation coefficient of 0.887, and Lin's concordance correlation coefficient of 0.884. This small difference between the Pearson's and Lin's correlation coefficients indicates a very slight bias in our method. Using the linear regression fit, we can calculate an effective range for T1-REQUIRE on T1-weighted spin-echo images as 523 to 3000 ms, the limit of our analysis.

In addition to correlation plots, the histograms of the culmination of the ten healthy controls are shown in *Figure 3.14a-b*. Although the T1 maps differ slightly, the same general shape can be seen, showing improved data harmonization over the T1-weighted images. Finally, representative slices of both T1 maps are shown in *Figure 3.15.*

3.5 Discussion

Overall, the T1-REQUIRE was validated in three different ways. First, a digital simulation run in MATLAB determined the feasibility of the algorithm as a whole. However, it did point out some potential pitfalls, including the potential need to account for T2, and likewise, proton density variations. Second, a phantom study showed that there was good agreement between T1-REQUIRE and the gold standard multiple-TI IR mapping sequence. In addition, it also showed that the reference standard used for the healthy volunteer study, the Look-Locker, generally

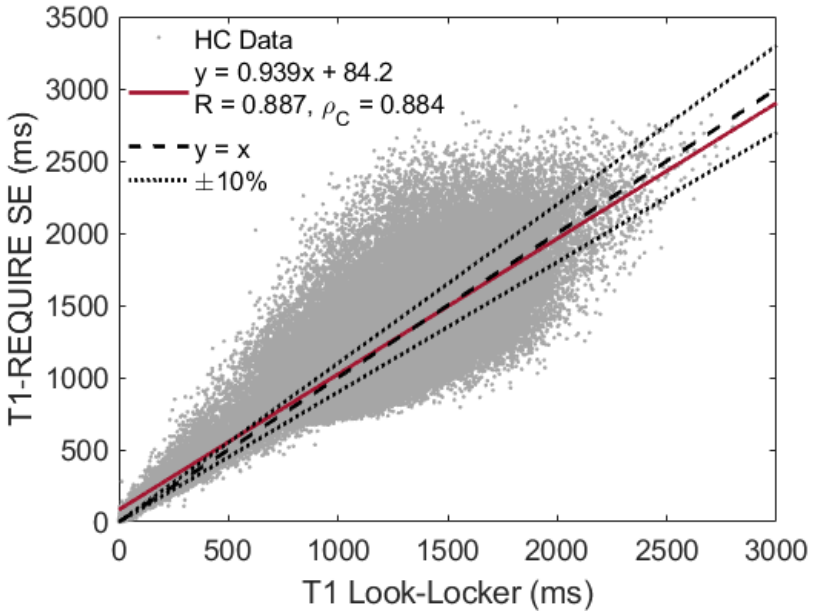

Figure 3.13: Results of healthy control study using corrected multiple-TI Look-Locker as reference standard T1 mapping and comparing with novel T1-REQUIRE method using spin-echo images. T1 maps were registered and convolved with an 4x4x1 voxel smoothing kernel before comparison.

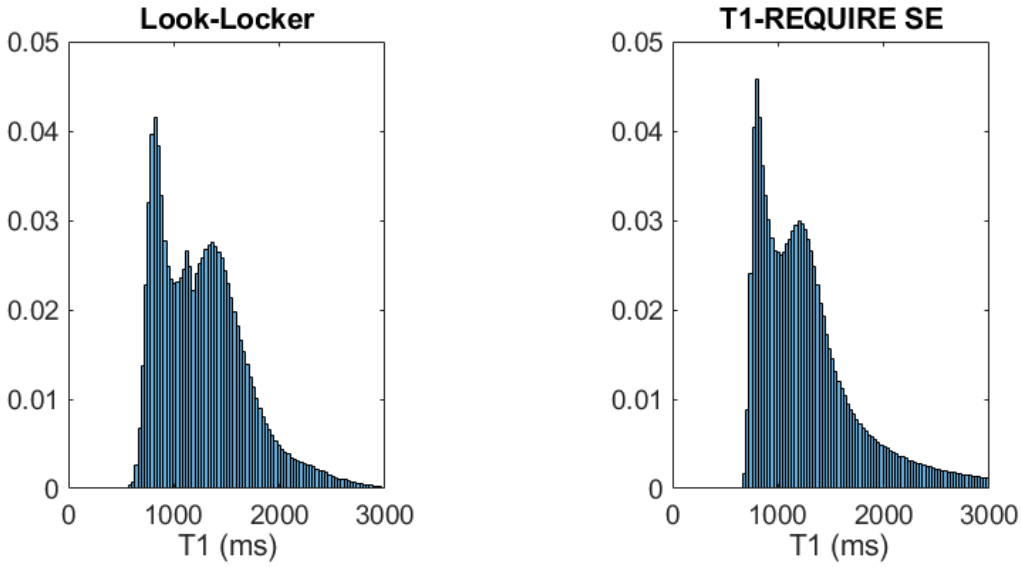

Figure 3.14: Histograms of T1 maps from 10 healthy control brains, with the reference Look-Locker method (a) and T1-REQUIRE on spin-echo images (b).

underestimated T1 when compared to the gold standard by about 11%. This was then corrected for any Look-Locker mapping sequence. Finally, a healthy volunteer study showed good agreement between the corrected reference standard and T1-REQUIRE in the range of 523 to 3000 ms, which should be sufficient for most imaging studies.

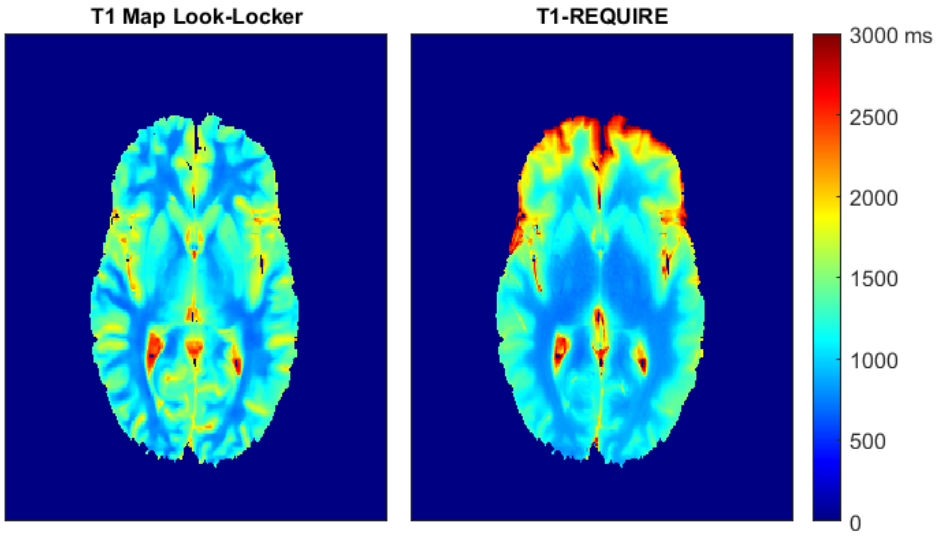

Figure 3.15: Example T1 maps generated by the reference standard Look-Locker (left) and T1-REQUIRE on spin-echo images (right).

Data harmonization of MRI data is an important aspect of machine learning that is often overlooked or understated. Without it, any results may be skewed by variability in scan- or scanner-specific properties. Relaxometry could have the dual ability to provide data harmonization along with providing interesting, tissue-specific information not previously seen. However, the downsides of relaxometry measurements often outweigh the benefit for clinicians, resulting in a lack of relaxometry datasets that are suitable for analysis via machine learning. By providing estimates of T1 using T1-weighted images, previously acquired weighted images can be converted to harmonized estimate T1 maps for big data studies.

Historically, MR relaxometry can be fit in a variety of ways, including an IR sequence with multiple TIs and a spin-echo with multiple repetition times. These sorts of methods have the advantage of accuracy but require long scan times prohibiting use in clinical studies. Other sequences have been developed to reduce scan times, such as the Look-Locker method and MR Fingerprinting (MRF). These can be implemented as a time-efficient method of acquiring quantitative MR parameters like T1.[64] But, as time-efficient as they can be, both are still an additional scan that clinicians do not often order or use for their clinical analysis of disease. In addition, MRF was only introduced within the last 5 years, meaning a large portion of information even in current datasets would not have been able to have run an MRF sequence. So, while MRF is a useful tool, it is a prospective tool with no applications retrospectively that is not very frequently utilized by clinicians. T1-REQUIRE can be used retrospectively with no additional sequences required, making it a useful addition to workflow for estimating T1.

These historical T1, T2, and proton density values, found in the literature, present a challenge, as T1 values vary across the same tissue type depending on location (i.e. parietal GM having a lower T1 than frontal gray matter – 1276 to 1322 ms, respectively). In addition, intra- and inter-scanner variability may result in additional error, as studies have found a 1% intra-scanner variability, 1% intra-vendor/inter-scanner variability, and an 8-10% inter-vendor variability across the whole brain due to factors like B0 field differences, B1 map variations, shimming procedure, etc.[65]

Many assumptions are made in the T1-REQUIRE algorithm. For the T2 correction, T2 varies along with T1 in diseased tissue which may lead to a source of error due to the T2 map being generated with the assumption of healthy tissue. However, error propagation analysis (derived from *Equation 2.1* showing how *S* varies with changes in T1 and T2 before equating

them) shows that the true T2 value of a voxel of average gray matter having an uncertainty of 50% would result in only a 5.6% uncertainty in T1, and the same in a voxel of average white matter would result in an uncertainty of 8.7% (*Equations 3.1a-c*).[66] Because of this, we argue that the estimation of T2 step for T1-REQUIRE of a spin-echo remains appropriate except in the most extreme cases of changes in T2. This is also exemplified in *Figure 3.10*, where the putamen and caudate nuclei visually appear to have T1 values relatively consistent with the literature even with the variation of T2 in deep gray matter.

$$\frac{\delta S}{S} = \frac{TR \cdot \delta T1}{T1^2\left(e^{TR/T1} - 1\right)} \qquad \textit{Equation 3.1a}$$

$$\frac{\delta S}{S} = \frac{TE \cdot \delta T2}{T2^2} \qquad \textit{Equation 3.1b}$$

$$\frac{\delta T1}{T1} = \frac{TE \cdot \delta T2 \cdot T1\left(e^{TR/T1} - 1\right)}{TR \cdot T2^2} \qquad \textit{Equation 3.1c}$$

There are limitations to this study. In addition to needing all three tissue types (GM, WM, CSF) in each slice for the fit, this study was also performed on a single 3T Philips Ingenia scanner with no changes to protocol (altering TR or TE, slice thickness, etc.). Also, factors such as coil sensitivity and flip angle variability were ignored in the brain. However, for applications elsewhere (i.e. prostate, cardiac, etc.), they may not be able to be ignored.

This pilot study shows the potential viability of T1-REQUIRE for retrospective quantification of relaxation times from weighted MR data as both an efficient estimation of T1 and a data harmonization technique for machine learning applications. More work needs to be done to expand the REQUIRE algorithm to other T1- and T2-weighted imaging sequences as well as validation of its potential in machine learning pipelines.

CHAPTER 4

VALIDATION OF T1-REQUIRE ON T1-WEIGHTED MPRAGE MR IMAGES

For Chapter 4 of this dissertation, the potential of T1-REQUIRE to be extended to more complicated MR sequences with more complex physical processes is investigated. The purpose of this chapter is to determine if T1-REQUIRE is applicable to sequences where the exact signal equation is unable to be derived directly, and instead must be estimated or simulated. The validation process will be similar to Chapter 3; however, no phantom studies were used for validation. Therefore, this chapter will be organized as follows: the introduction to MPRAGE, digital simulation methods and the results from those simulations, and the healthy volunteer study followed by the results of T1-REQUIRE via MPRAGE compared with both the reference standards and T1-REQUIRE via spin-echo MR images. Much of this Chapter will echo what was discussed in Chapter 3. That being said, the purpose of this chapter being separate is to show how more complicated sequences may be adapted and validated into the REQUIRE algorithm.

4.1 Introduction

MPRAGE is a widely used clinical and research scan that can generate high resolution, 3-D T1w MR images in a short period of time. The sequence itself consists of a 180-degree inversion pulse followed by a single segment of a 3-D gradient-echo image after an inversion time TI. There is a further delay time after the gradient-echo sequence to allow for relaxation, and then the process is repeated until the entirety of 3-D k-space has been covered, at which point a 3-D Fourier transform will produce an image of the object. This sequence is especially useful in anatomical imaging of the brain, as it has a large amount of contrast between gray and white matter to go along with its cubic millimeter isotropic resolution or better.

However, with this remarkable resolution, contrast, and speed comes an incredibly complex signal. After searching through the literature, there have been no derivations from first principles that have yielded a signal equation like there has been with the much simpler T1w spin-echo. Therefore, a different approach is required to estimate T1 from signal intensity values. As described in detail in Chapter 2 of this dissertation, an approximation of the behavior of the signal has been described by Brant-Zawadzki *et al*.[58]

The purpose of this chapter is to attempt to validate the T1-REQUIRE algorithm when it is not directly solving for the signal equation and instead is iteratively solving for the best approximate solution. To do this, validation was completed in two separate ways. First, simulations were run on the digital phantom used in Chapter 3 of this dissertation to determine the effects that estimating parameters not fully populated in the image headers had on the overall capability of the algorithm. Second, a healthy volunteer study allowed for the implementation of T1-REQUIRE *in vivo* to compare with the reference standard T1 mapping sequence. In addition, estimated T1 maps generated by running T1-REQUIRE on both the spin-echo and MPRAGE images were compared to determine the consistency of the algorithm at harmonizing data across sequences. Finally, a study using the same subjects on various scanners was run to determine the ability for T1-REQUIRE to harmonize data across scanner type and manufacturer.

4.2 Digital Simulation

4.2.1 Digital Phantom Construction

The same digital phantom that was constructed for Chapter 3 of this dissertation and described in detail in Section 3.2.1 was used for this simulation as well. However, only the T1 phantom was used, as T2 was not involved in the estimated signal equations for MPRAGE.

4.2.2 Simulation Design

Using the approximation of the signal intensities described previously along with user-defined parameters, a noiseless MPRAGE image was generated. Noise was then added to the image via a Gaussian distribution (again, as Rician noise can be approximated with a normal distribution if the SNR is greater than three). Using this new MPRAGE image, T1-REQUIRE was run to estimate the original T1 map. More detail on how this was done can be found in Section 2.2.4.

4.2.3 Variation of Imaging Equation Parameters

For validation of the MPRAGE, the simulation was used for a slightly different purpose. For most of the headers of the MPRAGE MR images, some of the required parameters were not filled while others were. The most missed parameter was the recovery time. So, to determine the effect of inputting the incorrect T_{rec}, the simulation was run with a set value for the imaging (T_{rec} = 800 ms) and an incorrect value for T1-REQUIRE (T_{rec} = 500-1500 ms). Similarly, this process was repeated for TR (TR = 8ms, TR = 1-20 ms) and the flip angle ($\alpha = 9^o$, $\alpha = 5\text{-}20^o$) to determine the effects of inputting an incorrect value. Finally, SNR was varied as well to determine the minimum SNR that T1-REQUIRE needs for an appropriate approximation (SNR = 5-100).

4.2.4 Data Analysis

Correlation plots were generated on a pixel-wise basis for non-zero pixels, and linear regression was performed to find the correlation slope and coefficients of determination (R^2) for each scenario. Further, Bland-Altman plots were created to find bias within the results, further confirmed by inspecting the histogram of the percent error images generated automatically.

Finally, the average of the absolute value of the error was used to compare various scenarios such as varying the T_{rec} to generate plots for visual analysis.

4.2.5 Results

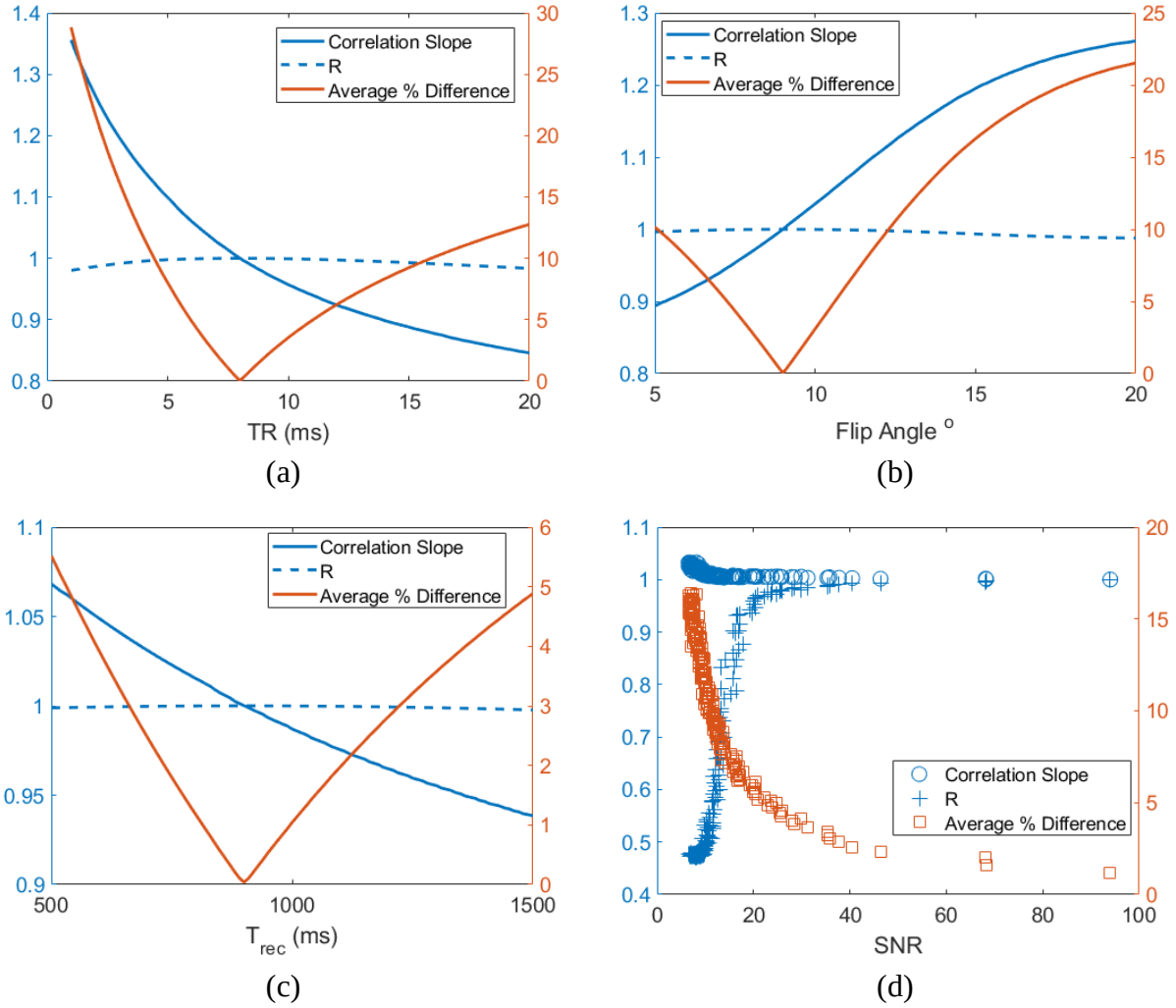

Figure 4.1: Results of T1-REQUIRE simulation using the MPRAGE signal equations and guessing potential missed header parameters.

The results of the simulation, shown in *Figures 4.1a-d*, give an indication of the importance of each parameter on determining the fit. The repetition time and flip angle seem to be essential in ensuring some sort of accuracy is achieved, as an incorrectly guessed or estimated repetition time and flip angle could lead to average percent differences well over 20%. However, this does not

seem to be the case for the recovery time or SNR; both seem to be relatively robust and could change significantly without a significant impact to the resulting T1 map.

4.3 Healthy Volunteer Study

4.3.1 MR Imaging of Subjects

Ten healthy controls (34.1 ± 10.3 years, 7 males, 3 females) were scanned in a Philips Ingenia 3T MRI scanner at our local institution. The protocol for these studies included a T1-mapping Look-Locker with multiple inversion times (TE = 4.6 ms, TR = 8 ms, TI = 150, 400, 750, 1500, 3500 ms, $\alpha = 12^{o}$, 240x196x65 mm^3 [240x240x13 pixels] FOV), a T1-weighted spin-echo (TE = 10 ms , TR = 525 ms, 240x196x65 mm^3 [240x240x13 pixels] FOV), and an MPRAGE (TE = 2.89 ms, TR = 8 ms, $\alpha = 9^{o}$, TI = 358 ms, T_{rec} = 400 ms, n = 176, 256x256x176 mm^3 [256x256x176 pixels] FOV). These three sequences were run back-to-back-to-back to reduce the risk of movement in between the three scans.

In addition, a second study was run to determine the validity of T1-REQUIRE for MPRAGE images across scanners. Two healthy volunteers (38.5 ± 3.5 years, both females) were scanned with some version of a MPRAGE sequence on six various 3T MRI scanners: 2 Philips Achieva, a Philips Ingenia, 2 GE Discovery MR750w GEM, and a GE Signa Architect. The scan parameters for each are listed in *Table 4.1*. Images were converted into T1 maps via T1-REQUIRE. No T1 mapping reference sequence was used; this study was purely to determine the reproducibility of T1-REQUIRE across various scanners types and manufacturers.

4.3.2 Data Analysis

Images were exported into MATLAB and converted into T1 maps either by the T1-REQUIRE algorithm as described in Chapter 2 (for both the T1w spin-echo and MPRAGE images)

Table 4.1: Scan Parameters for Multi-Scanner Experiment						
	GE Discovery #1	**GE Discovery #2**	**GE Signa Architect**	**Philips Achieva #1**	**Philips Achieva #2**	**Philips Ingenia**
Orientation	Axial	Axial	Axial	Axial	Axial	Axial
# Slices	182	174	174	160	180	167
Slice Thickness (mm)	1	1	1	1	1	1
FOV (mm)	256/256	256/256	250/256	250/199	250/225	240/240
Voxel Size (mm)	1x1x1	1x1x1	1 x 1 x1	1x1x1	1x1x1	1x1x1
TR (ms)	8.5	8.6	7.9	7.9	6.9	8.1
TE (ms)	3.2	3.2	3.1	3.5	3.5	3.7
TI (ms)	450	450	450	827.7	810	1010
# Channels	16	24	16	32	16	8

or via *Equations 1.3-1.4*. The T1 map generated via the Look-Locker was then corrected due to the underestimation found in the phantom study as described in Chapter 3 of this dissertation. The T1w spin-echo and MPRAGE images were registered to the Look Locker images via SPM12 prior to analysis. After conversion to T1 maps, all three were convolved with a 4x4x1 Gaussian smoothing kernel to reduce noise prior to analysis. Like both the digital simulation and phantom studies, correlation plots were generated between the T1 map estimated from the T1-REQUIRE and the other two T1 maps, and both Pearson's and Lin's Concordance Correlation Coefficients were calculated.

For the second study, no reference T1 mapping image was acquired. Instead, the T1-REQUIRE algorithm converted the MPRAGE images into T1 maps for comparison with each other. The T1-weighted images were registered with each other for each individual subject before

T1-REQUIRE was run. After conversion to T1 maps, a 4x4x1 smoothing kernel was convolved with the maps and T1-weighted images to reduce noise prior to comparison. Linear regression was run between maps converted from each sequence and the smoothed T1-weighted images, and the results were plotted to compare with the line of unity. In addition, a cumulative distribution function (CDF) was plotted for each T1-weighted image and T1 map to determine how well harmonized the data were.

4.3.3 Results of T1-REQUIRE vs Reference Standard

The resulting comparison T1 relaxation times from the ten healthy controls using the Look-Locker reference standard, T1-REQUIRE with the spin-echo MRIs, and T1-REQUIRE with the MPRAGE MRIs are shown in *Figure 4.2a-b.* For each data set, the T1-REQUIRE method for the was completed in less than a minute on a spin-echo image, including the conversion of files from DICOM to NIFTI formatting, and the conversion of multiple TI Look-Locker images to T1 maps was completed in an average 106 minutes on the same machine at the same resolution, a more than 100x increase in computational efficiency. For T1-REQUIRE on the MPRAGE images, the average computation time was around 7 minutes for a full estimated 3D T1-map, a 15x increase in computational efficiency even with a superior resolution over the Look-Locker images. When T1-REQUIRE was run on the registered MPRAGE images, the average computation time was just over a minute, again more than a 100x increase in computation time.

When comparing the T1 relaxation times from the T1-REQUIRE on MPRAGE images with those from the reference standard Look-Locker, linear regression produced a correlation slope of 0.949, intercept of 416 ms, Pearson's correlation coefficient of 0.849, and Lin's concordance correlation coefficient of 0.838. Again, there is a slight difference between the two correlation

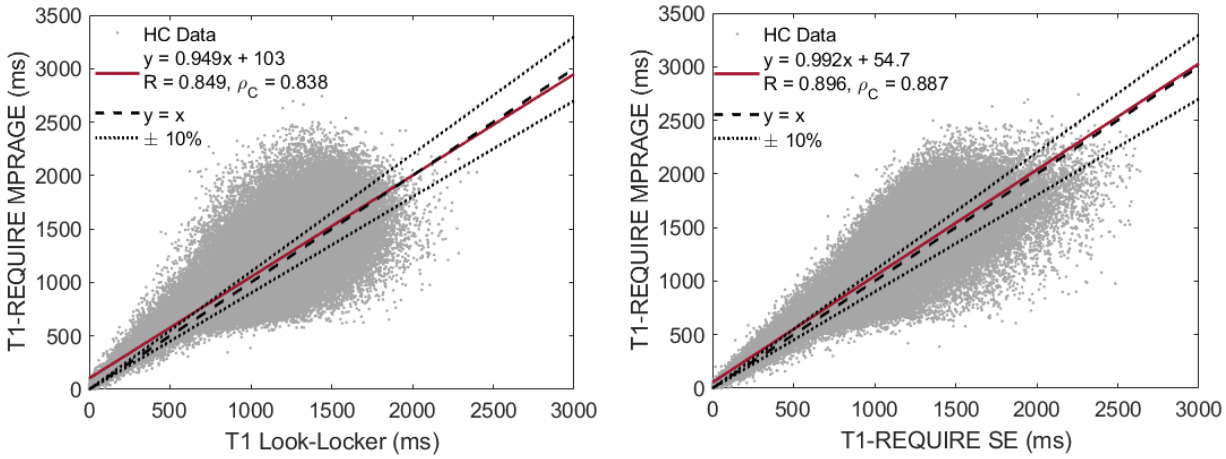

(a) (b)

Figure 4.2: Results of T1-REQUIRE on MPRAGE MR images versus reference standard (a), and T1-REQUIRE on MPRAGE MR images versus T1-REQUIRE on spin-echo MR images (b).

coefficients, but nothing concerning. Using the fit, we can calculate an effective range for T1-REQUIRE on T1-weighted MPRAGE images as 682 to 3000 ms.

To be effective as a data harmonization algorithm, it is important that T1-REQUIRE achieve the same or very similar results regardless of what sort of T1-weighted sequence is run. In that regard, we can do a similar analysis on T1-REQUIRE using both the spin-echo and MPRAGE images. Linear regression produces a correlation slope of 0.992, intercept of 54.7, Pearson's correlation coefficient of 0.896, and Lin's concordance correlation coefficient of 0.887, showing good agreement between the two with very little bias.

In addition to correlation plots, the histograms of the culmination of the ten healthy controls are shown in *Figure 4.3a-b*. *Figure 4.3a* shows the histograms of the weighted images, while *Figure 4.3b* shows those of the T1 maps. Although the T1 maps differ slightly, especially comparing the T1-REQUIRE from the MPRAGE image (right) with the reference T1

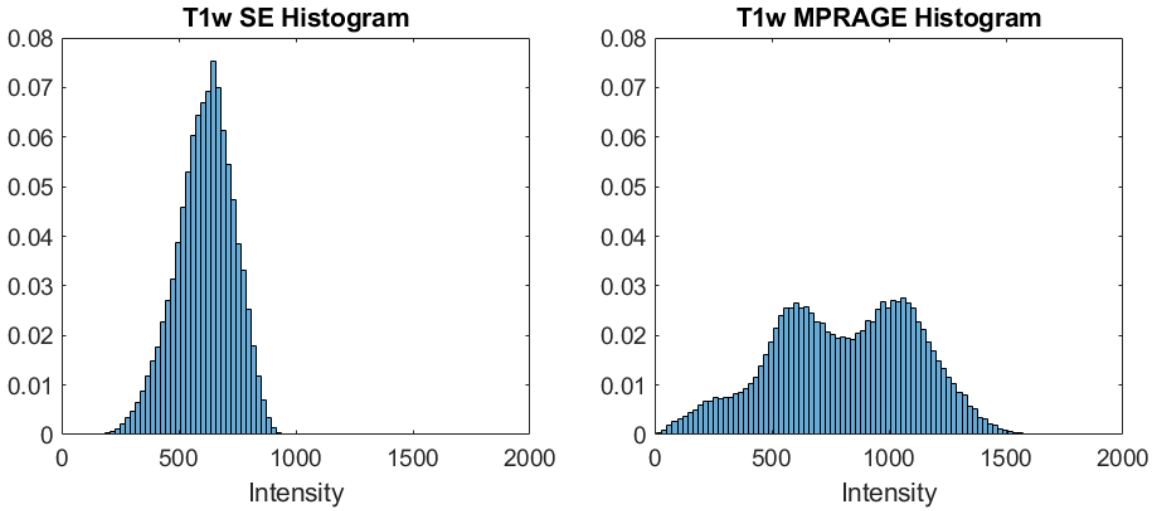

(a)

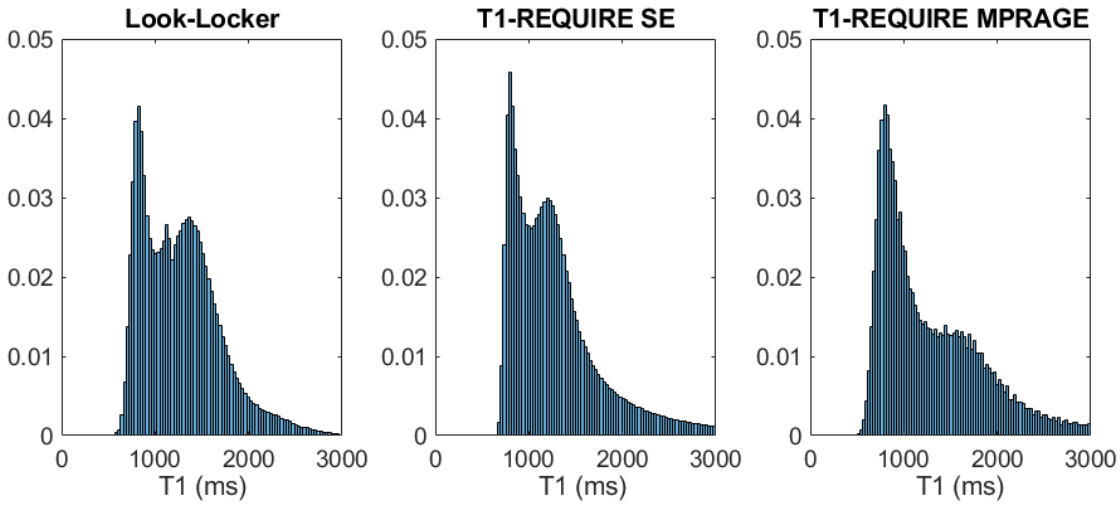

(b)

Figure 4.3: Histograms of 10 healthy control brains, including T1-weighted spin-echo and MPRAGE (a), and T1 maps generated via Look-Locker, T1-REQUIRE on spin-echo images, and T1-REQUIRE on MPRAGE images.

map (left), the same general shape can be seen, showing improved data harmonization over the T1-weighted images. Representative slices of the three T1 maps are shown in *Figure 4.4.*

4.3.4 Results of T1-REQUIRE Across Scanners

Figure 4.5 shows the results of the linear regression between either the original MPRAGE images (red dotted line) and T1-REQUIRE (black dashed line), along with the line of unity (cyan

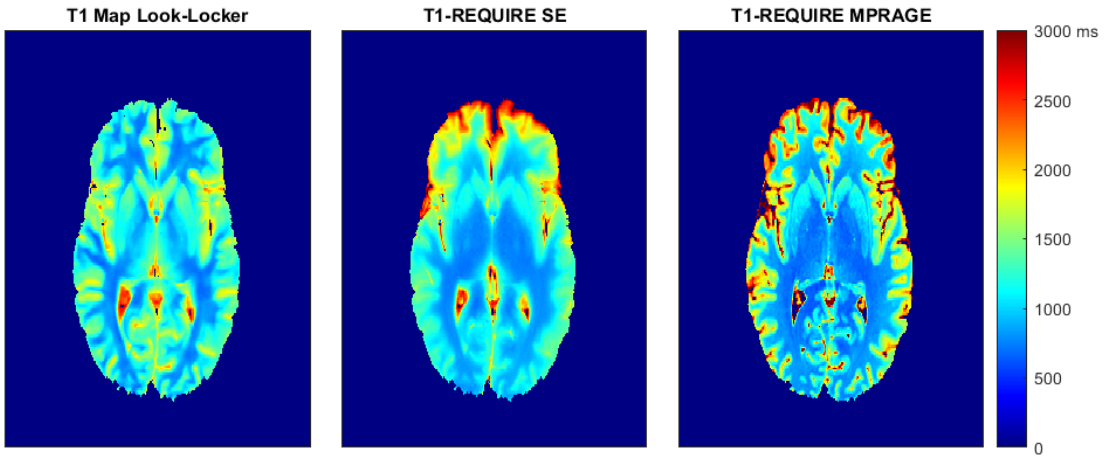

Figure 4.4: Example T1 maps generated by the reference standard Look-Locker (left), T1-REQUIRE on spin-echo images (middle), and T1-REQUIRE on MPRAGE images (right). Red areas around the cortex are probably due to partial volume effects of GM with CSF.

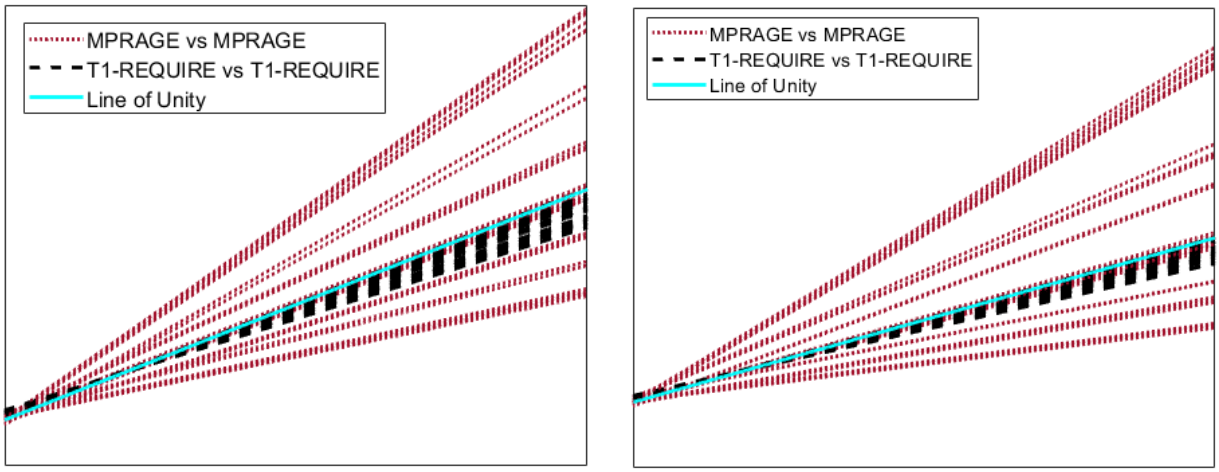

(a) (b)

Figure 4.5: Results from linear regression analysis comparing MPRAGE vs MPRAGE T1-weighted images (red dashed line) and corresponding T1-REQUIRE vs T1-REQUIRE (black dashed line) from Subject 1 (a) and Subject 2 (b) taken on 6 different scanners, along with the line of unity (cyan). Better normalization is indicated by a line closer to the cyan line of unity.

filled line) for both Subject 1 (left) and Subject 2 (right). Visual inspection shows that the spread of comparisons between T1 maps generated via T1-REQUIRE is much more consistent with each other and with the line of unity, providing evidence that T1-REQUIRE is a useful data harmonization tool across scanners. This result is consistent with the CDFs shown in *Figure 4.6*,

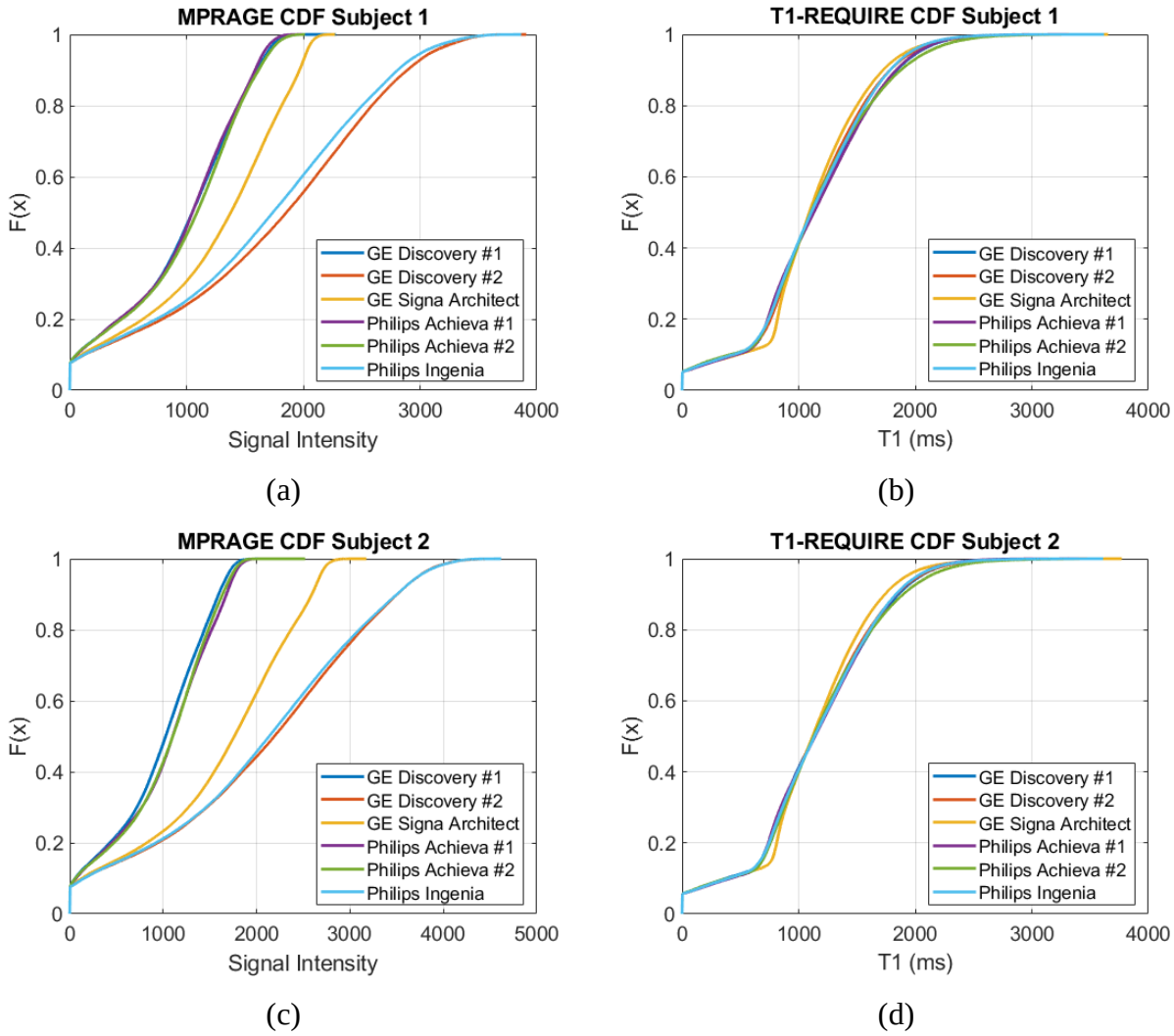

Figure 4.6: Comparison of CDFs from Subject 1 (a-b) and Subject 2 (c-d) for both the MPRAGE images (a,c) and T1-REQUIRE maps (b,d) from 6 different scanners. For both subjects, there was clear improvement in the normalization of the CDFs after applying T1-REQUIRE.

where the MPRAGE images have drastically varying CDFs that are much more uniform after T1-REQUIRE is completed.

4.4 Discussion

The results of the experiments run in this chapter show that T1-REQUIRE may be able to be expanded to other T1-weighted sequences. This is shown by good correlation between T1-REQUIRE run on MPRAGE images and the reference standard, along with T1-REQUIRE run on

both MPRAGE and spin-echo MR images. This shows the potential power of this methodology: by removing the sequence-dependent contrast from the image, it may now be possible to run studies on large datasets that involve weighted MR images but are run using different sequences.

In addition, the results of the experiment involving two subjects being scanned with a MPRAGE (or variation of MPRAGE) sequence over multiple scanners show the impact that T1-REQUIRE can have as a data harmonization algorithm across scanners. This, again, could be of huge importance as more and more big data studies are being completed. By using the REQUIRE algorithm, these studies have shown that the scanner and sequence dependence is removed, leading to improved data harmonization and potentially more applicable information, as T1 is a quantitative value unlike normal MR contrast.

However, the notion of this algorithm being impactful in big data studies needs to be tested more thoroughly. This was a pilot study run on a total of twelve subjects and may need to be scrutinized further to determine potential pitfalls and biases. That being said, the initial results show promise for both data harmonization and MR quantification. This idea will be investigated further in the following chapter (Chapter 5) of this dissertation.

CHAPTER 5

PREDICTION OF ACTIVE VERSUS INACTIVE MS LESIONS USING LOGISTIC REGRESSION

5.1 Introduction

As discussed in the introduction, Multiple Sclerosis (MS) is a chronic neuroinflammatory disease of the central nervous system characterized by focal demyelination of axons into lesions referred to as "plaques" throughout white matter.[67-70] To diagnose and track progression of the disease, magnetic resonance imaging (MRI) is used, as lesions show up clearly on standard MR weightings. However, MR features have only been shown to be moderately correlated with disability, implying that MS is a "clinico-radiological paradox" where disease appearing on MRI does not necessarily indicate clinical symptoms.[71-72] Studies have shown poor to moderate correlations between disability and radiological features such as white matter lesion load.[35-37, 73] Quantitative MR features, such as relaxometry, proton density (PD) imaging, and the magnetization transfer ratio (MTR) have been shown to better correlate with clinical outcomes.[74-77] This indicates that quantitative biomarkers may be more indicative of pathophysiology than weighted biomarkers. However, these are generally global features and do not always provide additional information about the lesions themselves.

One of the weighted biomarkers of new disease activity in MS is whether new lesions are enhanced when a gadolinium-based contrast agent (GBCA) is administered for a T1-weighted (T1w) post-contrast image. The current consensus is that disruptions in the blood-brain barrier (BBB) that allow for the contrast agent to leak through are indicative of active inflammation in that lesion.[67-68, 73] Eventually, these axons in these active lesions will begin to lose their myelin

sheath and perhaps even die, resulting in permanent damage. These lesions will show up as "black-holes" or regions of hypointensity on T1w imaging. Because there is no active inflammation in that area, the BBB will not allow contrast to leak into the lesion, and the lesion is no longer active. There is also an area of active interest in between the two states, where "gray-holes" appear and may be indicative of the remyelination process.

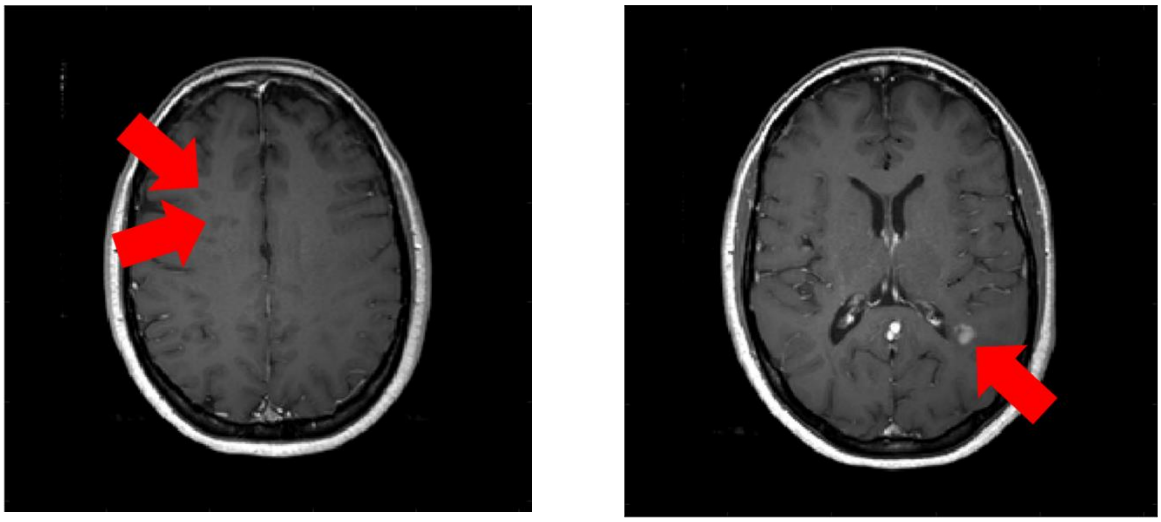

(a) (b)

Figure 5.1: MS lesions on T1w post-contrast MRIs showing dark lesions indicating inactive lesions (a) and bright spots indicating active lesions (b)

The above illustrates the need for physicians to be able to discern which lesions are active versus inactive and whether there is any new activity. Therefore, the GBCA is generally given to MS patients during their regular MR scans. This could pose a problem, as some studies have indicated that consistent administration of GBCAs can lead to deposition in the brain.[78-83] Patients in renal failure should also not receive contrast, as it can lead to potentially lethal nephrogenic systemic fibrosis.[83] In addition, the monetary costs of the GBCA itself, the staff to administer it, and the discomfort to the patient due to the intravenous injection all lends itself towards the conclusion that reducing the amount of GBCA MS patients receive is beneficial.

In this chapter, we investigated two ways to potentially use features derived from T1w pre-contrast images to predict the enhancement status of lesions. First, features derived directly from the T1w pre-contrast segmentations of the lesions were used with logistic regression to predict enhancement status. Second, the T1-REQUIRE algorithm described in Chapter 2 and validated in Chapters 3 and 4 of this dissertation was used to estimate a T1 map (qT1) from the T1w MR images. Using the lesion segmentations from these qT1 images, the same features were calculated and used to predict the enhancement status of the lesions. The results from these two predictive analyses were compared to determine if estimated quantitative MR features derived from the T1w MR images are any more predictive of enhancement status.

5.2 Methods and Materials

We performed a retrospective analysis of MRI exams collected as part of the normal evaluation of MS patients at our institution to determine the predictive value of features derives from pre-contrast MRI to predict gadolinium contrast agent enhancement, a marker of active inflammation.

5.2.1 Subjects

This study was approved by the Institutional Review Board of our local institution. 40 patients (32 females, 8 males, average age of 35.9 ± 10.0 years) with clinically diagnosed MS according to the revised McDonald criteria were included in this study. The patient data was a combination of two separate imaging datasets.

5.2.2 Imaging

All imaging was performed on either a Philips Achieva 3T or Philips Ingenia 3T whole-body scanner with a 16-channel head coil. Imaging data was combined from two independent imaging studies. Each patient underwent imaging at baseline, when symptoms first were reported,

and some had additional imaging at further time points for a total of 61 imaging datasets. For every patient, both a pre-contrast and post-contrast T1w spin-echo image in addition to a fluid-attenuated inversion recovery (FLAIR) image and further MR images consistent with the MS imaging protocol at our local institution.

5.2.3 Data Processing

All data processing was performed in commercially available software (MATLAB v2019b, The Mathworks, Nantick, MA, USA). The T1w pre- and post-contrast images at each time point, plus the FLAIR images and timepoints further along from the baseline, were all registered to the FLAIR baseline image using Statistical Parameter Mapping v12 (SPM12 - Wellcome Centre for Human Neuroimaging, University College London, UK). Once registered, MS lesions were segmented from all FLAIR images using a lesion prediction algorithm developed by Schmidt et al.[84] Lesion segmentations with volumes greater than 100 mm^3 were applied to the registered T1w pre- and post-contrast images, and 8 first-order features were derived from each image (*Table 5.1*). The lesions were separated into two classes. If the lesion had a T1w post-contrast maximum intensity greater than two standard deviations above the average white matter intensity on the T1w post-contrast image, it was considered to be contrast enhancing (CE). Otherwise, the lesion would be labeled as non-contrast enhancing (nCE). This was chosen as the discriminating factor between the two classes because it is similar to an assessment a neuroradiologist or neurologist would complete to determine enhancement versus non-enhancement. Visually, CE lesions would have areas of hyperintensity relative to the white matter, even if the entire lesion volume was not enhanced. Each time point, including those of the same patient, was considered independent.

In addition, T1-REQUIRE was also applied to the T1w pre-contrast images. As described in Chapter 2 of this dissertation, healthy tissue segmented via SPM12 and those tissues' T1, T2, and proton density values referenced in the literature along with the spin-echo signal equation was

Table 5.1: Chosen first-order features and their definitions.

Average	$\bar{X} = \frac{1}{n}\sum_{i=1}^{n} X_i$
Standard Deviation	$S = \sqrt{\frac{1}{n-1}\sum_{i=1}^{n}(X_i - \bar{X})^2}$
Median	η such that $P(X_i < \eta) = P(X_i > \eta) = \frac{1}{2}$
Maximum	X_n
Minimum	X_1
Range	$X_n - X_1$
Skewness	$s_1 = \frac{\frac{1}{n}\sum_{i=1}^{n}(X_i - \bar{X})^3}{\left[\frac{1}{n}\sum_{i=1}^{n}(X_i - \bar{X})^2\right]^{3/2}}$
Kurtosis	$k_1 = \frac{\frac{1}{n}\sum_{i=1}^{n}(X_i - \bar{X})^4}{\left[\frac{1}{n}\sum_{i=1}^{n}(X_i - \bar{X})^2\right]^{2}}$

used to generate an estimated T1 map (qT1) was derived from the T1w pre-contrast images (*Figure* 1). The lesion segmentations were then applied to the qT1 pre-contrast images, and the same 8 first-order features were calculated. The lesion class was the same as with the weighted images, as the weighted image is used clinically to determine enhancement status so it would be inappropriate to redefine what constituted a CE lesion.

5.2.4 Data Analysis

The mean feature values were compared using a Student's t-test to identify differences between CE and nCE lesions. Significance was set at the 95% confidence level ($p < 0.05$) corrected for multiple comparisons via the Bonferroni correction. Logistic regression was performed on the 8 features extracted from both the T1w and qT1 pre-contrast images using MATLAB, and receiver operator characteristic (ROC) analysis was performed and the area under the curve (AUC) was used to determined diagnostic accuracy. Comparison of AUC values for significance was achieved using the method described by Hanley and McNeil, with $p < 0.05$ considered significant.[85] 5-fold cross validation was completed on both the T1w and qT1 datasets to determine total accuracy. To compare accuracies, a test of hypothesis concerning a system of two proportions was completed, again with the results considered significant when $p < 0.05$.[86]

5.2.5 Testing/Training on Distinct Datasets

To determine the effectiveness of the qT1 images generated by T1-REQUIRE, the collected datasets were separated into training and testing classes based on which of the two original datasets they came from (Dataset #1 or Dataset #2). Then, logistic regression analysis was completed using Dataset #1 to train and Dataset #2 to test, and vice versa. This was completed for both the T1w feature sets and qT1 feature sets to determine if T1-REQUIRE provided additional benefit as a data harmonization algorithm.

5.3 Results

5.3.1 Segmentation and Classification of Lesions

From an initial sample of 61 complete exams, 4 (6.5%) were rejected for further analysis because incomplete headers caused an error in the image registration step of the analysis pipeline.

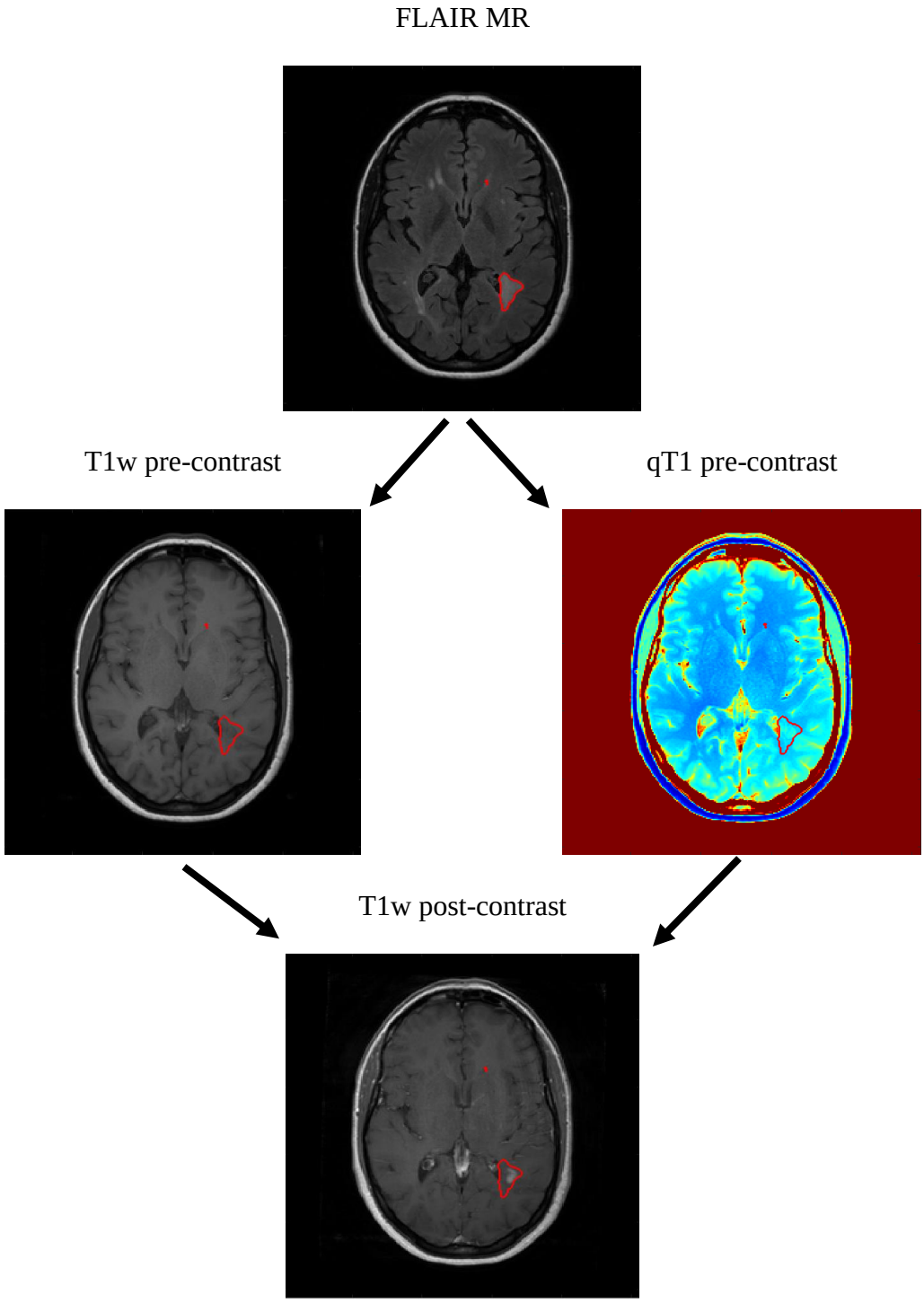

Figure 5.2: Flowchart depicting the analysis pipeline, beginning with the segmentation from the FLAIR image, application of the lesion segmentation to the T1w and qT1 pre-contrast images, and the comparison of the trained logistic regression classifier output with the truth from the T1w post-contrast image.

This left 57 time points with the required MR images which were analyzed. After segmentation, a total of 1,665 lesions were segmented. Most of these were sparse voxels within the "dirty" white matter. After the volume criteria of greater than 100 mm^3 was applied, a total of 263 lesion were identified. Of these, 104 were classified as CE, while the remaining 159 were classified as nCE.

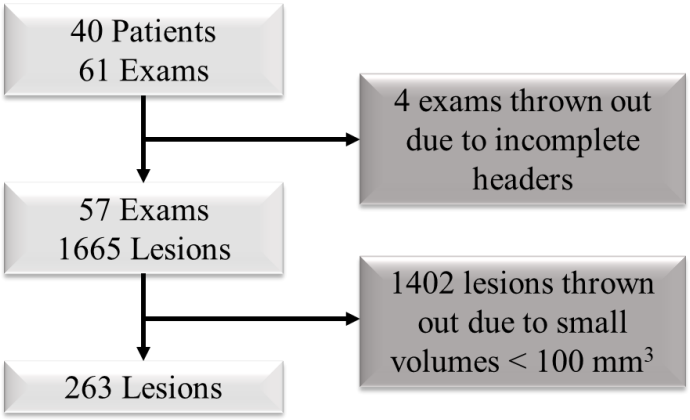

Figure 5.3: Flowchart of dataset selection criteria and removal of data.

5.3.2 T1w Analysis

Using the features derived from the T1w pre-contrast images of the lesions, a student's t-test was applied to each feature with a Bonferroni correction for multiple comparisons setting the significant p-value at 0.00625 (8 total features). Three features were determined to be significant: the standard deviation of the lesion (p = 0.00301), the minimum voxel value within the lesion (p = 0.000255), and the range of voxel values (p = 4.1E-12). A boxplot of the features between the two classes is shown in *Figure 5.4.*

Logistic regression was run on the T1w data for three different combinations of features, followed by an ROC curve and AUC value. When all T1w pre-contrast features were included, an

AUC of 0.914 was achieved (*Figure 5.5*). Beta values and p-values for the coefficients are shown in *Table 5.2.* After running 5-fold cross validation (*Table 5.3*, *Figure 5.6*), a total accuracy of 0.833 was calculated.

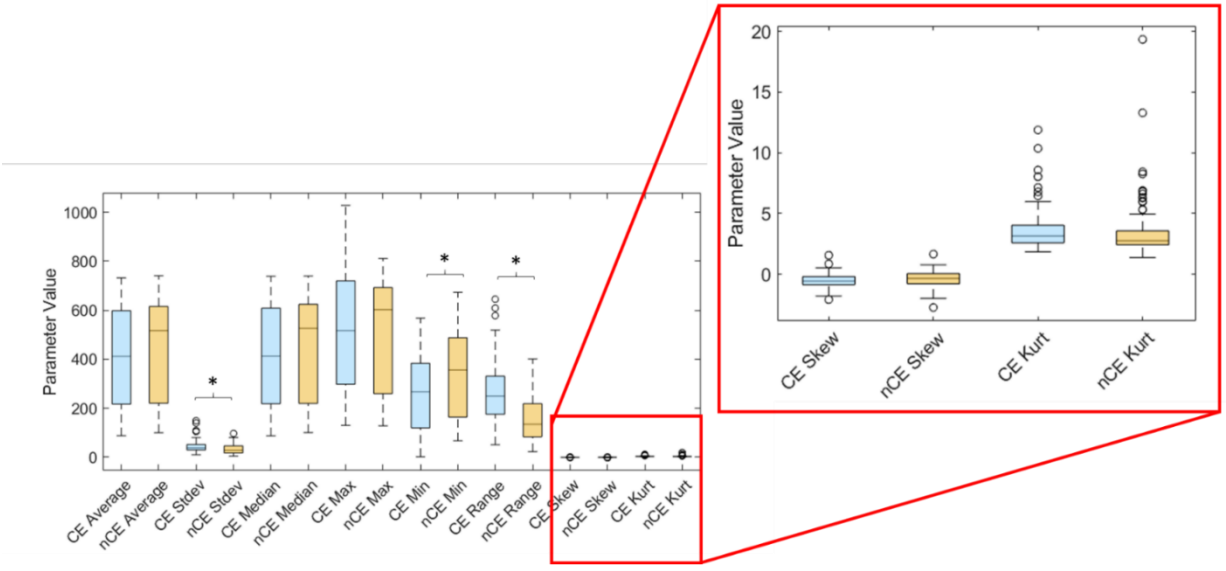

Figure 5.4: Boxplot for 8 features derived from T1w data divided into two classes: CE and nCE. Significant differences indicated by asterisks.

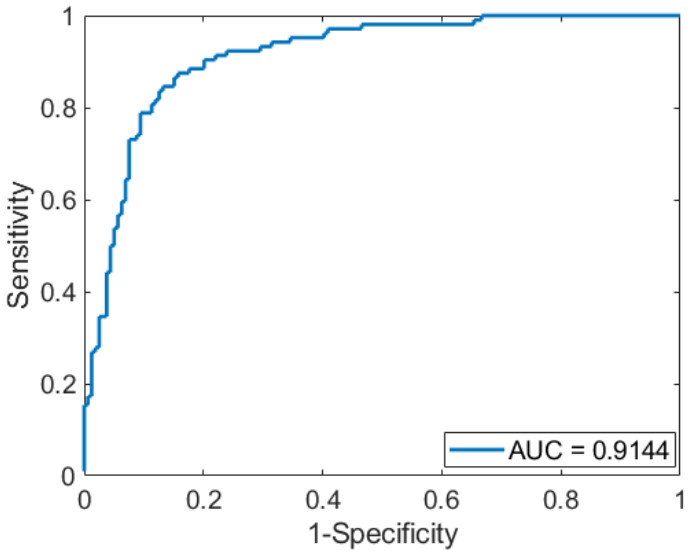

Figure 5.5: ROC curve for logistic regression fit of features extracted from T1w data.

Table 5.2 Beta values and significance from logistic regression analysis of features extracted from T1w data.		
Feature	**Beta**	**p-value**
X0	-0.541	0.401
X1 (Average)	0.0267	0.676
X2 (Stdev)	-0.188	3.84E-7
X3 (Median)	-0.0261	0.640
X4 (Max)	-7.16E6	0.304
X5 (Min)	7.16E6	0.304
X6 (Range)	7.16E6	0.304
X7 (Skewness)	-1.19	0.0555
X8 (Kurtosis)	-0.314	0.0323

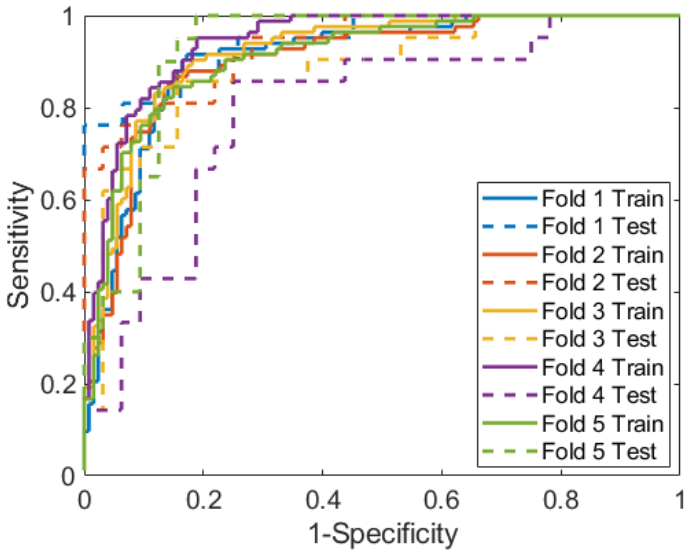

Figure 5.6: ROC curves for training and testing datasets using 5-fold cross validation with logistic regression operator on T1w data.

5.3.3 qT1 Analysis

Using the features derived from the qT1 pre-contrast images of the lesions, a student's t-test was applied to each feature with a Bonferroni correction for multiple comparisons setting the significant p-value at 0.00625 (8 total features). Six features were found to be significantly

Table 5.3: AUCs from 5-fold cross validation study on T1w data.		
Fold #	**AUC Train**	**AUC Test**
1	0.906	0.945
2	0.902	0.933
3	0.918	0.881
4	0.942	0.795
5	0.910	0.925
Avg (SD)	0.916 (0.0159)	0.896 (0.0613)

different between the groups: standard deviation (p = 2.07E-8), maximum intensity (p = 6.29E-17), minimum intensity (p = 1.22E-21), range of intensities (p = 2.97E-22), skewness (p = 1.20E-11), and kurtosis (p = 9.59E-6). A boxplot of the features between the two classes is shown in *Figure 5*.7.

Logistic regression was run on the qT1 data for three different combinations of features, followed by an ROC curve and AUC value. When all qT1 pre-contrast features were included, an AUC of 0.927 was achieved (*Figure 5.8*). Beta values and p-values for the coefficients are shown in *Table 5.4*. After applying 5-fold cross validation to the qT1 data (*Table 5.5, Figure 5.9*), an accuracy of 0.848 was calculated.

5.3.4 T1w versus qT1 Comparison

When comparing the AUC values from the ROC curves using the qT1 and T1w data, there was no significant differences in the two (p = 0.328). Similarly, after using a test of hypothesis concerning a system of two proportions, we again find no significant difference between the T1w and qT1 datasets (p = 0.317).

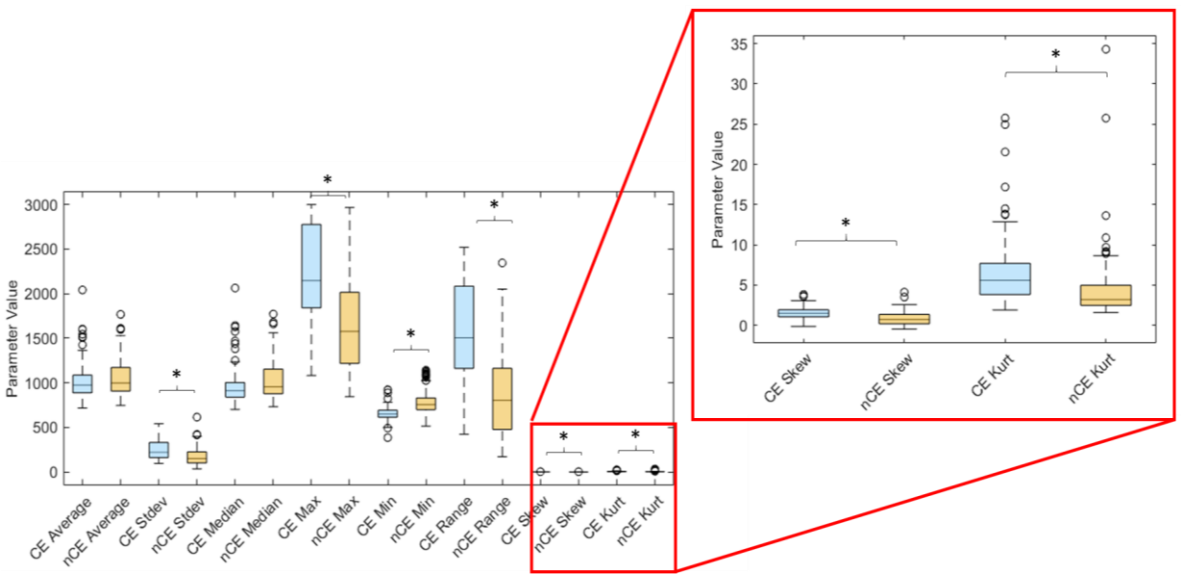

Figure 5.7: Boxplot for 8 features derived from qT1 data divided into two classes: CE and nCE. Significant differences indicated by asterisks.

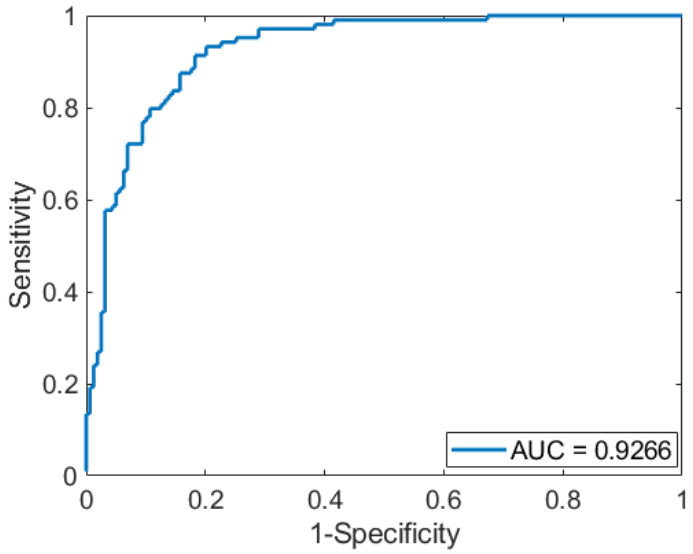

Figure 5.8: ROC curve for logistic regression fit of features extracted from qT1 data.

Table 5.4 Beta values and significance from logistic regression analysis of features extracted from qT1 data.		
Feature	**Beta**	**p-value**
X0	4.81	0.0224
X1 (Average)	0.0144	0.374
X2 (Stdev)	-0.0243	0.0122
X3 (Median)	0.000830	0.943
X4 (Max)	1.67E5	0.733
X5 (Min)	-1.67E5	0.733
X6 (Range)	-1.67E5	0.733
X7 (Skewness)	2.36	0.00259
X8 (Kurtosis)	-0.298	0.00738

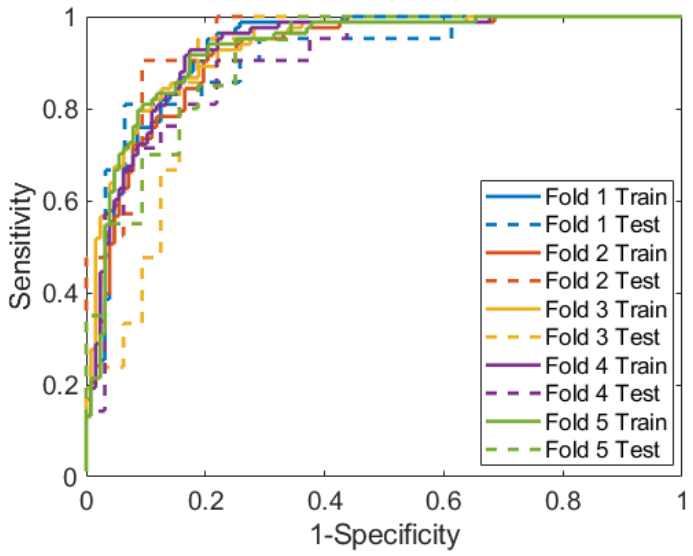

Figure 5.9: ROC curves for training and testing datasets using 5-fold cross validation with logistic regression operator on qT1 data.

Table 5.5: AUCs from 5-fold cross validation study on qT1 data.		
Fold #	**AUC Train**	**AUC Test**
1	0.929	0.920
2	0.916	0.945
3	0.932	0.893
4	0.929	0.903
5	0.929	0.913
Avg (SD)	0.927 (0.0063)	0.915 (0.0197)

5.3.5 Testing/Training on Distinct Datasets

However, an additional test was run. The data acquired were a combination of two datasets. To test the usefulness of the T1-REQUIRE algorithm, the T1w and qT1 data from Dataset #1 were used to train the logistic regression algorithms for testing on Dataset #2 and vice versa. When the T1w data was used, the logistic regression algorithm was able to train on Dataset #1 and test on Dataset #2, with a training AUC of 0.927 and testing AUC of 0.889. However, the logistic regression algorithm failed to converge to a solution when training on the T1w data in Dataset #2 and testing on Dataset #1.

Conversely, the qT1 data converted via T1-REQUIRE was able to successfully train and test on both datasets. When Dataset #1 was used to train and Dataset #2 used to test, a training AUC of 0.930 and testing AUC of 0.823 was found. When Dataset #2 was used to train and Dataset #1 was used to test, a training AUC of 0.944 and testing AUC of 0.797 was calculated.

5.4 Discussion

In this chapter, a pipeline was developed that incorporated the automatic segmentation of and feature extraction from MS lesions. In addition, it was found that first-order gray-level features derived from the T1w pre-contrast MRIs of the lesions had the potential to be indicative of contrast

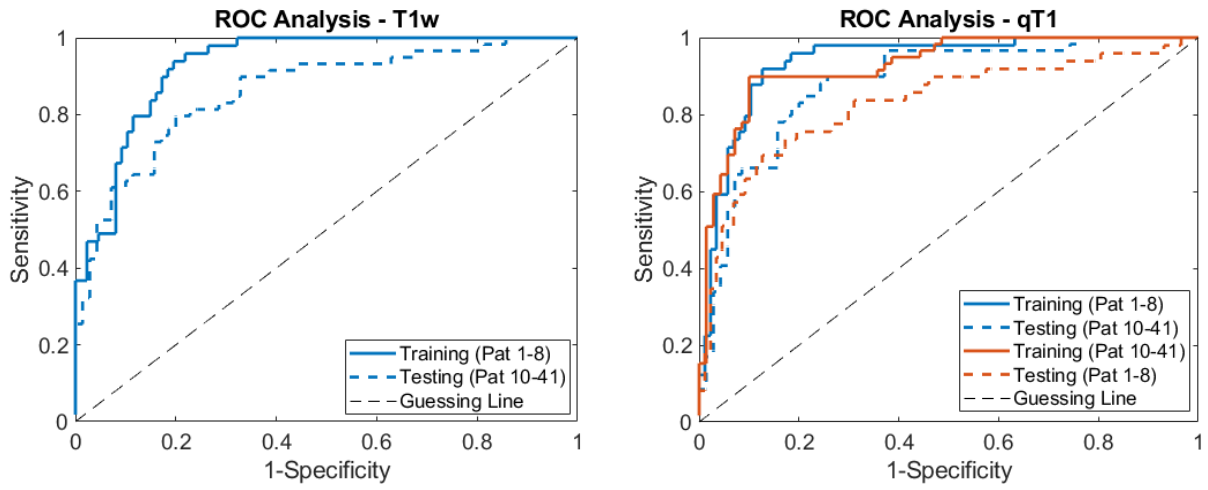

(a) (b)

Figure 5.10: Training/Testing ROC analysis when training on Dataset #1 and testing on Dataset #2 and vice versa for the T1w data (a) and qT1 data (b).

enhancement of lesions on the T1w post-contrast MRIs. The AUC of a logistic regression algorithm applied to the T1w features was 0.914, with an accuracy of 0.833. In addition, the T1w MRIs were converted to estimated T1 maps using a novel post-processing algorithm (T1-REQUIRE), and a similar analysis showed that logistic regression on the qT1 features resulted in a non-significant increase in the AUC (0.927) and accuracy (0.848). However, the qT1 data was able to successfully train and test on both datasets, while the T1w data was not, providing evidence of the T1-REQUIRE algorithm's usefulness.

Regardless of the differences in T1w and qT1 data, this analysis shows that it may be possible to use features from the T1w pre-contrast image to predict whether a MS lesion will enhance or not if GBCA would be given. This could be essential to cutting costs, reducing scan time, and protecting the well-being of patients with MS, and MRIs with contrast are common practice for the monitoring of their disease.

Other studies have shown that it is possible to use quantitative MR features to determine the enhancement status of MS lesion. Such studies have looked at quantitative T1 values, PD, and MTR values to determine differences between enhancing and non-enhancing lesions, and some have even used models to predict enhancement status.[87-89] However, these studies, while resulting in significant differences between mean values in enhancing and non-enhancing, have AUCs on the order of 0.83, significantly less than this study. In addition, those studies employed complicated quantitative techniques that increased time and cost with no benefit clinically for a neurologist or neuroradiologist. By using multiple first-order featured derived from both the T1w and qT1 lesion segmentations, we outperformed the previous studies using only scans that are already included in the clinical workflow. This provides evidence that other features like the texture of the MS lesion given by the standard deviation of values may be indicative of the biological process resulting in the disruption of the BBB. More research should be performed into the most predictive features and their relationship to the microenvironment within the lesion before fully concluding that features derived from T1w MRIs or qT1 images are able to accurately determine enhancement status.

One of the most important results of this study, though, was the ability to improve data harmonization with T1-REQUIRE. Because future studies may rely on training on one dataset and testing on another, it is essential that a data harmonization step must be completed. T1-REQUIRE was shown to do this using two separate datasets to an acceptable degree; the logistic regression algorithm was able to test and train on both Dataset #1 and Dataset #2 after T1-REQUIRE was applied, but not before. This provides initial evidence that T1-REQUIRE could be a useful addition to a big data or machine learning pipeline with minimal intrusion.

Limitations to this study include the lack of type of MS diagnosis (primary progressive versus secondary progressive versus relapsing remitting) that may confound the results. In addition, the lesion segmentation algorithm used is not clinically used, which may result in some discrepancies in what would be considered a lesion. However, because the algorithm was shown to have dice coefficients similar to that of two independent readers for larger lesion sizes, this should not be an issue.[84] Finally, this was a small study on only Philips' MR scanners that was intended to investigate the use of multiple features in a logistic regression predictor. A large study should be run to validate the accuracy of using T1 features derived from pre-contrast MR images before considering replacing the use of GBCA clinically for MS patient.

In conclusion, the study performed in this chapter shows that a multi-feature analysis using features derived from segmentations of T1w pre-contrast MS lesions was effective in predicting whether a lesion would enhance if GBCA was administered. In addition, moderate but insignificant improvement was shown using the same features derived from the qT1 MR image. However, the T1-REQUIRE algorithm did show promise as a data harmonizer when using separate datasets to test and train.

CHAPTER 6

SUMMARY AND FUTURE DIRECTIONS

This chapter presents a summary of the findings and contributions of this dissertation and gives outlines some ideas to further the presented work. In summary, this dissertation shows the results of an automatic, retrospective MR quantification algorithm and validates this novel algorithm against reference standard relaxometry techniques. Furthermore, the REQUIRE algorithm was tested on a combination of two datasets consisting of patients with MS in a multi-feature study of the contrast enhancement status of MS lesions. We did this in two ways; First, we compared the same logistic regression algorithm for prediction contrast enhancement with a random selection of training and testing data. Second, we compared the results of the same logistic regression methodology when we separated the data into its original two datasets.

6.1 Summary

Chapter 2 of this dissertation gives a detailed description of the physics behind and implementation of the REQUIRE algorithm. The REQUIRE algorithm differs from normal data harmonization algorithms by not only presenting a non-linear, physics-based approach to normalization, but also generating MR maps that reflect the properties of the tissue contained in each voxel. This can potentially help in both big data studies and relaxometry studies.

Chapter 3 shows the results of the validation of the REQUIRE algorithm on T1w spin-echo MR images. These were chosen for the initial validation due to the simplicity of the spin-echo MR sequence and the applicability of a T1w MRI for our eventual target disease of MS. Because of the sensitivity of the spin-echo signal equation to both variations in proton density and T2, necessary corrections were developed and applied to the MR image to create a pseudo-T1w image.

After being transformed into a T1 map by the REQUIRE algorithm, we found good comparison with the reference standard in both the case of a gadolinium/agar phantom and a healthy volunteer study. The healthy volunteer study also gave a range of T1 values for T1-REQUIRE to be applicable to ± 10% (523 to 3000 ms), which is an appropriate range for most cases of anatomical MR studies of the brain. A high correlation coefficient and Lin's concordance correlation coefficient also give evidence for T1-REQUIRE being comparable to the reference standard. Visual inspection of the histograms of the reference standard T1 maps and the T1-REQUIRE maps show similar overall shapes and distributions, again supporting the fact that a simple, physics-based, non-linear transform may be used as an estimate of T1. In addition, T1-REQUIRE was able to efficiently estimate T1, with over a 100-fold decrease in computation time compared to the Look-Locker method.

Chapter 4 expanded upon Chapter 3 of this dissertation by applying a similar methodology to a T1w MPRAGE MR sequence. By choosing a more complicated sequence, we were hoping to show the versatility of the REQUIRE algorithm to even more complex MR methods. Two studies were completed in Chapter 4. The first one involved the same healthy volunteer study as in Chapter 3, where we showed that there was good correlation between T1-REQUIRE with the MPRAGE images and the reference standard. Slightly more bias was detected, as shown in the discrepancy between the Pearson's and Lin's correlation coefficients, but an applicable range where T1 was ± 10% was determined to be from 682 to 3000 ms. In addition, T1-REQUIRE was compared between the MPRAGE and spin-echo MR sequences, with very good agreement and high correlation between the two.

The second study described in Chapter 4 determined the ability for T1-REQUIRE to remove scanner and sequence parameter dependence by using the same two healthy volunteers

and scanning them on multiple scanners. This study shows the viability of T1-REQUIRE to aid in data harmonization, as there was a marked decrease in variability when comparing T1 maps generated by T1-REQUIRE than there was when comparing MPRAGE images. In addition, the comparison of T1 maps generated by T1-REQUIRE was much more closely clustered around the line of unity for both subjects, thus providing evidence that T1-REQUIRE was effectively harmonizing the data.

Chapter 5 showed an example of the usage of T1-REQUIRE in a practical, clinical study. Using a multi-feature approach on both the T1w and qT1 MR images, logistic regression showed that there are defining features that can separate MS lesions into enhancing and non-enhancing classes without the need for gadolinium contrast agent injection. This, if confirmed in a larger study, could reduce the need for GCBAs, resulting in more patient comfort and less potential side effects and risks without removing the necessary information of active versus inactive MS lesions. We showed that a multi-feature approach achieved an accuracy of between 83-85%, with AUC values around 0.9-0.92. We believe that with more data, this accuracy can increase, potentially removing the need for GBCAs with MS patients. In addition, we also showed that although T1-REQUIRE did not significantly improve results when choosing the testing and training data randomly, it did improve the results when testing on one dataset and training on a separate one. This, again, highlights the potential use of T1-REQUIRE as a data harmonization algorithm for MR studies.

6.2 Future Directions

There are two categories of projects that could be explored in the future to further the work described in this dissertation. The first involves the development and validation of the REQUIRE

algorithm, and the second involves the testing of the applicability of REQUIRE to answer clinical questions.

6.2.1 Furthering the Development and Validation of the REQUIRE Algorithm

1. Other factors need to be explored in order to better validate the REQUIRE algorithm. Specifically, tests that involve the determination of the effect of variability in flip angle and coil sensitivity would be of potential interest. More options could include removing raw k-space data from the scanner to reconstruct without any proprietary filters.
2. More exploration should be conducted into scanning the same subjects on the same scanners with the same sequence but varied parameters (i.e. varying TR and TE for multiple T1w spin-echo images). This was not completed in our studies but could show the robustness of the REQUIRE algorithm to remove sequence parameters. Caution must be taken to ensure that the weighting remains the same for each image, however; otherwise, the signal may become dominated by the opposing weighting and result in significant errors in the analysis.
3. A bigger study should be completed to determine the inter-scanner variability for T1-REQUIRE among the major scanner manufacturers and models. We included a limited study consisting of two subjects with six scanners total, but this is not sufficient. Ideally, the REQUIRE algorithm would remove all variability between scanners; we cannot confidently say this is the case with such a small study.
4. The REQUIRE algorithm should be expanded to other T1w MR sequences along with other MR weightings. Options that could be of interest for T1w MR imaging could include fast low-angle shot (FLASH) and short inversion time recovery (STIR) sequences. It would be important to expand the REQUIRE algorithm to other weightings as well, especially T2w

images. More specifically, the comparison between a T2w image and a FLAIR image would be interesting to explore, as any mismatch could be indicative of underlying pathology as with various CNS tumors.[90-91]

6.2.2 Applications of REQUIRE Algorithm

There are a multitude of potential clinical applications of the REQUIRE algorithm. This section will highlight a few specific ones. It is worth mentioning that all the diseases mentioned involve the brain; this is due to the REQUIRE algorithm only being tested thus far in brain imaging.

1. As explained in both Chapters 1 and 5 of this dissertation, MS is a very heterogeneous disease and is a "clinico-radiological paradox", where radiological evidence of disease is not necessarily indicative of clinical disability or disease progression. In addition, MS patients routinely undergo MRI scans to aid in their disease management. This means that there are large amounts of longitudinal MS patient data that could be explored to answer questions about the disease. The REQUIRE algorithm can contribute to this potential analysis by harmonizing the data and providing quantitative maps to add even more information to the study.
2. As mentioned previously in this chapter, CNS tumors could also be a target for the REQUIRE algorithm. Various quantitative factors could be used to understand the genomic expression within and between similar tumors, and potentially help clinicians determine what treatments could be most effective for a patient's specific tumor type.
3. Another potential target for the REQUIRE algorithm is aneurysms. Factors such as k_{trans} have been looked at to determine the thickness of the aneurysm wall. The REQUIRE algorithm could replace the T1 mapping step necessary for the determination of this value.[92]

6.3 Final Thoughts

More and more research being completed in the world of medical imaging involves the usage of quantitative values from large datasets. The REQUIRE algorithm has the ability to be easily implemented into these workflows as both a quantification or relaxometry algorithm to produce MR maps and as a data harmonization algorithm to reduce inter- and intra-scanner and sequence variability for these studies. Although it is in its infancy, the evidence provided shows that the REQUIRE algorithm efficiently does both of those tasks and could be a useful addition to big data MR studies.

REFERENCES

1. OECD (2021), Magnetic resonance imaging (MRI) exams (indicator). doi: 10.1787/1d89353f-en (Accessed on 13 September 2021).

2. Plewes, D. B., & Kucharczyk, W. (2012). Physics of MRI : A Primer. *Journal of Magnetic Resonance Imaging*, *35*, 1038–1054. https://doi.org/10.1002/jmri.23642

3. Mills, A. F., Sakai, O., Anderson, S. W., & Jara, H. (2017). Principles of quantitative MR imaging with illustrated review of applicable modular pulse diagrams. *Radiographics*, 37(7), 2083–2105. https://doi.org/10.1148/rg.2017160099

4. Filippi, M., Rocca, M. A., Horsfield, M. A., Rovaris, M., & Pereira, C. (1998). Increased Spatial Resolution Using a Three- dimensional T1-Weighted Gradient-Echo MR Sequence Results in Greater Hypointense Lesion Volumes in Multiple Sclerosis. *American Journal of Neuroradiology*, *19*(2), 235–238.

5. Rosenkrantz, A. B., Mendiratta-Lala, M., Bartholmai, B. J., Ganeshan, D., Abramson, R. G., Burton, K. R., … Lenchik, L. (2015). Clinical Utility of Quantitative Imaging. *Academic Radiology*, 22(1), 33–49. https://doi.org/10.1016/j.acra.2014.08.011

6. Margaret Cheng, H. L., Stikov, N., Ghugre, N. R., & Wright, G. A. (2012). Practical medical applications of quantitative MR relaxometry. *Journal of Magnetic Resonance Imaging*, 36(4), 805–824. https://doi.org/10.1002/jmri.23718

7. Prescott, J. W. (2013). Quantitative imaging biomarkers: The application of advanced image processing and analysis to clinical and preclinical decision making. *Journal of Digital Imaging*, 26(1), 97–108. https://doi.org/10.1007/s10278-012-9465-7

8. Lescher, S., Jurcoane, A., Veit, A., Bähr, O., Deichmann, R., & Hattingen, E. (2014). Quantitative T1 and T2 mapping in recurrent glioblastomas under bevacizumab: earlier detection of tumor progression compared to conventional MRI. *Neuroradiology*, 57(1), 11–20. https://doi.org/10.1007/s00234-014-1445-9

9. Carneiro, A. A. O., Vilela, G. R., De Araujo, D. B., & Baffa, O. (2006). MRI relaxometry: Methods and applications. *Brazilian Journal of Physics*, 36(1 A), 9–15. https://doi.org/10.1590/S0103-97332006000100005

10. De Haro, L. P., Karaulanov, T., Vreeland, E. C., Anderson, B., Hathaway, H. J., Huber, D. L., … Flynn, E. R. (2015). Magnetic relaxometry as applied to sensitive cancer detection and localization. *Biomedizinische Technik*, 60(5), 445–455. https://doi.org/10.1515/bmt-2015-0053

11. Blystad, I., Warntjes, J. B. M., Smedby, Lundberg, P., Larsson, E. M., & Tisell, A. (2020). Quantitative MRI using relaxometry in malignant gliomas detects contrast enhancement in

peritumoral oedema. *Scientific Reports*, 10(1), 1–9. https://doi.org/10.1038/s41598-020-75105-6

12. Manfredonia, F., Ciccarelli, O., Khaleeli, Z., Tozer, D. J., Sastre-Garriga, J., Miller, D. H., & Thompson, A. J. (2007). Normal-appearing brain T1 relaxation time predicts disability in early primary progressive multiple sclerosis. *Archives of Neurology*, 64(3), 411–415. https://doi.org/10.1001/archneur.64.3.411

13. Deichmann, R., & Haase, A. (1992). Quantification of T1 values by SNAPSHOT-FLASH NMR imaging. *Journal of Magnetic Resonance (1969)*, *96*(3), 608–612. https://doi.org/10.1016/0022-2364(92)90347-A

14. Panda, A., Mehta, B. B., Coppo, S., Jiang, Y., Ma, D., Seiberlich, N., Griswold, M. A., & Gulani, V. (2017). Magnetic resonance fingerprinting – An overview. *Current Opinion in Biomedical Engineering*, *3*(1), 56–66. https://doi.org/10.1016/j.cobme.2017.11.001

15. Trial, M., Tanenbaum, X. L. N., Tsiouris, X. A. J., Johnson, X. A. N., Naidich, X. T. P., Delano, X. M. C., Melhem, X. E. R., Quarterman, X. P., Parameswaran, X. S. X., Shankaranarayanan, X. A., Goyen, X. M., & Field, X. A. S. (2017). Synthetic MRI for Clinical Neuroimaging : Results of the Magnetic Resonance Image Compilation (MAGiC) Prospective ,. *American Journal of Neuroradiology*, *38*, 1103–1110.

16. NINDS Multiple Sclerosis Information Page. National Institute of Neurological Disorders and Stroke https://web.archive.org/web/20160210042232/http://www.ninds.nih.gov/disorders/multiple_sclerosis/detail_multiple_sclerosis.htm (2015).

17. Compston, A. & Coles, A. Multiple sclerosis. The Lancet 359, 1221–1231 (2002).

18. Ascherio, A. & Munger, K. L. Environmental risk factors for multiple sclerosis. Part I: The role of infection. *Ann. Neurol.* 61, 288–299 (2007).

19. Vidal-Jordana, A. & Montalban, X. Multiple Sclerosis. *Neuroimaging Clin. N. Am*. 27, 195–204 (2017).

20. Lucchinetti, C., Bruck, W., Parisi, J., Scheithauer, B., Rodriguez, M., & Lassmann, H. (2000). Heterogeneity of multiple sclerosis lesions. *Annals of Neurology*, *47*(6), 707–717.

21. Friese, M. A., Schattling, B., & Fugger, L. (2014). Mechanisms of neurodegeneration and axonal dysfunction in multiple sclerosis. *Nature Reviews Neurology*, *10*(4), 225–238. https://doi.org/10.1038/nrneurol.2014.37

22. Adams, C. W. M. (1975). The onset and progression of the lesion in multiple sclerosis. *Journal of the Neurological Sciences*, *25*(2), 165–182. https://doi.org/10.1016/0022-510X(75)90138-0

23. Ascherio, A., & Munger, K. L. (2007). Environmental risk factors for multiple sclerosis. Part I: The role of infection. *Annals of Neurology*, *61*(4), 288–299. https://doi.org/10.1002/ana.21117

24. Lublin, F. D., Reingold, S. C. & National Multiple Sclerosis Society (USA) Advisory Committee on Clinical Trials of New Agents in Multiple Sclerosis*. Defining the clinical course of multiple sclerosis: Results of an international survey. *Neurology* 46, 907–911 (1996).

25. Lublin, F. D. et al. Defining the clinical course of multiple sclerosis: The 2013 revisions. *Neurology* 83, 278–286 (2014).

26. Poser, C. M., Paty, D. W., Scheinberg, L., McDonald, W. I., Davis, F. A., Ebers, G. C., Johnson, K. P., Sibley, W. A., Silberberg, D. H., & Tourtellotte, W. W. (1983). New diagnostic criteria for multiple sclerosis: Guidelines for research protocols. *Annals of Neurology*, *13*(3), 227–231. https://doi.org/10.1002/ana.410130302

27. Rovira, À. (2017). Advances in the Diagnosis, Characterization, and Monitoring of Multiple Sclerosis. *Neuroimaging Clinics of North America*, *27*(2), xvii–xviii. https://doi.org/10.1016/j.nic.2017.02.001

28. Vidal-Jordana, A., & Montalban, X. (2017). Multiple Sclerosis: Epidemiologic, Clinical, and Therapeutic Aspects. *Neuroimaging Clinics of North America*, *27*(2), 195–204. https://doi.org/10.1016/j.nic.2016.12.001

29. National MS Society (2021). Types of MS. https://www.nationalmssociety.org/What-is-MS/Types-of-MS (Accessed 14 September 2021).

30. Young, I. R. et al. Nuclear Magnetic Resonance Imaging of the Brain in Multiple Sclerosis. *The Lancet* 318, 1063–1066 (1981).

31. Poser, C. M. et al. New diagnostic criteria for multiple sclerosis: Guidelines for research proto-cols. *Ann. Neurol*. 13, 227–231 (1983).

32. Thompson, A. J. et al. Diagnosis of multiple sclerosis: 2017 revisions of the McDonald criteria. *Lancet Neurol*. 17, 162–173 (2018).

33. Saslow, L., Li, D. K. B., Halper, J., Banwell, B., Barkhof, F., Barlow, L., Costello, K., Damiri, P., Dunn, J., Giri, S., Maes, M., Morrow, S. A., Newsome, S. D., Oh, J., Paul, F., Quarterman, P., Hecke, W. Van, Ven, K. Van De, & Wallin, M. T. (2020). An International Standardized Magnetic Resonance Imaging Protocol for Diagnosis and Follow-up of Patients with Multiple Sclerosis. International Journal of MS Care, 22(5), 226–232. https://doi.org/10.7224/1537-2073.2020-094

34. Noseworthy, J. H., Vandervoort, M. K., Wong, C. J. & Ebers, G. C. Interrater variability with the Expanded Disability Status Scale (EDSS) and Functional Systems (FS) in a multiple sclerosis clinical trial. Neurology 40, 971–971 (1990).

35. van Walderveen, M. A. A. et al. Correlating MRI and clinical disease activity in multiple sclero-sis: Relevance of hypointense lesions on short-TR/short-TE (T1-weighted) spin-echo images. Neurology 45, 1684–1690 (1995).

36. Truyen, L. et al. Accumulation of hypointense lesions (‘black holes’) on T1 spin-echo MRI correlates with disease progression in multiple sclerosis. Neurology 47, 1469–1476 (1996).

37. van Walderveen, M. A. A. et al. Hypointense Lesions on T1-Weighted Spin-Echo Magnetic Resonance Imaging: Relation to Clinical Characteristics in Subgroups of Patients With Multiple Sclerosis. Arch. Neurol. 58, (2001).

38. Gawne-Cain, M. L. et al. MRI lesion volume measurement in multiple sclerosis and its correla-tion with disability: a comparison of fast fluid attenuated inversion recovery (fFLAIR) and spin echo sequences. J. Neurol. Neurosurg. Psychiatry 64, 197–203 (1998).

39. Ciccarelli, O., Brex, P. A., Thompson, A. J. & Miller, D. H. Disability and lesion load in MS: a reassessment with MS functional composite score and 3D fast FLAIR. J. Neurol. 249, 18–24 (2002).

40. Mostert, J. P. et al. T2 lesions and rate of progression of disability in multiple sclerosis: T2 lesions and progression in MS. Eur. J. Neurol. 17, 1471–1475 (2010).

41. Barkhof, F. MRI in multiple sclerosis: correlation with expanded disability status scale (EDSS). Mult. Scler. J. 5, 283–286 (1999).

42. Ge, Y. et al. Magnetization transfer ratio histogram analysis of gray matter in relapsing-remitting multiple sclerosis. AJNR Am. J. Neuroradiol. 22, 470–475 (2001).

43. Oreja-Guevara, C. et al. Magnetization Transfer Magnetic Resonance Imaging and Clinical Changes in Patients With Relapsing-Remitting Multiple Sclerosis. Arch. Neurol. 63, 736 (2006).

44. Vrenken, H. et al. Magnetization transfer ratio measurement in multiple sclerosis normal-appearing brain tissue: limited differences with controls but relationships with clinical and MR measures of disease. Mult. Scler. J. 13, 708–716 (2007).

45. Rudick, R. A., Fisher, E., Lee, J.-C., Duda, J. T. & Simon, J. Brain atrophy in relapsing multiple sclerosis: relationship to relapses, EDSS, and treatment with interferon β-1a. Mult. Scler. J. 6, 365–372 (2000).

46. von Gumberz, J. et al. Short-term MRI measurements as predictors of EDSS progression in relapsing-remitting multiple sclerosis: grey matter atrophy but not lesions are predictive in a real-life setting. PeerJ 4, e2442 (2016).

47. Barkhof, F. The clinico-radiological paradox in multiple sclerosis revisited. Curr. Opin. Neurol. 15, 239–245 (2002).

48. Bitsch, A. et al. A longitudinal MRI study of histopathologically defined hypointense multiple sclerosis lesions: Longitudinal Study of Hypointense T1 Lesions. Ann. Neurol. 49, 793–796 (2001).

49. Gracien, R.-M. et al. Assessment of cortical damage in early multiple sclerosis with quantitative T 2 relaxometry: Cortical T 2 in Early Multiple Sclerosis. NMR Biomed. 29, 444–450 (2016).

50. Zellini, F., Niepel, G., Tench, C. R. & Constantinescu, C. S. Hypothalamic involvement assessed by T1 relaxation time in patients with relapsing—remitting multiple sclerosis. Mult. Scler. J. 15, 1442–1449 (2009).

51. Neema, M. et al. 3 T MRI relaxometry detects T2 prolongation in the cerebral normal-appearing white matter in multiple sclerosis. NeuroImage 46, 633–641 (2009).

52. Margaret Cheng, H.-L., Stikov, N., Ghugre, N. R. & Wright, G. A. Practical medical applications of quantitative MR relaxometry. J. Magn. Reson. Imaging 36, 805–824 (2012).

53. Papadopoulos, K. et al. TI-relaxation time changes over five years in relapsing-remitting multiple sclerosis. Mult. Scler. J. 16, 427–433 (2010).

54. Manfredonia, F. et al. Normal-Appearing Brain T1 Relaxation Time Predicts Disability in Early Primary Progressive Multiple Sclerosis. Arch. Neurol. 64, 411 (2007).

55. Deo, R. C. (2015). Machine learning in medicine. Circulation, 132(20), 1920–1930. https://doi.org/10.1161/CIRCULATIONAHA.115.001593

56. Cleophas, T. J., & Zwinderman, A. H. (2020). Machine learning in medicine - a complete overview. In Machine Learning in Medicine - A Complete Overview. https://doi.org/10.1007/978-3-030-33970-8

57. Shan Suthaharan. (2016). Machine Learning Models and Algorithms for Big Data Classification Thinking with Examples for Effective Learning. In Integrated Series in Information Systems (Vol. 36).

58. Brant-Zawadzki, M., Gillan, G. D., & Nitz, W. R. (1992). MP RAGE: A three-dimensional, T1-weighted, gradient-echo sequence - Initial experience in the brain. *Radiology*, *182*(3), 769–775. https://doi.org/10.1148/radiology.182.3.1535892

59. Wansapura, J. P., Holland, S. K., Dunn, R. S. & Ball, W. S. NMR relaxation times in the human brain at 3.0 tesla. J. Magn. Reson. Imaging JMRI 9, 531–538 (1999).

60. Condon, B., Patterson, J., Jenkins, A., Wyper, D., Hadley, D., Grant, R., … Teasdale, G. (1987). MR relaxation times of cerebrospinal fluid. Journal of Computer Assisted Tomography. https://doi.org/10.1097/00004728-198703000-00001

61. Bojorquez, J. Z., Bricq, S., Acquitter, C., Brunotte, F., Walker, P. M., & Lalande, A. (2017). What are normal relaxation times of tissues at 3 T? Magnetic Resonance Imaging, 35, 69–80. https://doi.org/10.1016/j.mri.2016.08.021

62. Gracien RM et. al. (2016). The relationship between gray matter quantitative MRI and disability in secondary progressive multiple sclerosis. PLoS One, 11(8). https://dx.doi.org/10.1371%2Fjournal.pone.0161036

63. Lin, L. I. (1989). A Concordance Correlation Coefficient to Evaluate Reproducibility. *Biometrics*, *45*(1), 255–268.

64. Panda, A., Mehta, B. B., Coppo, S., Jiang, Y., Ma, D., Seiberlich, N., Griswold, M. A., & Gulani, V. (2017). Magnetic resonance fingerprinting – An overview. Current Opinion in Biomedical Engineering, 3(1), 56–66. https://doi.org/10.1016/j.cobme.2017.11.001

65. Li, X., Morgan, P. S., Ashburner, J., Smith, J., & Rorden, C. (2016). The first step for neuroimaging data analysis: DICOM to NIfTI conversion. Journal of Neuroscience Methods, 264, 47–56. https://doi.org/10.1016/j.jneumeth.2016.03.001

66. Bevington, P., & Robinson, D. (2003). Data Reduction and Error Analysis for the Physical Sciences (3rd ed.). McGraw-Hill Higher Education.

67. Wingerchuk, D. M., Lucchinetti, C. F., & Noseworthy, J. H. (2001). Multiple Sclerosis: Current Pathophysiological Concepts. Laboratory Investigation, 81(3), 263–281.

68. Frohman, E., Racke, M., & Raine, C. (2006). Multiple Sclerosis - The Plaque and Its Pathogenesis. New England Journal of Medicine, 354, 942–955.

69. Compston, A., & Coles, A. (2002). Multiple sclerosis. 359, 1221–1231.

70. Vidal-Jordana, A., & Montalban, X. (2017). Multiple Sclerosis: Epidemiologic, Clinical, and Therapeutic Aspects. Neuroimaging Clinics of North America, 27(2), 195–204. https://doi.org/10.1016/j.nic.2016.12.001

71. Barkhof, F. (2002). The clinico-radiological paradox in multiple sclerosis revisited. Current Opinion in Neurology, 15(3), 239–245.

72. Mollison, D., Sellar, R., Bastin, M., Mollison, D., Chandran, S., Wardlaw, J., & Connick, P. (2017). The clinico-radiological paradox of cognitive function and MRI burden of white matter lesions in people with multiple sclerosis: A systematic review and meta-analysis. PLoS ONE, 12(5), 1–16.

73. Sahraian, M. A., Radue, E. W., Haller, S., & Kappos, L. (2010). Black holes in multiple sclerosis: Definition, evolution, and clinical correlations. Acta Neurologica Scandinavica, 122(1), 1–8. https://doi.org/10.1111/j.1600-0404.2009.01221.x

74. Li, X., Van Gelderen, P., Sati, P., De Zwart, J. A., Reich, D. S., & Duyn, J. H. (2015). Detection of demyelination in multiple sclerosis by analysis of T 2 ∗ relaxation at 7 T. NeuroImage: Clinical, 7, 709–714. https://doi.org/10.1016/j.nicl.2015.02.021

75. Giacomini, P. S., Levesque, I. R., Ribeiro, L., Narayanan, S., Francis, S. J., Pike, G. B., & Arnold, D. L. (2009). Measuring demyelination and remyelination in acute multiple sclerosis lesion voxels. Archives of Neurology, 66(3), 375–381. https://doi.org/10.1001/archneurol.2008.578

76. Sheth, V., Shao, H., Chen, J., Vandenberg, S., Corey-Bloom, J., Bydder, G. M., & Du, J. (2016). Magnetic resonance imaging of myelin using ultrashort Echo time (UTE) pulse sequences: Phantom, specimen, volunteer and multiple sclerosis patient studies. NeuroImage, 136, 37–44. https://doi.org/10.1016/j.neuroimage.2016.05.012

77. Rovira, A., Auger, C., & Alonso, J. (2013). Magnetic resonance monitoring of lesion evolution in multiple sclerosis. Therapeutic Advances in Neurological Disorders, 6(5), 298–310. https://doi.org/10.1177/1756285613484079

78. Choi, J. W., & Moon, W. (2019). Gadolinium Deposition in the Brain: Current Updates. Korean Journal of Radiology, 20(1), 134–147.

79. Guo, B. J., Yang, Z. L., & Zhang, L. J. (2018). Gadolinium Deposition in Brain: Current Scientific Evidence and Future Perspectives. Frontiers in Molecular Neuroscience, 11(September), 1–12. https://doi.org/10.3389/fnmol.2018.00335

80. Kanda, T., Ishii, K., Kawaguchi, H., Kitajima, K., & Takenaka, D. (2014). High Signal Intensity in the Dentate Nucleus and Globus Pallidus on Images: Relationship with Increasing Cumulative Dose of a Gadolinium-. Radiology, 270(3).

81. Lenkinski, R. E. (2019). Gadolinium Deposition and Retention in the Brain: Should We Be Concerned? Radiology: Cardiothoracic Imaging, 2, 2018–2020.

82. Smith, T. E., Steven, A., & Bagert, B. A. (2019). Gadolinium Deposition in Neurology Clinical Practice. Ochsner Journal, 17–25. https://doi.org/10.31486/toj.18.0111

83. Kanda, T., Oba, H., Toyoda, K., & Kitajima, K. (2016). Brain gadolinium deposition after administration of gadolinium based contrast agents. Japanese Journal of Radiology, 34(1), 3–9. https://doi.org/10.1007/s11604-015-0503-5

84. Schmidt, P., Gaser, C., Arsic, M., Buck, D., Forschler, A., Berthele, A., Hoshi, M., Rudiger, I., Volker, S., Zimmer, C., Hemmer, B., & Muhlau, M. (2012). An automated tool for detection of lesions in Multiple Sclerosis. NeuroImage, 59, 3774–3783.

85. Hanley, J., & McNeil, B. (1982). The Meaning and Use of the Area under a Receiver Operating Characteristic (ROC) Curve. Radiology, 143, 29–36.

86. Sullivan, L. (n.d.). Hypothesis Testing for Means and Proportions. Boston University School of Public Health. https://sphweb.bumc.bu.edu/otlt/mph-modules/bs/bs704_hypothesistest-means-proportions/bs704_hypothesistest-means-proportions_print.html

87. Levesque, I. R., Giacomini, P. S., Narayanan, S., Ribeiro, L. T., Sled, J. G., Arnold, D. L., & Pike, G. B. (2010). Quantitative Magnetization Transfer and Myelin Water Imaging of the Evolution of Acute Multiple Sclerosis Lesions. Magnetic Resonance in Medicine, 63, 633–640. https://doi.org/10.1002/mrm.22244

88. Jurcoane, A., Wagner, M., Schmidt, C., Mayer, C., Gracien, R., Hirschmann, M., Deichmann, R., Volz, S., Ziemann, U., & Hattingen, E. (2013). Within-Lesion Differences in Quantitative MRI Parameters Predict Contrast Enhancement in Multiple Sclerosis. Journal of Magnetic Resonance Imaging, 38, 1454–1461. https://doi.org/10.1002/jmri.24107

89. Blystad, I., Hakansson, I., Tisell, A., Ernerudh, J., Smedby, O., Lundberg, P., & Larsonn, E. (2016). Quantitative MRI for Analysis of Active Multiple Sclerosis Lesions without Gadolinium-Based Contrast Agent. American Journal of Neuroradiology, 37(1), 94–100.

90. Patel SH, Poisson LM, Brat DJ, Zhou Y, Cooper L, Snuderl M, Thomas C, Franceschi AM, Griffith B, Flanders AE, Golfinos JG, Chi AS, Jain R. T2-FLAIR Mismatch, an Imaging Biomarker for IDH and 1p/19q Status in Lower-grade Gliomas: A TCGA/TCIA Project. (2017) Clinical cancer research : an official journal of the American Association for Cancer Research. 23 (20): 6078-6085. doi:10.1158/1078-0432.CCR-17-0560

91. Broen MPG, Smits M, Wijnenga MMJ, Dubbink HJ, Anten MHME, Schijns OEMG, Beckervordersandforth J, Postma AA, van den Bent MJ. The T2-FLAIR mismatch sign as an imaging marker for non-enhancing IDH-mutant, 1p/19q-intact lower-grade glioma: a validation study. (2018) Neuro-oncology. 20 (10): 1393-1399. doi:10.1093/neuonc/noy048

92. Vakil P, Ansari SA, Cantrell CG, Eddleman CS, Dehkordi FH, Vranic J, Hurley MC, Batjer HH, Bendok BR, Carroll TJ. Quantifying Intracranial Aneurysm Wall Permeability for Risk Assessment Using Dynamic Contrast-Enhanced MRI: A Pilot Study. AJNR Am J Neuroradiol. 2015 May;36(5):953-9. doi: 10.3174/ajnr.A4225.

LIST OF PUBLICATIONS AND PRESENTATIONS

Peer-Reviewed Publications

Hasse A, Javed A, Carroll TJ. "Features Derived from T1 Pre-Contrast MRI Predict Contrast Enhancement of Plaques in Multiple Sclerosis: a Pilot Study." (In preparation).

Hasse A, Jeong Y, Foxley S, Javed A, Carroll TJ. "A Method for Harmonizing T1 Image Contrast in the Brain: T1 REtrospective Quantification Using Internal REferences (T1-REQUIRE) Algorithm." (In review).

Zhang M, **Hasse A**, Carroll TJ, Pearson A, Cipriani N, Ginat DT. "Differentiating low and high grade mucoepidermoid carcinoma of the salivary glands using CT texture analysis." *Gland Surgery* 10 (5), 2021 May. https://doi.org/10.21037/gs-20-830

Hasse A, Dapash M, Jeong Y, Ansari SA, Carroll TJ, Lesniak M, Ginat DT. "Correlation of post-contrast T1-weighted MRI surface regularity, tumor bulk, and necrotic volume with Ki67 and p53 in glioblastomas." *Neuroradiology*. 2019 April 24. https://doi.org/10.1007/s00234-019-02204-1

Presentations

Hasse A, Jeong Y, Foxley S, Javed A, Carroll TJ. "Validation of T1 REtrospective Quantification Using Internal REferences (T1-REQUIRE) Algorithm in Healthy Volunteers" e-poster presented at ASNR 56th Annual Meeting, Virtual. May 22-26, 2021.

Hasse A, Dapash M, Jeong Y, Su S, Cummings A, Ansari SA, Ginat DT, Carroll TJ. "Association of geometric features with genetic markers in glioblastoma multiforme." e-poster

presented at ISMRM 27th Annual Meeting and Exhibition, Montreal, QC, Canada. May 11-16, 2019.

Hasse A, Jeong Y, Javed A, Carroll TJ. "Validation of retrospective T1 quantitation using Grey Matter, White Matter, and Cerebrospinal Fluid reference values." poster presented at NIBIB Training Grantees Conference, Bethesda, MD, June 21-22, 2018.

Hasse A, Jeong Y, Ansari S, Collins J, Carroll TJ. "Development of an Automatic Tumor Detection and Segmentation Algorithm using Multi-contrast MR and Linear Discriminant Analysis." oral presentation at ASNR 56th Annual Meeting, Vancouver, BC, Canada, June 3-7, 2018.

Kawaji K, **Hasse A**, Singh A, Narang A, Wang H, Carroll T.J., Patel A "A Versatile MOLLI-based Inversion Time (TI) scout sequence for Myocardial Nulling Determination in emerging Late Gadolinium Enhanced CMR Variants: A Phantom Study" poster presented at ISMRM 25th Annual Meeting and Exhibition, Honolulu, HI, April 22-27, 2017.